"FEDERICO II" UNIVERSITY OF NAPLES

DOCTORATE IN APPLIED BIOLOGY
(XXVI Cycle)

In vitro *and* in vivo *crosstalk between gut and pre-/pro-biotics*

Tutor
Prof. Ezio Ricca

Ph.D student
Blanda Di Luccia

Coordinator
Prof. Ezio Ricca

INDEX

pagg.

OUTLINE OF THE THESIS

This PhD Thesis reports the results of my research in the laboratory of Prof. Ezio Ricca at the Department of Biology of the Federico II University of Naples, Italy. During these three years I focused my studies on the effects of molecules of various origin on intestinal epithelial cells and on the role of the microbiota in the gut homeostasis, using two different experimental approaches: *in vitro* and *in vivo* model systems. The Thesis is organized in four chapters addressing specific topics. The first three chapters are focused on the effect of bacterial molecules (putative peptides produced by intestinal isolates of *Lactobacilli spp.*, CHAPTER 1; Competence and Sporulation Factor –CSF produced by intestinal isolates of *Bacillus subtilis* strains, CHAPTER 2) or plant molecules (whole-leaf extracts of *Aloe arborescens*, CHAPTER 3) on epithelial cells (*in vitro* approach) with particular attention to intestinal epithelial cells, to better understand how they affect cellular proliferation and death. CHAPTER 4 analyzes the variations of intestinal microbiota composition in rats (*in vivo* approach) under different diet regimens, by using a metagenomic approach.

In most part of my work, I focused on the crosstalk set between commensal bacteria and intestinal epithelial cells, based on microbial *quorum-sensing* molecules. It is well known the intestinal microbiota is a unique ecological niche where microorganisms live in a balanced relationship with other species and the host. Our gut microbiota can be pictured as a microbial organ placed within a host organ: i) it is composed of different cell lineages with a capacity to communicate with one another and the host, ii) it consumes, stores, and redistributes energy, iii) it mediates physiologically important chemical transformations and iv) it maintains and repairs itself through self-replication.

Our relationship with components of this microbiota is often described as commensal (one partner benefits and the other is apparently unaffected) as opposed to mutualistic (both partners experience increased fitness). However, use of the term commensal generally reflects our lack of knowledge, or at least an agnostic (noncommittal) attitude about the contributions of most citizens of this microbial society to our own fitness or the fitness of other community members (Backhead et al., 2005). It's well known that this relationship is complex and incompletely understood, often involving bidirectional signals and interactions that not only influence the behavior of microflora but also host responses essential to the maintenance of intestinal homeostasis. In this contest, many beneficial bacteria, including members of the *Lactobacillus* or *Bacillus* genera, have been promoted as probiotics for the treatment or prevention of a number of diseases (Hong et al., 2005). The mechanism(s) by which they exert their protective effects in the gastrointestinal tract is not well understood but is likely to involve pathogen control or exclusion as well as protection of host tissues against inflammatory responses. However, the biochemical basis of the biological response of eukaryotes to bacterial quorum-sensing signal molecules is still at an early stage, and virtually nothing is known about the impact of Gram-positive peptide signals on host cells. Furthermore, it has to be underlined that all bacilli and lactobacilli used in my studies are intestinal isolates from healthy human adult volunteers, previously characterized (Fakhry et al., 2008; Fakhry et al., 2009). Here a brief summary of the content of each chapter is reported.

In **CHAPTER 1**, I report the effects of secreted molecules of an intestinal strain of *Lactobacillus gasseri* (SF1183) on HCT116 cells, a model of intestinal epithelial cells. With my work I have shown that the bacterial strain secretes, during its stationary phase

of growth, a small molecule, most likely a peptide, able to reduce the TNF-alpha induced-apoptosis of HCT116 cells. These results have been published in 2013: ***Di Luccia B***, Manzo N, Baccigalupi L, Calabrò V, Crescenzi E, Ricca E, Pollice A. (2013). *Lactobacillus gasseri SF1183 affects intestinal epithelial cell survival and growth*. PLoS One. 2013 Jul 23;8(7):e69102.

In **CHAPTER 2**, I studied the effects of the Competence and Sporulation Factor (CSF) secreted by various intestinal strains of *Bacillus subtilis* on HT29, used as a model of intestinal epithelial cells. CSF is a cationic pentapeptide corresponding to the C-terminal 5 amino acids of the 40 amino acid polypeptide encoded by the *phrC* gene (Kunst et al., 1997) and acts in *quorum sensing* factor (Lazazzera et al., 1997) altering *Bacillus* population behavior in pure culture (Solomon et al.,1996). It has been shown that CSF produced by a laboratory collection strain of *B. subtilis,* induces the heat-shock protein 27 (Hsp27) in human intestinal epithelial cells (Fujita et al., 2007). Hsps confer protection against a wide variety of stresses protecting intestinal epithelial cells from oxidative injury and hence contribute to the maintenance of intestinal homoeostasis (Tao et al., 2006). During my studies, I developed a genetic system to evaluate the presence of CSF in bacterial conditioned growth media and used it to screen a collection of intestinal isolates of *B. subtilis*. When compared to a laboratory strain of *B. subtilis* (PY79) most isolates were shown to produce high amounts of CSF and only few of them were unable to produce the *quorum-sensing* peptide. Some of the intestinal isolates were able to grow anaerobically and also in those condition CSF production was observed. As expected, all CSF-containing media were able to induce Hsp27 to levels similar to those observed with the laboratory collection strain and after heat shock. Surprisingly, one of the strain that does not produce CSF is still able to

induce an heat-shock response, suggesting the also other bacterial molecules can be sensed by epithelial cells. Then, a proteomic approach was used to investigate potential other cell targets of the bacterial molecule. The total proteic extracts of HT29 cells treated and not-treated with CSF were analysed by 2D-PAGE-MS/MS to identify proteins up- or down-regulated in the treated sample compared with the not-treated. A preliminary analysis of the proteins affected by CSF is reported. A manuscript reporting these results is in preparation.

In the **CHAPTER 3**, it has been proposed a biochemical and cellular approach to explore the beneficial activity of *Aloe arborescens* leaf-extracts. *Aloe arborescens* is known to be rich in beneficial phytotherapeutic, anticancer, and radio-protective properties. It is commonly used as a pharmaceutical ingredient for its effect in burn treatment and ability to increase skin wound healing properties. However, very few studies have addressed its biological effects at molecular level. In this contest, my experiments showed that *Aloe arborscens* extracts have antiproliferative properties on epithelial cancer cells and prodifferentiative effects on immortalized cheratinocytes promoting the production of antimicrobial molecules. These results have been included in the publication: ***Di Luccia B***, Manzo N, Vivo M, Galano E, Amoresano A, Crescenzi E, Pollice A, Tudisco R, Infascelli F, Calabrò V. (2013). *A biochemical and cellular approach to explore the antiproliferative and prodifferentiative activity of Aloe Arborescens leaf extract*. Phytother Res. doi: 10.1002/ptr.4939.

Moreover, I studied the changes of microbiota composition in rats fed with different diets by using a metagenomic approach (**CHAPTER 4**), to investigate how these variations could affect the physiology of the whole organism. The Western diet, rich in

fat and carbohydrates, has been clearly associated to the development of obesity and diabetes in several industrialized countries. Fructose, an abundant component of the western diet, has been proposed as a major inducer of the metabolic syndrome, a combination of health disorders significantly increasing the risk of developing obesity and diabetes. In addition to being associated to the human health, the diet is known to strongly affect the composition of the gut microbiota. However, it is still not clear whether the alteration of the microbial composition of the gut is a consequence or rather one of the causes of the health disorders due to the diet. We used a rat model of obesity to assess whether the gut microbiota was linked to the development of the fructose-induced metabolic syndrome and showed that an antibiotic treatment as well as a fecal transplant was able to abolish early signs of fructose-induced metabolic syndrome. A metagenomic approach was used to evaluate the bacterial composition of the gut of rats under the various diet regimens. These data point to the reduced bacterial diversity of the gut as one of causative factors of the metabolic syndrome. A manuscript summarizing these results has been just submitted for publication.

Finally, in the **APPENDIX** of the thesis I report an unrelated study about the characterization of a pigmented spore-forming bacterium (*Bacillus pumilus* SF214) able to produce a hydrosoluble orange carotenoid. Although I don't discuss in details this argument here, I published the results of this work in 2013: Manzo N, ***Di Luccia B***, Isticato R, D'Apuzzo E, De Felice M, Ricca E. (2013)**.** *Pigmentation and sporulation are alternative cell fates in Bacillus pumilus SF214***.** PLoS One. 2013 Apr 25;8(4):e62093. Briefly, I observed that in *B. pumilus* SF214 the pigmentation is strictly regulated and high pigment production was observed during the late stationary growth phase in a minimal medium and at growth temperatures lower than the optimum. Only a

subpopulation of stationary phase cells produced the pigment, indicating that the stationary culture contains a heterogeneous cell population and that pigment synthesis is a bimodal phenomenon. The fraction of cells producing the pigment varied in the different growth conditions and occured only in cells not devoted to sporulation. Only some of the pigmented cells were also able to produce a matrix. Pigment and matrix production in SF214 appear then as two developmental fates both alternative to sporulation. Since the pigment has an essential role in the cell resistance to oxidative stress conditions, we propose that within the heterogeneous population different survival strategies can be followed by the different cells.

Backhed F., Ley RE., Sonnenburg JL., Peterson DA., Gordon JI (2005)**.** *Host-Bacterial Mutualism in the Human Intestine*. Science **307**, 1915; DOI: 10.1126/science.1104816.

Fakhry S., Sorrentini I., Ricca E., De Felice M., Baccigalupi L. (2008). *Characterization of spore forming Bacilli isolated from the human gastrointestinal tract*. J Appl Microbiol, 105(6):2178-86

Fakhry S., Manzo N., D'Apuzzo E., Pietrini L., Sorrentini I., Ricca E., De Felice M. and Baccigalupi L. (2009). *Characterization of intestinal bacteria tightly bound to the human ileal epithelium*. Res Microbiol **160**: 817-823

Fujiya M, Musch MW, Nakagawa Y, Hu S, Alverdy J, Kohgo Y, Schneewind O, Jabri B, Chang EB. *The Bacillus subtilis quorum-sensing molecule CSF contributes to intestinal homeostasis via OCTN2, a host cell membrane transporter*. Cell Host Microbe. 2007 Jun 14;1(4):299-308.

Hong HA, Duc Ie H, Cutting SM (2005). *The use of bacterial spore formers as probiotics*. FEMS Microbiol. Rev. 29: 813-835.

Kunst, F., Ogasawara, N., Moszer, I. & 148 other authors (1997). *The complete genome sequence of the Gram-positive bacterium Bacillus subtilis*. Nature 390, 249–256

Lazazzera, B.A., Solomon, J.M., and Grossman, A.D. (1997). *An exported peptide functions intracellularly to contribute to cell density signaling in B. subtilis*. Cell 89, 917–925.

Solomon, J. M., B. A. Lazazzera, and A. D. Grossman. 1996. *Purification and characterization of an extracellular peptide factor that affects two different developmental pathways in Bacillus subtilis*. Genes Dev. **10**:2014–2024.

CHAPTER 1

Lactobacillus gasseri *SF1183 affects intestinal epithelial cell survival and growth*

Blanda Di Luccia[¶1], *Nicola Manzo*[¶1], *Loredana Baccigalupi*[1], *Viola Calabrò*[1], *Elvira Crescenzi*[2], *Ezio Ricca*[1], *Alessandra Pollice**[1]

[1]*Department of Biology, University of Naples Federico II-MSA-Via Cinthia 26-80126 Naples, Italy*

[2]*Istituto di Endocrinologia ed Oncologia Sperimentale-CNR-via S. Pansini, 5- 80131 Naples, Italy.*

Published in July 2013 on *PLoS ONE* 8(7):e69102.

1.1 Abstract

It is now commonly accepted that the intestinal microbiota plays a crucial role in the gut physiology and homeostasis, and that both qualitative and quantitative alterations in the compositions of the gut flora exert profound effects on the host's intestinal cells. In spite of this, the details of the interaction between commensal bacteria and intestinal cells are still largely unknown and only in few cases the molecular mechanisms have been elucidated. Here we analyze the effects of molecules produced and secreted by *Lactobacillus gasseri* SF1183 on human intestinal HCT116 cells. *L. gasseri* is a well known species of lactic acid bacteria, commonly associated to the human intestine and SF1183 is a human strain previously isolated from an ileal biopsy of an healthy volunteer. SF1183 produces and secretes, in a growth phase-dependent way, molecule(s) able to drastically interfere with HCT116 cell proliferation. *L. gasseri* molecule(s) stimulate a G1-phase arrest of the cell cycle by up-regulation of p21WAF1 rendering cells protected from intrinsic and extrinsic apoptosis.

1.2 Introduction

Several recent studies have shown that commensal bacteria, forming the human gut microbiota, establish complex symbiotic interactions with cells of the gastrointestinal tract (GIT) and that these interactions significantly contribute to human health [1,2,3,4]. Metagenomic experiments have indicated that the vast majority of the intestinal bacteria belong to two phyla, the Gram-negative Bacteroidetes and the Gram-positive Firmicutes, including the large class of Clostridia and the lactic acid bacteria [5,6]. However, the composition of the gut microbiota is known to change transiently as a consequence of a variety of factors such as age, diet, enteral infections, pharmacological treatments and immunosuppression [7,8,9]. Changes in the microbiota composition

have also been associated to several diseases, such as chronic inflammation of the Gastro-Intestinal tract (GIT), diabetes and obesity [7,10,11,12,13,14], and the oral administration of members of the microbiota has been considered as a potential clinical tool to relieve intestinal dysfunctions [15,16,17,18,19,20]. Interest in the beneficial functions of the human microbiota has resulted in the selection of specific strains with putative health-promoting capacities that are recognized as probiotics and are generally selected from isolates of the *Lactobacillus* or *Bifidobacterium* species. Probiotic bacteria have been shown capable to modulate systemic inflammation, cell proliferation and apoptosis, and such properties proposed as useful for future immunomodulatory and cancer prevention strategies [13,14,21,22]. *In vitro* studies have reported the anti-proliferative and pro-apoptotic effects of *Lactobacillus* and *Bifidobacterium* spp. in various cancer cell lines [23,24,25,26], while *in vivo* studies have shown the inhibitory activity of probiotics on liver, bladder and colon tumours in animal models [27,28,29,30].

The molecular mechanisms of interaction between intestinal cells and bacteria have been studied in detail only in few cases and often quorum-sensing autoinducers, communication molecules released by bacteria at high densities, have been shown to modulate host responses either directly or through regulation of bacterial genes involved in gut colonization and host signalling [31,32]. An example in this context is the quorum-sensing pentapeptide CSF (Competence and Sporulation Factor) of *Bacillus subtilis* that is taken up by Caco-2 cells via the membrane transporter OCTN2 (organic cation transporter 2) and that contributes to eukaryotic cell homeostasis activating survival pathways (p38 MAP kinase and protein kinase B/ Akt) [33]. In other cases the secreted bacterial effectors have not been identified: still unidentified molecules secreted by *Lactobacillus rhamnosus* GG were shown to prevent cytokine-induced

apoptosis on two different intestinal cell model systems (YAMC-young adult mouse colon; HT29-colon carcinoma) [34]; molecules secreted by *L. reuteri* were shown to potentiate tumour necrosis factor (TNF-α)-induced apoptosis in myeloid leukemia derived cells. In the latter example *L. reuteri* molecules were found to: i) suppress NF-kB activation by inhibiting IkBa degradation; ii) downregulate nuclear factor-kB (NF-kB)-dependent gene products affecting cell proliferation and survival; iii) promote apoptosis by enhancing mitogen-activated protein kinase (MAPK) activities including c-Jun N-terminal kinase and p38 MAPK [35].

Lactobacillus gasseri is a well characterized species of low GC gram-positive bacteria, known to represent one of the major homofermentative *Lactobacillus* of the human intestine [36]. We have isolated the SF1183 strain of *L. gasseri* from an ileal biopsy of a human healthy volunteer and, in particular, from the fraction of bacteria tightly associated to the epithelial cells. SF1183 was shown to have antimicrobial activity against a panel of enteropathogens and to form a matrix (biofilm) in standard laboratory as well as in simulated intestinal conditions [36].

This study investigates the effects of molecules produced and secreted by *L. gasseri* SF1183 on colorectal HCT116 cells, both at the molecular and cellular level. Since HCT116 cells are responsive to TNFα-induced apoptosis [37,38], we tested their response to the presence of *L. gasseri* SF1183 supernatant. Moreover, we extended our analysis to the effects of another inducer of apoptosis to evaluate the specificity of the observed effect.

1.3 Results and Discussion

1.3.1 The conditioned medium (CM) of *L. gasseri* SF1183 protects HCT116 cells from TNFα induced apoptosis. Among the most common features of chronic

intestinal inflammations, such as Crohn and irritable bowel diseases (IBDs), is the increase in the production of inflammatory cytokines, epithelial cell apoptosis and immune cell infiltration, leading to disruption of the intestinal epithelial integrity. TNFα is among the cytokines more largely produced under these conditions. It is known to regulate both anti- and pro-apoptotic signaling pathways and determine the cell fate by controlling the balance between the two pathways [39]. To study the effects of molecules secreted by *L. gasseri* on TNFα-induced apoptosis we used the TNFα sensitive HCT116 human colon cancer cells as a model of intestinal epithelial cells [37]. As a marker of apoptosis we followed the proteolytic cleavage of PARP-1, a regulator of the DNA base excision repair pathway essential for the maintenance of genomic integrity and for survival in response to genotoxic insults [40]. PARP-1 is known to be specifically proteolysed by the Caspase 3 to a 24 kDa DNA-binding domain (DBD) and a 89 kDa catalytic fragment during the execution of the apoptotic program [41]. To set up the experimental conditions, HCT116 cells were incubated with 1 nM TNFα for various times and cell extracts analyzed by western blotting with anti-PARP-1 antibody. As shown in Figure 1A, the amount of proteolyzed PARP-1 increased with the time of exposure to TNFα. Therefore we decided to use 8 hours of treatment with 1 nM TNFα to detect either induction or inhibition of PARP cleavage, for all therein experiments involving a TNF-α activation.

A filter-sterilized conditioned medium (CM) of a *L. gasseri* SF1183 culture was added (20% v/v) to HCT116 cells and incubated for 16 hours. Then, TNFα was added and, after additional 8 hours of incubation, cells were harvested and whole extracts analyzed by western blotting with anti-PARP-1 antibody. As shown in Figure 1B the bacterial CM alone did not have any effect on PARP-1 cleavage while was able to significantly reduce the TNFα-induced proteolytic activation of PARP-1.

L. gasseri is a homofermentative bacterium that, therefore, grows producing lactic acid as the only metabolic end-point of carbohydrate metabolism.

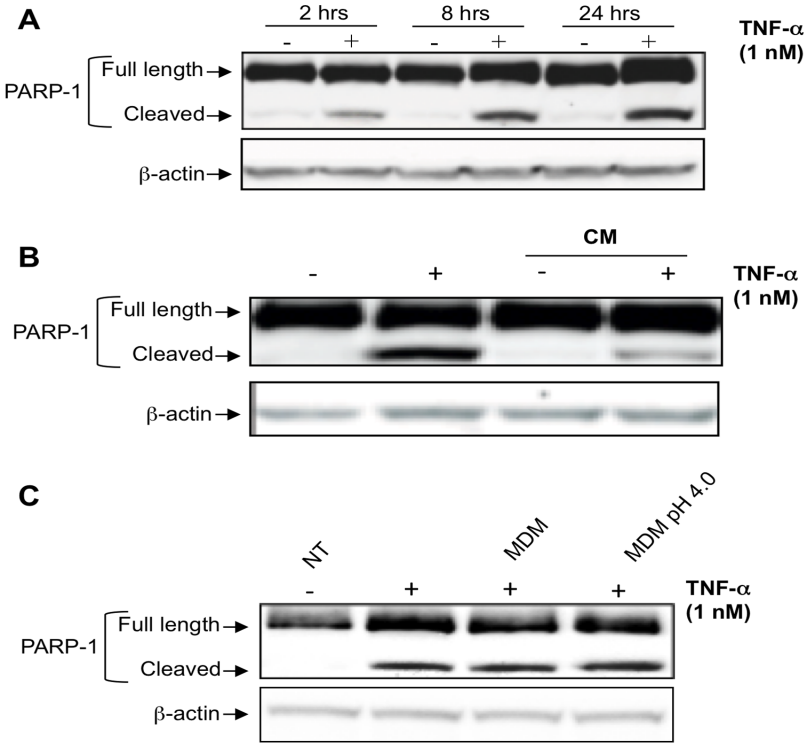

Fig 1. HCT116 cell response to* L. gasseri *CM with or without TNFα treatment. *Western blot with anti-PARP-1 antibody of whole cell extracts from HCT116 cells incubated in (A) complete cell culture medium supplemented or not with TNFα (1 nM) for 2, 8 or 24 hours; (B) complete cell culture medium supplemented or not with CM (20%v/v) for 16 hours before treatment with 1nM TNFα for 8 hours; (C) complete cell culture medium supplemented or not with TNFα (1 nM) for 8 hours and MDM (20%v/v) or MDM + lactic acid pH4 (20%v/v). After the treatments cells were collected, lysed and protein concentration determined. Equal amount of cell lysates were fractionated on SDS-PAGE and analyzed by western blotting with antibodies against PARP-1. Actin was used as a loading control.*

As a consequence, its growth medium is acidified during growth to reach a final pH value of 4.0. To verify that the reduction in the extent of PARP-1 cleavage was due to secreted molecules and not to the acidification of the growth medium, the same experiment of Figure 1B was performed adding to HCT116 cells the same amount (20% v/v) of the fresh bacterial growth medium (MDM) either at its normal pH (pH 7.0) or acidified to pH 4.0 with lactic acid. As shown in Fig. 1C, both media did not have any

effect on TNFα-induced cleavage of PARP-1 suggesting that the CM of *L. gasseri* SF1183 contains molecules with anti-apoptotic activity.

1.3.2 The CM of *L. gasseri* SF1183 contains bioactive soluble molecule(s) secreted during the stationary phase of growth. As a first step toward the characterization of molecule(s) involved in the observed effect, we decided to size-separate the CM of *L. gasseri* by using a 3 kDa molecular mass cut-off filter. As Figure 2A clearly shows we observed bioactivity largely in the filtrate, indicating a small (less than 3 kDa) molecular mass for the effector(s) molecule(s). Further, different enzymatic treatments of the CM indicated that bioactivity is proteinase-K sensitive, suggesting a proteinaceous nature (Figure 2B). Often bacteria secrete bioactive molecules during their stationary phase of growth. We thus tested the CM of *L. gasseri* cultures at different stages of growth and observed bioactivity produced only in early and late stationary phase of growth (24 and 48 hours of growth, respectively) (Figure 2). All experiments therein reported have been performed by using the size-fractionated (< 3 kDa) CM of a late stationary culture of *L. gasseri* SF1183.

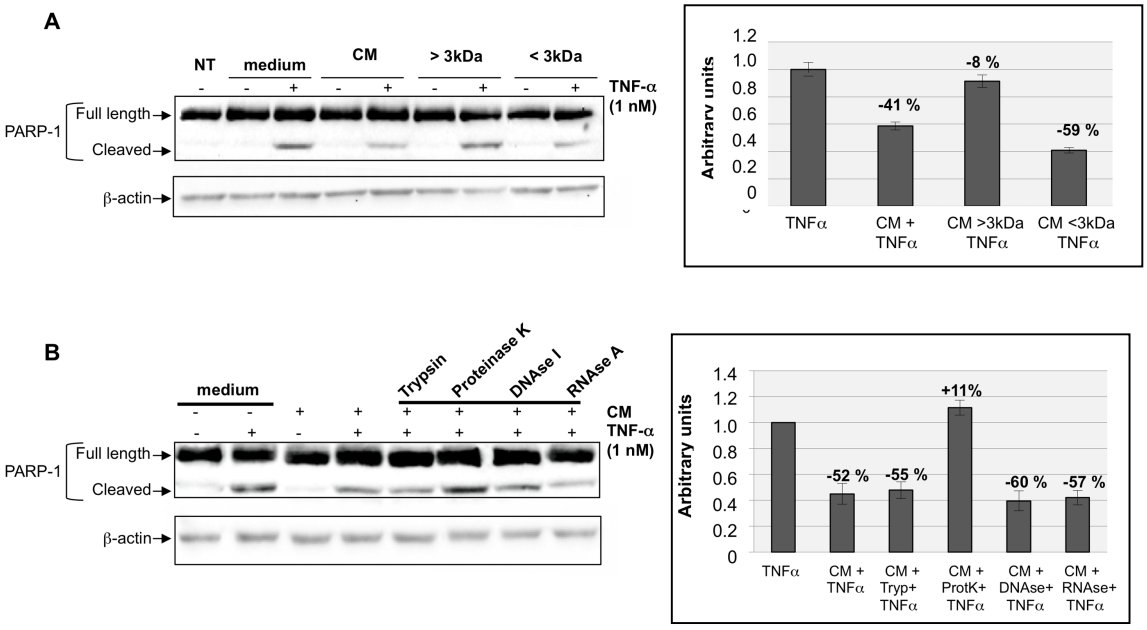

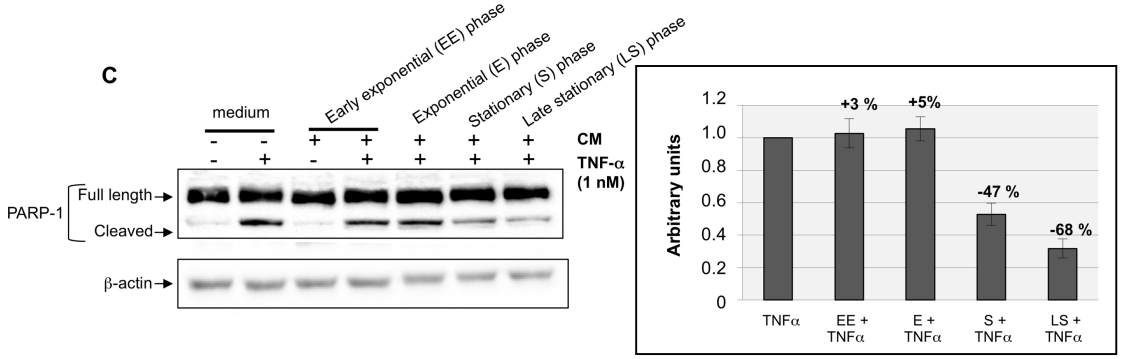

Fig. 2* L. gasseri *secretes bioactive soluble molecule(s) of proteinaceous nature during the stationary phase of growth. *HCT116 cells were incubated in complete cell culture medium supplemented or not with TNFα (1 nM) for 8 hours and with A) CM fractionated with a cut-off of 3 kDa, or B) CM treated with different enzymes [Trypsin, Proteinase K, DNAse I, RNAse A], or C) CM of cultures at the indicated phases of growth. After the treatments, cells were collected, lysed and total cell extracts were analyzed by western blotting with antibodies against PARP-1. Actin was used as a loading control. PARP-1 band intensity was evaluated by ImageQuant analysis on at least two different expositions to assure the linearity of each acquisition. Values expressed as ratio with the corresponding actin values and normalised to the reference point (PARP-1 cleavage in medium). Percentage of increase (+) or decrease (—) with respect to the intensity of the reference point are indicated.*

1.3.3 The CM of *L. gasseri* SF1183 affects cell proliferation of HCT116 cells. To characterize the cellular response to *L. gasseri* secreted molecules, we analyzed HCT116 cell number and viability after growth in presence of CM. Briefly, cells were incubated for 24 hours with CM of *L. gasseri* (20% vol/vol) and then analyzed both for the number of cells by counting in a Burker chamber and for cell viability by MTS assay. As Figure 3A shows, the CM caused a 30% reduction in the number of cells. The MTS assay (Figure 3B) showed a reduction in cell viability of the same order of magnitude.

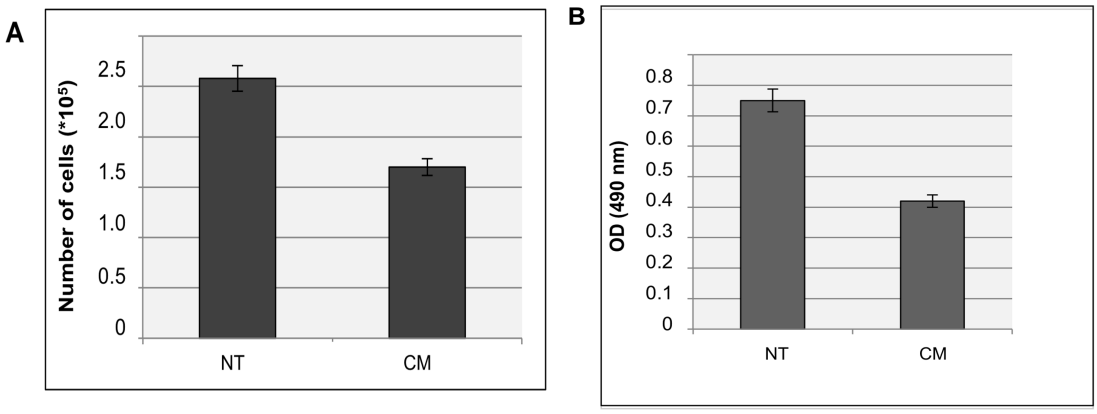

Fig. 3. The CM of* L. gasseri *SF1183 affects HCT116 cell number but not cell viability. *Proliferating HCT116 cells were incubated in complete cell culture medium supplemented or not with CM (20%v/v). After 24 hours (A) controls (NT) and CM-treated (CM) cells were collected and counted in a Burker chamber; or (B) incubated with 3-(4,5-dimethylthiazol-2-yl)-5-(3-carboxymethoxyphenyl)-2-(4-sulfophenyl)-2H-tetrazolium as a substrate and the absorbance of converted formazan measured at 490nm.*

To get more insights into the cellular response, we looked at the cell-cycle distribution profile and at the expression of cell cycle-related molecular markers in HCT116 cells exposed to TNFα and/or to the CM of *L. gasseri*.

The cell cycle distribution was analyzed by flow cytometry and showed that treatment with TNFα causes a drastic increase in the subG1 cell population (from 4 to 28%) while the pre-treatment of cells with the CM of *L. gasseri* strongly reduced the TNFα induced effect (Figure 4A), thus supporting our previous data indicating a reduction in the extent of PARP-1 cleavage (see Figure 1B, 2B, 2C). Importantly, we found that the CM alone caused a significant increase (up to 18%) in the G1 population of cells with a compensatory decrease in S/G2 cells, indicating that cells were unable to resume the cell cycle at normal phase transit rate (Figure 4A), consistently with previous MTS and proliferation data. This suggests that, indeed, molecules secreted from *L. gasseri* can drastically interfere with proliferation of HCT116 cells, rendering them less prone to TNFα induced apoptosis.

Expression of the cell cycle markers p21WAF1 and pERKs was also investigated to explore the effects of the CM of *L. gasseri* at the molecular level. p21WAF1 (also known as cyclin-dependent kinase inhibitor 1) is a regulator of cell cycle progression at the S phase that acts as an inhibitor of cyclin-dependent kinase, and occupies a central position in the regulation of the cell cycle in many tissues [42,43].

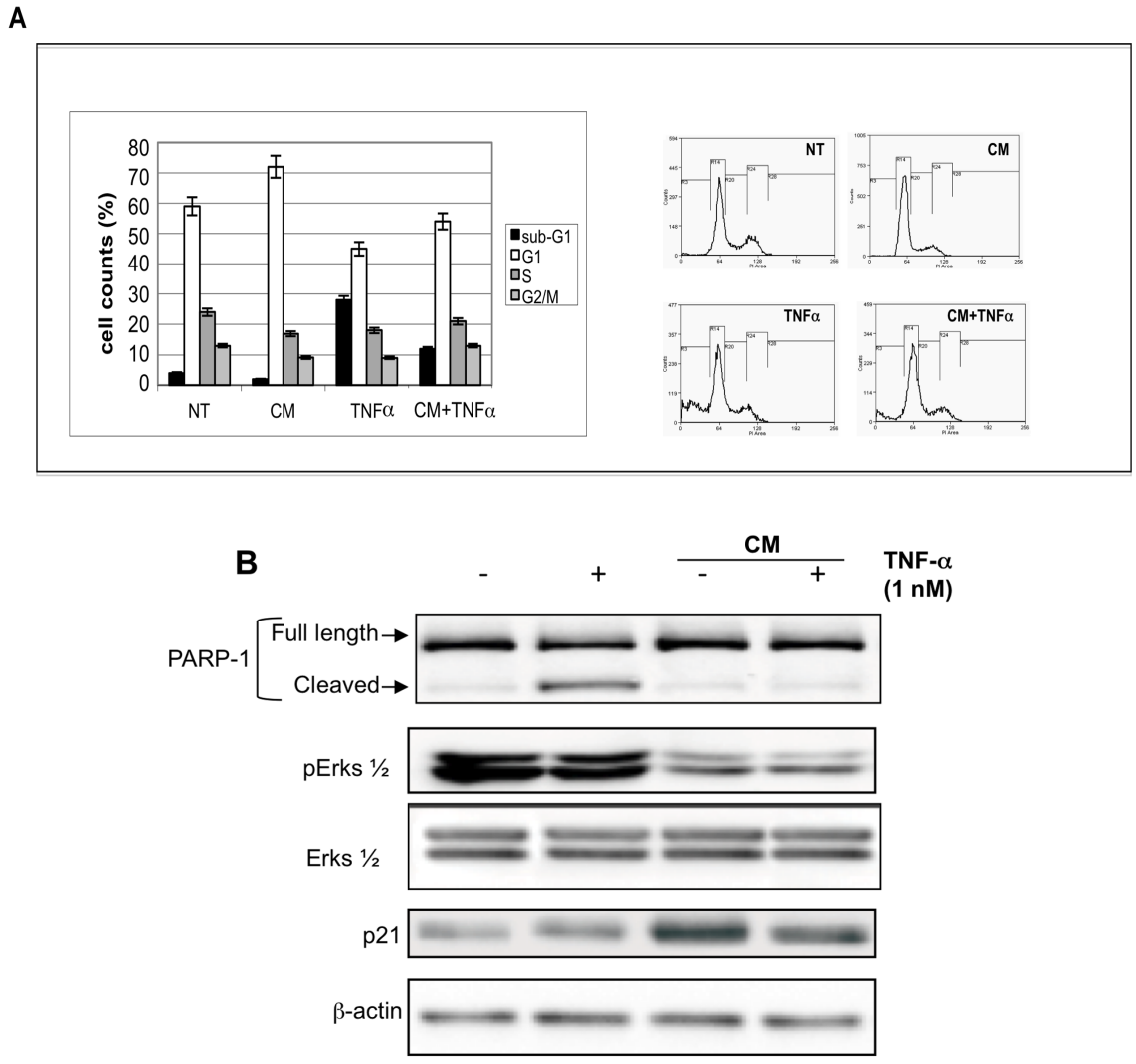

Fig. 4 The CM of* L. gasseri *SF1183 affects cell proliferation of HCT116 cells. *Proliferating HCT116 cells were incubated in complete cell culture medium supplemented or not with CM (20%v/v) and/or TNFα (1nM). After the treatments, cells were collected and treated for flow-cytometric analysis (A) or western blot (B) with the indicated antibodies.*

Levels of p21WAF1 protein are regulated during the cell cycle at the levels of transcription and protein degradation, although many questions remain on the

mechanism of p21 proteolysis [44,45]. ERK1,2 (Extracellular signal-regulated kinases) are members of the mitogen-activated protein kinase (MAPK) super family that can mediate cell proliferation and apoptosis. Activated (phosphorylated) ERKs, are usually associated with active cell proliferation [46], while p21 increase correlates with a G1 cell cycle arrest [47]. Immunoblots with the appropriate antibodies showed that treatment with CM significantly induced p21WAF independently from TNFα (Figure 4B; compare lanes 1-2 with 3-4) while pERKs expression was inhibited in CM treated cells, strongly supporting the antiproliferative effect of molecule(s) present in *L. gasseri* supernatant.

Altogether these experiments clearly indicate that *L. gasseri* supernatant exerts a cytostatic but not a cytotoxic effect on epithelial colon cells.

1.3.4 The CM of *L. gasseri* SF1183 protects HCT116 cells from cisplatin induced apoptosis. To test whether bioactive molecules present in *L. gasseri* supernatant could exert anti-apoptotic effects against other apoptosis-inducers we preincubated HCT116 cells with CM and then treated them with 30 μM cisplatin to induce the intrinsic apoptotic pathway. As shown in Figure 5A cytofluorimetric analysis indicate that a G1 cell cycle arrest is induced by CM addition which causes cells to be more resistant to cisplatin induced apoptosis. These observations are supported, at the molecular level, with an increase in p21WAF1 levels and a decrease of ERKs activation when CM was added to the cells (Figure 5B, lanes 1,2). Consistently, pretreatment of cells with CM determined a reduction in the extent of PARP-1 cleavage when cells were subjected to cisplatin action (Figure 5B, lanes 3,4).

Altogether our results clearly indicate that probiotic *L. gasseri* protects intestinal epithelial cells from apoptosis induced by inflammatory cytokines or cytotoxic drugs, causing cell cycle arrest.

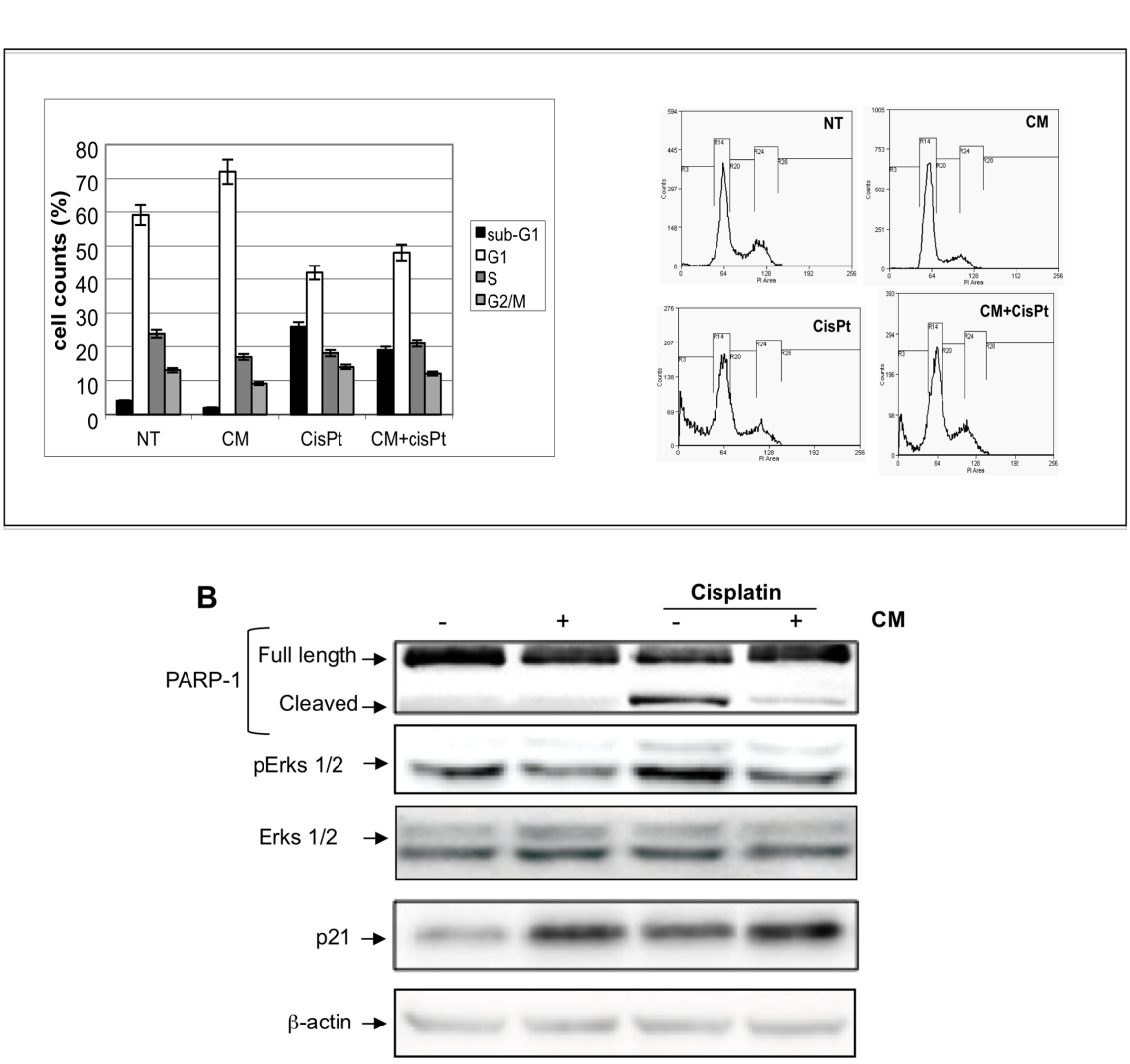

Fig. 5 The anti-apoptotic effect of* L. gasseri *is not specific for TNFα-induced apoptosis. *Proliferating HCT116 cells were incubated in complete cell culture medium supplemented or not with CM (20%v/v) and/or cisplatin (30μM). After the treatments, cells were collected and treated for flow-cytometric analysis (A) or western blot (B) with the indicated antibodies.*

1.4 Conclusions

The main result of this report is that the conditioned medium of a stationary culture of the human isolate SF1183 of *L. gasseri* contains molecule(s) able to affect cell

proliferation of HCT116 cells, protecting them from intrinsic as well as extrinsic, TNFα-induced, apoptosis. Chronic inflammations cause an increase in inflammatory cytokines (such as TNFα), epithelial cell apoptosis and immune cell infiltration, leading to disruption of the intestinal epithelial integrity. Therefore, a reduction of cell proliferation could protect epithelial barrier integrity and help in reconstituting tissutal homeostasis.

The *L. gasseri* molecule(s) responsible of the observed effects is proteinaceous, has a small (less than 3 kDa) size and its synthesis is growth phase-dependent, occuring only in bacterial cells in stationary phase. Those properties are suggestive of bacterial quorum-sensing autoinducers, communication molecules produced at high cell density and known to act as modulator of bacterial host responses [31,32,33]. Unfortunately, the definition of the chemical nature of the molecule(s) secreted by *L. gasseri* SF1183 and able to affect HCT116 cells has been so far unsuccessful. The size-fractionated (less than 3 kDa) CM of *L. gasseri* was analyzed by gel filtration chromatography with a Superdex Peptide 10/300 GL (GE Healthecare Life Sciences) column and two main peaks were obtained (Suppl. Mat Fig. S1). Chromatographic fractions containing either one of the two peaks were tested for the ability to reduce the TNFα-induced cleavage of PARP-1 (Suppl. Mat Fig. S2A). Only one of the fractions (Fraction 1) was shown to reduce the TNFα-induced cleavage of PARP-1 at the same extent of the unfractionated CM (Suppl. Mat Fig. S2B). Unfortunately, attempts to analyze Fraction 1 by mass-spectrometry have been so far unsuccessful, probably because of the minimal concentration of molecules in the fraction. To define the chemical nature of the molecule(s) affecting HCT116 cells and identify its cellular and molecular targets will then be a future and challenging task.

1.5 Materials and Methods

1.5.1 Bacterial growth and preparation of conditioned medium

Lactobacillus gasseri (SF1183) was grown in MRS broth (Difco, Detroit, MI) for 24 hours at 37°C and the culture diluted and used to inoculate MDM (Glucose 10 g/L, Sodium acetate 5g/L, KH_2PO_4 3 g/L, K_2HPO_4 3 g/L, $MgSO_4$ * $7H_2O$ 0.2 g/L, L-Alanine 0.10 g/L, L-Arginine 0.10 g/L, L-Aspartic acid 0.20 g/L, L-Cysteine 0.20 g/L, L-Glutamic 0.20 g/L, L-Histidine 0.10 g/L, L-Isoleucine 0.10 g/L, L-Leucine 0.10 g/L, L-Lysine 0.10 g/L, L-Methionine 0.10 g/L, L-Phenylalanine 0.10 g/L, L-Serine 0.10 g/L,L-Tryptophan 0.10 g/L, L-Tyrosine 0.10 g/L, L-Valine 0.10 g/L, Nicotinic acid 0.001 g/L, Pantothenic acid 0.001 g/L, Pyridoxal 0.002 g/L, Riboflavin 0.001 g/L, Cyanocobalamin 0.001 g/L, Adenine 0.01 g/L, Guanine 0.01 g/L, Uracil 0.01 g/L) minimal medium. Cells of SF1183 were then grown anaerobically for 48 hours at 37°C. The culture was centrifuged (3000 rpm for 10 min at RT) and the supernatant (conditioned medium, CM) was filtered-sterilized through a 0.22 mm low-protein binding filter (Millex; Millipore, Bedford, MA). CM treated with proteases and nucleases was prepared as described above and size fractionated (3-kDa cutoff spin column; Centricon, Millipore). Before treatment with trypsin (GIBCO) or proteinase K (Invitrogen), or DNasi I, or RNasi A (Invitrogen) at a final 100 ug/ml concentration for 60 min at 37°C the pH of CM was neutralized with concentrated NaOH (10 N). After the enzymatic treatments CM was acidified to pH 4.0 using concentrated HCl and fractionated as described above to remove the enzymes.

1.5.2 Cell culture and treatment with bacterial CM

HCT116 cells (ATCC CCL 247) derived from a poorly-differentiated colonic adenocarcinoma and were maintained in RPMI 1640 supplemented with 10% fetal

bovine serum and 1% penicillin-streptomycin. Cells were cultured at 37°C in humidified atmosphere of 5% CO_2. The bacterial CM was employed for the treatment at 20% v/v concentration in complete growth medium. After incubation of 16 hours with CM (20% v/v), TNFα (1 nM, Millipore) or Cisplatin (30 μM, Sigma) was added and cells harvested after 8 hours or 24 hours of treatment. Cells were lysed and cell extracts prepared for Western blot and FACS analysis, respectively, as described below.

1.5.3 SDS-PAGE and Western Immunoblot analysis

Cells were harvested in lysis buffer (50 mM Tris-HCl pH 7.5, 5 mM EDTA, 150 mM NaCl, 1% NP-40, 1 mM phenylmethylsulfonyl fluoride, 0.5% sodium deoxycholate, and protease inhibitors) and total protein extract prepared as previously described [48]. Briefly, cell lysates were incubated on ice for 40 minutes, and the extracts were centrifuged at 13200 rpm for 15 minutes to remove cell debris. Protein concentration was determined by the Bio-Rad protein assay (Bio-Rad). After the addition of 2x Laemmli buffer (SIGMA), samples were boiled at 100°C for 5 minutes and resolved by SDS-polyacrylamide gel electrophoresis (10% or 12%). Proteins were transferred to polyvinylidenedifluoride (PVDF) membranes (Millipore) as previously described [49]. The membranes were blocked in 5% w/v milk buffer (5% w/v non-fat dried milk, 50 mM Tris, 200 mM NaCl, 0,2% Tween 20) and incubated with primary antibody diluted in 5% w/v milk or bovine serum albumine buffer for 2 hours at room temperature or overnight at 4°C. Primary antibodies were anti-rabbit PARP-1 (Cell Signalling), anti-rabbit pErks 42/44 (Cell Signalling), anti-rabbit p21WAF1 (Santa-Cruz Biotechnology), anti-goat β-actin (Santa-Cruz Biotechnology). Data were visualized by enhanced chemiluminescence method (ECL, GE-Healthcare) using HRP-conjugated secondary antibody (Santa-Cruz Biotechnology) incubated 1 hour at room temperature, and

analysed by Quantity One ®software of ChemiDoc ^{TM}XRS system (Bio-Rad).

1.5.4 Cell growth and flow cytometry analysis

HCT116 cells were plated in 35mm dishes at the cell density of 2,5 x 10^5 cells/plate. For cell growth analysis, cells were cultured in complete growth medium supplemented or not with bacterial CM at 20% v/v concentration for 24 hours. After the treatment, cells were collected and counted in a Burker chamber. Flow cytometry analysis was performed as previously described [50]. Briefly, cells were washed twice with PBS and harvested with 0.05% trypsin in 0.15% Na_2EDTA. Cells were then centrifuged, washed in PBS, fixed with ice-cold 70% ethanol, and stored overnight at 4°C. Fixed cells were washed in PBS and then incubated with propidium iodide (50 μg/ml) and RNAse A (10 μg/ml) for 30 min at room temperature. Data acquisition was performed using a CyAn ADP Flow Cytometer (Beckman Coulter, Inc., Milano, Italy) and Summit Software.

1.5.5 MTS assay

HCT116 cells were cultured at a density of 2,5x10^5 cells per well in flat bottomed 6-well plates and supplemented or not with CM (20% v/v) for 24 hours. After treatment, CellTiter 96® AQ_{UEOUS} One Solution Reagent (Promega, Madison, WI) was added to each well according to the manufacturer's instructions. After 30 minutes cell viability was determined by measuring the absorbance at 490nm using a Multiskan spectrum (Thermo Electron Corporation).

1.6 Acknowledgments

We thank Elio Pizzo for helping us with the chromatography experiments and Luciano Di Iorio for technical assistance.

1.7 References

1. Macpherson AJ, Harris NL (2004) Interactions between commensal intestinal bacteria and the immune system. *Nat Rev Immunol* 4: 478-485.
2. Lozupone CA, Stombaugh JI, Gordon JI, Jansson JK, Knight R (2012) Diversity, stability and resilience of the human gut microbiota. *Nature* 13: 489:220-230.
3. Clemente JC, Ursell LK, Parfrey LW, Knight R (2012) The impact of the gut microbiota on human health: an integrative view. *Cell* 148:1258-1270.
4. Kau AL, Ahern PP, Griffin NW, Goodman AL, Gordon JI (2011) Human nutrition, the gut microbiome and the immune system. *Nature* 474:327-336.
5. Eckburg PB, Bik EM, Bernstein CN, Purdom E, Dethlefsen L, et al. (2005) Diversity of the human intestinal microbial flora. *Science* 308:1635-1638.
6. Mahowald MA, Rey FE, Seedorf H, Turnbaugh PJ, Fulton RS, et al. (2009) Characterizing a model human gut microbiota composed of members of its two dominant bacterial phyla. *Proc. Natl. Acad. Sci. USA* 106:5859-5864.
7. Turnbaugh PJ, Hamady M, Yatsunenko T, Cantarel BL, Duncan A et al. (2009) A core gut microbiome in obese and lean twins. *Nature* 457:480-484.
8. De Filippo C, Cavalieri D, Di Paola M, Ramazzotti M, Poullet JB et al. (2010) Impact of diet in shaping gut microbiota revealed by a comparative study in children from Europe and rural Africa. *Proc Natl Acad Sci USA* 107:14691-14696
9. Biagi E, Candela M, Franceschi C, Brigidi P. (2011) The aging gut microbiota: new perspectives. *Ageing Res Rev.* 10:428-439.
10. Wen L, Ley RE, Yu P, Volchkov PY, Stranges PB et al. (2008) Innate immunity and intestinal microbiota in the development of Type 1 diabetes. *Nature* 455:1109-1113.

11. Li M, Wang B, Zhang M, Rantalainen M, Wang S, et al. (2008) Symbiotic gut microbes modulate human metabolic phenotypes. *Proc Natl Acad Sci USA* 105:2117-2122.

12. Zhang H, DiBaise JK, Zuccolo A, Kudrna D, Braidotti M et al. (2009) Human gut microbiota in obesity and after gastric bypass. *Proc Natl Acad Sci USA* 106:2365–2370.

13. O'Mahony L, McCarthy J, Kelly P, Shanahan F, Quigley EM. (2005) *Lactobacillus* and *Bifidobacterium* in irritable bowel syndrome: symptom responses and relationship to cytokine profiles. *Gastroenterol.* 128:541-551.

14. Sokol H, Pigneur B, Watterlot L, Lakhdari O, Bermúdez-Humarán LG et al. (2008) *Faecalibacterium prausnitzii* is an anti-inflammatory commensal bacterium identified by gut microbiota analysis of Crohn disease patients. *Proc Natl Acad Sci USA* 105:16731-16736.

15. Gilliland SE, Nelson CR, Maxwell C (1985) Assimilation of cholesterol by *Lactobacillus acidophilus Appl Environ Microbiol* 49: 377–381.

16. Salminen S, Bouley C, Boutron-Ruault, MC, Cummings JH, Franck A, et al. (1998) Functional food science and gastrointestinal physiology and function. *Br J Nutr* 80: S147–S171.

17. Perdigon G, Fuller R, Raya, R (2001) Lactic acid bacteria and their effect on the immune system. *Curr Issues Intest Microbiol* 2: 27–42.

18. Rafter J (2003) Probiotics and colon cancer. *Best Pract Res Clin Gastroenterol* 17: 849–859.

19. Isolauri E, Salminen S, Ouwehand AC (2004) Microbial–gut interactions in health and disease. *Best Pract Res Clin Gastroenterol* 18: 299–313.

20. Guarner F, Bourdet-Sicard R, Brandtzaeg P, Gill HS, McGuirk P et al. (2006) Mechanisms of disease: the hygiene hypothesis revisited. *Nat Clin Pract Gastroenterol Hepatol* 3: 275–284.
21. Kato I, Endo-Tanaka, K, Yokokura T. (1998) Suppressive effects of the oral administration of Lactobacillus casei on type II collagen-induced arthritis in DBA/1 mice. *Life Sci* 63:635–644.
22. Sheil B, McCarthy J, O'Mahony L, Bennett MW, Ryan P et al. (2004) Is the mucosal route of administration essential for probiotic function ? Subcutaneous administration is associated with attenuation of murine colitis and arthritis. *Gut* 53: 694–700.
23. Fichera GA, Giese G (1994) Non-immunologically mediated cytotoxicity of Lactobacillus casei and its derivative peptidoglycan against tumor cell lines. *Cancer Lett* 85:93–103.
24. Biffi A, Coradini D, Larsen R, Riva L, Di Fronzo G. (1997) Antiproliferative effect of fermented milk on the growth of a human breast cancer cell line. *Nutr Cancer* 28:93–99.
25. Kim JY, Woo, HJ, Kim YS, Lee JH (2002) Screening for antiproliferative effects of cellular components from lactic acid bacteria against human cancer cell lines. *Biotechnol Lett* 24: 1431–1436.
26. Orlando A, Refolo MG, Messa C, Amati L, Lavermicocca P et al. (2012) Antiproliferative and proapoptotic effects of viable or heat-killed *Lactobacillus paracasei* IMPC2.1 and *Lactobacillus rhamnosus* GG in HGC-27 gastric and DLD-1 colon cell lines. *Nutr Cancer* 64:1103-1111.
27. Reddy BS, Rivenson A (1993) Inhibitory effect of *Bifidobacterium longum* on colon, mammary, and liver carcinogenesis induced by 2-amino-3-

methylimidazo[4,5-f]quinoline, a food mutagen. *Cancer Res.* 53:3914–3918.

28. Lim, BK, Mahendran R, Lee YK, Bay BH (2002) Chemopreventive effect of *Lactobacillus rhamnosus* on growth of a subcutaneously implanted bladder cancer cell line in the mouse. *Jpn J Cancer Res* 93:36–41.
29. Candela M, Guidotti M, Fabbri A, Brigidi P, Franceschi C et al. (2011) Human intestinal microbiota: cross-talk with the host and its potential role in colorectal cancer. *Crit Rev Microbiol.* 37:1-14.
30. Matsumoto M, Kurihara S, Kibe R, Ashida H, Benno Y. (2011) Longevity in mice is promoted by probiotic-induced suppression of colonic senescence dependent on upregulation of gut bacterial polyamine production. *PLoS One* 6:e23652.
31. Sperandio V, Torres AG, Kaper JB (2002) Quorum sensing *Escherichia coli* regulators B and C (QseBC): a novel two-component regulatory system involved in the regulation of flagella and motility by quorum sensing in *E. coli. Mol. Microbiol.* 43:809, 2002.
32. Merritt J, Qi F, Goodman SD, Anderson MH, Shi W (2003) Mutation in luxS affects biofilm formation in *Streptococcus mutans*. *Infect Immun* 71:1972-1979.
33. Fujiya M, Musch MW, Nakagawa Y, Hu S, Alverdy J et al. (2007) The *Bacillus subtilis* Quorum-Sensing Molecule CSF Contributes to Intestinal Homeostasis via OCTN2, a Host Cell Membrane Transporter. *Cell Host & Microbe* 1:299–308.
34. Yan F, Polk DB (2002) Probiotic Bacterium Prevents Cytokine-induced Apoptosis in Intestinal Epithelial Cells. *J Biol Chem.* 277:50959-50965.
35. Iyer C, Kosters A, Sethi G, Kunnumakkara AB, Aggarwal BB et al (2008) Probiotic *Lactobacillus reuteri* promotes TNF-induced apoptosis in human myeloid leukemia-derived cells by modulation of NF-**k**B and MAPK signalling. *Cellular Microbiology* 10:1442–1452

36. Fakhry S, Manzo N, D'Apuzzo E, Pietrini L, Sorrentini, I, et al. (2009).Characterization of intestinal bacteria tightly bound to the human ileal epithelium. *Res. Microbiol.* 160:817-823
37. Zwacka M R, Stark L, Dunlop MG (2000) NF-kB kinetics predetermine TNFalpha sensitivity of colorectal cancer cells. *J Gene Med* 2:334-343.
38. Roemer M M, Roemer K (2001) p21 Waf1/Cip1 can protect human colon carcinoma cells against p53-dependent and p53-independent apoptosis induced by natural chemopreventive and therapeutic agents. *Oncogene* 20:3387-3398.
39. Yan F, John SK and Polk DB (2001) Kinase suppressor of Ras determines survival of intestinal epithelial cells exposed to tumor necrosis factor *Cancer Res* 61:8668-8675.
40. D'Amours D, Sallmann FR, Vishva MD, Poiriers GG (2001) Gain-of-function of poly(ADP-ribose) polymerase-1 upon cleavage by apoptotic proteases: implications for apoptosis. *J Cell Sci* 114:3771-3778
41. Kaufmann, SH, Desnoyers S, Ottaviano Y, Davidson NE, Poirier GG (1993) Specific proteolytic cleavage of poly(ADP-ribose) polymerase: an early marker of chemotherapy-induced apoptosis. *Cancer Res*. 53:3976-3985.
42. Sherr, CJ, Roberts JM (1999) CDK inhibitors positive and negative regulators of G1-phase progression. *Genes Dev.* 13:1501–1512.
43. Weinberg WC, Denning MF (2002) p21Waf1 control of epithelial cell cycle and cell fate. *Crit Rev Oral Biol Med.* 13:453-464.
44. Bloom J, Amador V, Bartolini F, DeMartino G, Pagano M (2003) Proteasome-Mediated Degradation of p21 via N-Terminal Ubiquitinylation *Cell* 115:71–82.
45. Pollice A, Vivo M, La Mantia G (2008) The promiscuity of ARF interactions with the proteasome. *FEBS Letters* 582:3257–3262.

46. McCubrey JA, Steelman LS, Chappell WH et al (2007) Roles of the Raf/MEK/ERK pathway in cell growth, malignant transformation and drug resistance. *Biochim. Biophys. Acta* 1773:1263–1284

47. El-Deiry WS, Tokino T, Velculescu VE, Levy DB, Parsons R et al. (1993) WAF1, a potential mediator of p53 tumor suppression. *Cell* 75:817-825.

48. Vivo M, Di Costanzo A, Fortugno P, Pollice A, Calabrò V et al. (2009) Downregulation of ΔNp63α in keratinocytes by p14ARF-mediated SUMo-conjugation and degradation. *Cell Cycle* 8:3545-3551.

49. Vivo M, Ranieri M, Sansone F, Santoriello C, Calogero RA et al (2013) Mimicking p14ARF Phosphorylation Influences Its Ability to Restrain Cell Proliferation. *PLoS One* 8:e53631.

50. Di Luccia B, Manzo N, Vivo M, Galano E, Amoresano A et al. (2013) A Biochemical and Cellular Approach to Explore the Antiproliferative and Prodifferentiative Activity of *Aloe Arborescens* Leaf Extract. *Phytother Res*. doi: 10.1002/ptr.4939.

1.8 Supporting Information

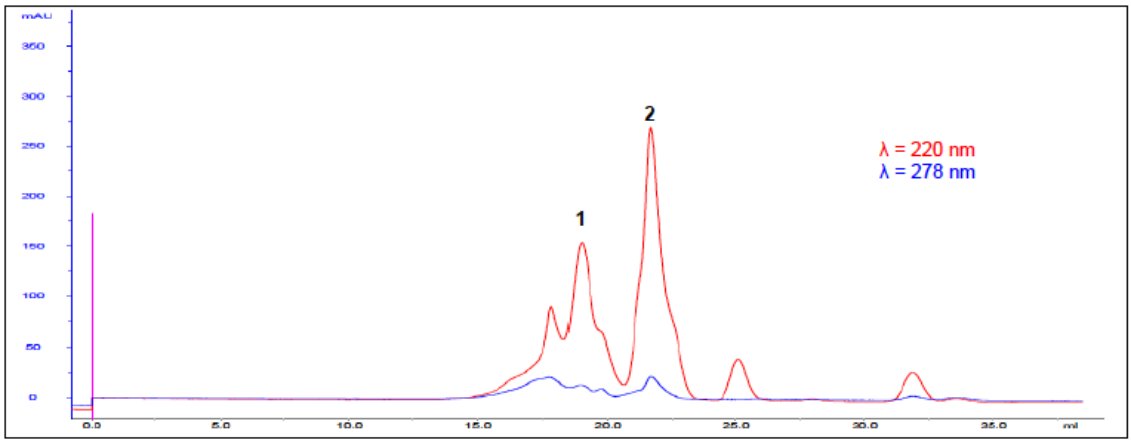

Fig. S1. *The CM of* L. gasseri *was size fractionated with a 3 kDa molecular mass cut-off filter and loaded on a gel filtration chromatographic column (Superdex Peptide 10/300 GL, GE Healthecare Life Sciences). The elution buffer was AMAC 0.3 M. Two main peaks were observed at 220 nm.*

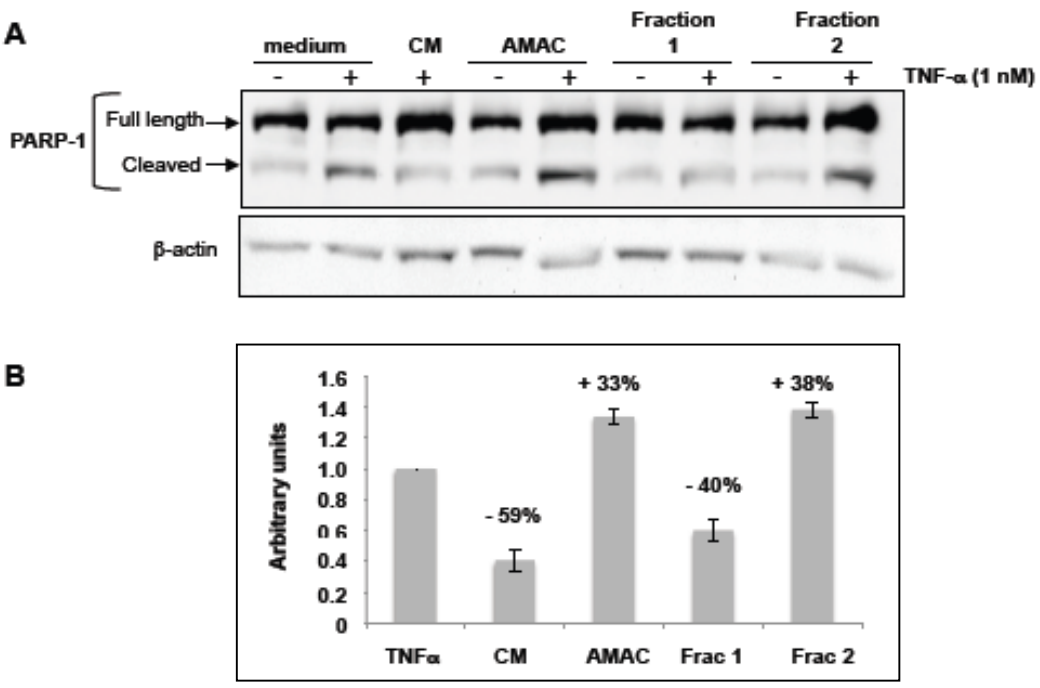

Fig. S2. *Chromatographic fractions from the experiment of Fig. S1 were tested by western blotting with anti-PARP-1 antibody (A). As a control, cells were also treated with the elution buffer (AMAC 0,3 M). (B) Densitometric analysis of the western blot. PARP-1 band intensity was evaluated by ImageQuant analysis on at least two different expositions to assure the linearity of each acquisition. Values are expressed as ratio with the corresponding actin values and normalised to the reference point (PARP-1 cleavage in medium). Percentage of increase (+) or decrease (—) with respect to the intensity of the reference point are indicated.*

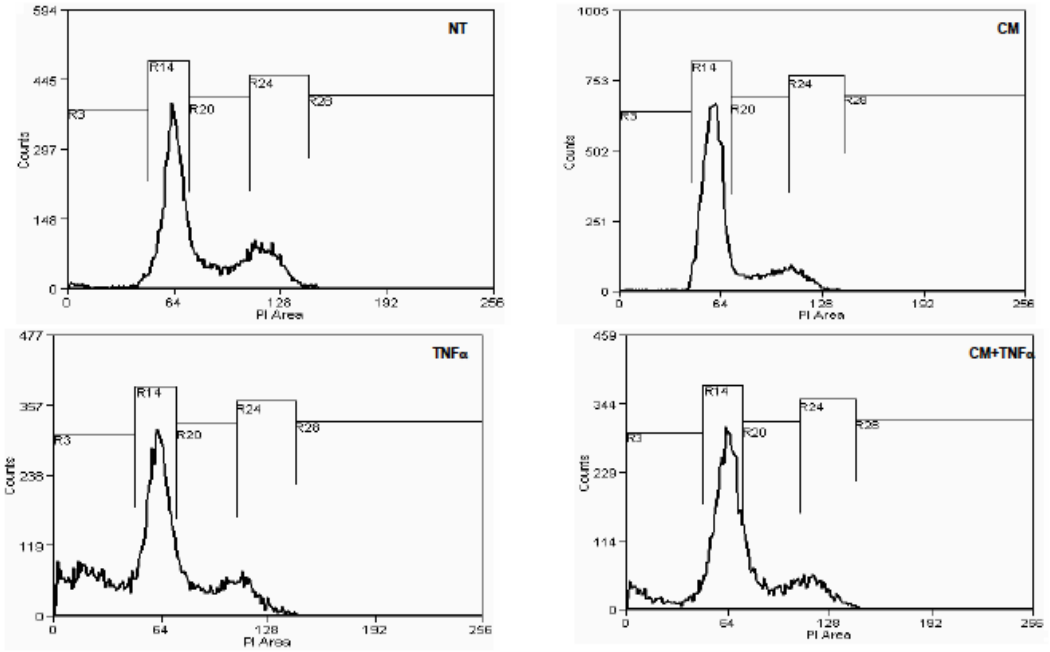

Fig. S3. Enlargment of part of Fig. 4 showing the output of the FACS analysis.

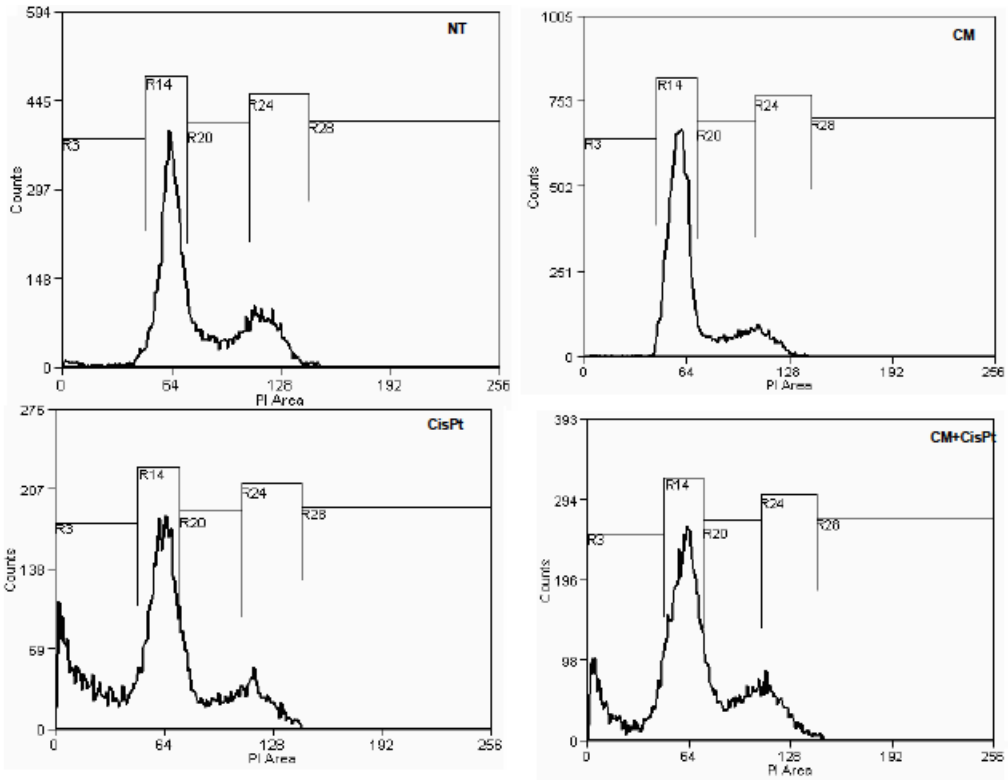

Fig. S4. Enlargment of part of Fig. 5 showing the output of the FACS analysis.

CHAPTER 2

Intestinal isolates of **Bacillus subtilis** *produce molecules able to interact with intestinal epithelial cells*

manuscript in preparation

2.1 Abstract

Bacteria use *quorum-sensing* molecules to communicate within and across species. In this regulatory system an inducing molecule is secreted during growth, accumulates outside the cell and is then sensed by the producing organism, as well as by other cells that respond to the signal expressing specific sets of genes. *Quorum-sensing* molecules are also recognized by eukaryotic cells and examples are: i) a molecule produced by *Pseudomonas aeruginosa* shown to activate the p38 mitogen-activated protein kinase and phosphorilate the eukaryotic translation initiation factor eIF2a in macrophages and bronchial epithelial cells and ii) the *Bacillus subtilis* pentapeptide, known as CSF (competence and sporulation factor) shown to induce cytoprotective heat shock proteins (HSPs) and prevent oxidant-induced intestinal epithelial cell injury. We developed a genetic system to evaluate the presence of CSF in bacterial conditioned growth media and used it to screen a collection of intestinal isolates of *B. subtilis*. Most isolates produced high amounts of CSF and some of them were able to do that also in anaerobic growth conditions. The conditioned medium of all CSF-producing strains was able to induce Hsp27 while only one strain not producing CSF was still able to induce Hsp27. A proteomic approach was used to investigate the molecular mechanisms underlying this induced-cytoprotective effect. Total protein extracts of HT29 cells treated and not-treated with CSF were analysed by 2D-PAGE-MS/MS to identify proteins up- or down-regulated in the treated sample.

2.2 Introduction

The gastrointestinal tract (GIT) is the site of the largest and most complex environment in the mammalian host. In the adult human, the total microbial population (ca. 10^14 cells) is estimated to exceed the total number of mammalian cells by at least an order of

magnitude (Berg RD, 1996). The GIT features several diverse "macro" environments, including the oral cavity, the stomach, the small intestine (including the three major regions, the duodenum, jejunum, and ileum), and the large intestine (colon). The density of bacteria along the GI tract can vary greatly, from 10^3/ml near the gastric outlet to 10^10/ml at the ileo-cecal valve to 10^11 to 10^12/ml in the colon (Borrellio SP, 2002). Within these "macro" environments are several "micro" environments where bacteria can live, such as the lumen of the bowel, the mucus layer overlying the epithelium, mucus within intestinal crypts, and the surface of mucosal epithelial cells. Given the enormous number and diversity of bacteria that comprise the GI environment, it would not be surprising if the members of this community were to somehow communicate among themselves to coordinate various processes ranging from maintenance of the commensal population to aiding or resisting infectious diseases (Kaper JB and Sperandio V, 2005). Over the last decade an important paradigm shift has been our changing perspective of bacteria as unicellular and non-co-operative to socially interactive and capable of multicellular behavior. Bacteria are clearly capable of complex patterns of co-operative behavior that result from the coordination of the activities of individual cells. This is primarily achieved through the deployment of small diffusible signal molecules (sometimes called 'pheromones' or 'autoinducers') which are generally considered to facilitate the regulation of gene expression as a function of cell population density. This phenomenon is termed '*quorum sensing*' (QS). As the bacterial population density increases, so does the synthesis of QS signal molecules and consequently, their concentration in the external environment rises. Once a threshold concentration has been attained, activation of a signal transduction cascade leads to the induction or repression of QS target genes, often incorporating those required for QS signal molecule synthesis, so providing an auto-regulatory mechanism for amplifying

signal molecule production. Consequently, the size of the 'quorum' is not fixed but will depend on the relative rates of production and loss of the signal molecule, which will, in turn, vary depending on the local environmental conditions (Williams P, 2007). In general QS systems facilitate the coordination of population behavior to enhance access to nutrients or specific environmental niches, collective defense against other competitor organisms or community escape where survival of the population is threatened. Although QS has primarily been studied in the context of single species, the expression of QS systems may be manipulated by the activities of other bacteria within complex microbial consortia which employ different QS signals and by higher organisms.

Three major QS circuits have been described: one is used primarily by gram-negative bacteria, one is used primarily by gram-positive bacteria, and one has been proposed to be a hybrid system. The gram-negative QS system involves the use of acyl homoserine lactones (AHLs) as autoinducers, which then bind to response regulators that affect gene expression. The gram positive bacteria use oligopeptide autoinducers that are detected by two-component systems. The third QS system is proposed to be a hybrid system because it is characterized by autoinducers very similar to ones used by gram-negative, but these molecules activate a signal cascades in target cells that is generally found in gram-positive. Moreover, QS signal molecules can also be subdivided according to whether they interact with receptors at the cell surface (e.g. the staphylococcal AIPs) or are internalized (e.g. the AHLs, AQs, the Phr peptides of *Bacillus subtilis* and the mating pheromones of *Enterococcus faecalis*).

In a typical gram-negative bacterial quorum-sensing circuit the autoinducer is an acylated homoserine lactone (AHL) synthesized by a LuxI-type enzyme. Cytoplasmically synthesized autoinducer diffuses passively through the bacterial

membrane and accumulates both intra- and extracellularly in proportion to cell density. When the stimulatory concentration of the AHL is achieved, a LuxR-type protein binds it. LuxR-AHL complexes bind to promoters of quorum sensing-regulated target genes and activate transcription. Over 50 species of gram- negative bacteria produce AHLs that differ only in the acyl side chain moiety, and each LuxR-type protein is highly selective for its cognate AHL signal molecule. Additional complexity exists in many of these circuits, such as the use of multiple AHL autoinducers and LuxR proteins that can act either in parallel or in series.

In the quorum sensing circuit of a gram-positive bacterium the autoinducers are short, usually modified peptides processed from precursors. The signals are actively exported out of the cell, and they interact with the external domains of membrane bound sensor proteins. Signal transduction occurs by a phosphorylation cascade that culminates in the activation of a DNA binding protein that controls transcription of target genes. Specificity exists because each sensor protein is highly selective for a given peptide signal. Similar to gram-negative bacteria, gram-positive bacteria can use multiple autoinducers and sensors. Some peptide autoinducers act exclusively from the outside, while others elicit a specific set of gene expression changes from the outside and are also transported back into the cell where they trigger a different set of behavioral changes.

The third model system is studied in gram-negative bacterium *Vibrio harveyi*. This quorum sensing circuit controls bioluminescence. *V. harveyi* produces two autoinducers termed HAI-1 and AI-2. HAI-1 is a typical gram-negative-like AHL and the second autoinducer, AI-2, is unexpectedly a furanosyl borate diester. HAI-1 and AI-2 signal transduction occurs via a gram-positive-like phosphorylation cascade (Bassler BL, 2002).

While the quorum sensing systems involved in bacterial communication are well-know, the mechanism(s) by which different bacteria (pathogens and/or probiotics) exert their effects in a cross-kingdom quorum-sensing system is not clearly understood. As well as promoting pathogen success, certain QS signal molecules exert beneficial effects on the host. Although the mechanism(s) used by probiotic bacteria, such as certain bacilli and lactobacilli, to exert protective effects in the gastro-intestinal tract is not clear, it is likely to involve pathogen control or exclusion as well as protection of host tissues against inflammatory responses. Interestingly, among probiotics it's known that the *Bacillus subtilis* strain has a protective effect on the host that involves a pentapeptide QS signal molecule, the competence and sporulating factor, CSF (also called PhrC).

In *Bacillus subtilis*, sporulation and the development of genetic competence (the natural ability to import exogenous DNA) are stimulated as cells grow to high cell density. As with other gram-positive bacteria, cell density control in *B. subtilis* is mediated by extracellular peptides (Lazzazzera BA and Grossmann AD, 1998). The development of genetic competence is stimulated by two peptide factors, ComX pheromone, a modified 10-aminoacid peptide (Magnuson R., el al. 1994), and the competence and sporulation factor (CSF), an unmodified five-aminoacid peptide (Solomon JM, et al. 1996). ComX pheromone and CSF stimulate transcription of the *srfA* operon which encodes a small protein ComS required for competence development (D'Souza C., et al. 1994), and the surfactin biosynthetic enzymes (Nakano MM, et al. 1991). Transcription from the *srfA* promoter is activated by the phosphorylated form of the response regulator ComA (Nakano MM and Zuber P., 1991), and activity of ComA is controlled by a kinase, ComP, and a phosphatase, RapC. ComP, a membrane-bound histidine protein kinase, is required for activation of ComA while RapC, a putative aspartyl-phosphate phosphatase, inhibits activation of ComA. ComX pheromone, whose active form

production needs ComQ, stimulates gene expression, apparently by stimulating the kinase ComP, whereas CSF stimulates gene expression, apparently by inhibiting the phosphatase RapC. ComX pheromone most likely works at the cell surface, and CSF is actively transported into the cell by the oligopeptide permease Opp (also known as Spo0K), where it interacts with intracellular receptors. Furthermore, σ^H, the spo0H gene product, activates transcription of *phrC*. Transcription of *phrC* was found to be controlled by two promoters: P1, which precedes *rapC*, the gene upstream of *phrC*; and P2, which directs transcription of *phrC* only. Both RapC and CSF were found to be part of autoregulatory loops that affect transcription from P1, which is activated by ComA~P. RapC negatively regulates its own expression, presumably due to its ability to inhibit accumulation of ComA~P. CSF positively regulates its own expression, presumably due to its ability to inhibit RapC activity. Transcription from P2, which is controlled by the alternate sigma factor σ^H, increased as cells entered stationary phase, contributing to the increase in extracellular CSF at this time. In addition to controlling transcription of *phrC*, σ^H appears to control expression of at least one other gene required for production of CSF.

CSF has a remarkable constellation of activities for a five amino- acid peptide. At relatively low extracellular concentrations (1 to 5 nM), CSF stimulates expression of *srfA* by inhibiting the phosphatase RapC. However, high concentrations of CSF (> 20 nM) inhibit expression of *srfA*, perhaps by inhibiting activity of the kinase ComP. In addition to its effects on expression of ComA~P-controlled genes, high concentrations of CSF (>20 nM) can stimulate sporulation under some conditions (Lazzazera BA., et al. 1997). CSF appears to stimulate sporulation, at least in part, by inhibiting the activity of the phosphatase RapB, an aspartyl-phosphate phosphatase that dephosphorylates Spo0F~P, an essential component of the phosphorelay that controls sporulation.

Production of mature CSF involves several steps, starting with transcription and translation of *phrC*, the gene encoding the precursor of CSF. The 40-amino-acid primary product of *phrC* has a signal sequence and putative peptidase cleavage sites, indicating that a 11- to 25-amino-acid peptide is exported via a Sec-dependent pathway. Pre-CSF is then processed to the mature five-amino-acid form. It seems likely that there is a specific peptidase that recognizes and cleaves pre-CSF. Such a peptidase would be a good candidate for a σ^H -controlled gene product required for CSF production. (Lazzazzera BA., et al 1999).

Interestingly, in a cross-kingdom *quorum-sensing* system CSF induces the expression of heat-shock-inducible protein 27 (Hsp27) in the human colonic epithelial cell line Caco2 and in ligated mouse intestinal loops (Fujiya et al., 2007). Hsps confer protection against a wide variety of stresses and, when overexpressed, can protect intestinal epithelial cells from oxidative injury and so contribute to the maintenance of intestinal homeostasis. Intestinal epithelia express many heat shock proteins, including inducible Hsp27(human)/Hsp25(murine) and Hsp70 and constitutively expressed heat shock cognate Hsc70. The nomenclature, Hsp27 and Hsp25, defines the related small heat shock proteins of approximate molecular weight of 27 kDa and 25 kDa of human and murine cells, respectively (Morimoto, 1993 and Morimoto, 2002). Physiological expression of inducible heat shock proteins like Hsp27/25 and Hsp70 is maintained by microbial-derived molecules, including pattern recognition ligands (Rakoff-Nahoum et al., 2004), accounting for their predominant expression in surface colonocytes.

In this contest, the biological activity of CSF is within the concentration range required for QS in *B. subtilis* (10–100 nM), an important consideration given that some of observed activities of QS molecules on mammalian cells are only apparent at high, non-physiological concentrations (Pritchard, 2006). Fujiya et al. (2007) also identified a

mammalian apical membrane oligopeptide transporter (OCTN2) which is required for CSF uptake. CSF and OCTN2-mediated CSF transport are both required to protect Caco2 cells against oxidant- mediated injury and loss of epithelial barrier function.

Here, we investigated about the efficiency of *B. subtilis spp*. isolated from ileum of healthy-human volunteers, to produce and secrete CSF and thus, to induce Hsp27 in human intestinal epithelial cell line HT29. Moreover, we used a proteomic approach to identify other CSF targets.

2.3 Results

2.3.1 CSF-production by intestinal isolates of *Bacillus subtilis*

The conditioned medium (CM) of various intestinal isolates of *Bacillus subtilis* (Fakhry S., et al. 2008) was analyzed to detect the presence of CSF. As an assay we followed the production of beta-galactosidase activity of an engineerized strain of *B. subtilis* carrying the CSF-inducible promoter *sfrA* fused to *lacZ* in a *comQ-phrC* null background. In this strain CSF is not produced and the β-gal activity can be induced by exogenous CSF. In Fig. 1, it's shown that all the intestinal isolates, but two (SF185, SF155) were able to produce and secrete the bioactive pentapeptide. Five strains (SFB2, SF106, SF195, SF151, SF154) produced higher CSF amounts and three strains (SF128, SF152 and SF153) lower CSF amounts than the laboratory strain PY79 (Fig. 1). The same assay was also performed to evaluate if these isolates were able to produce the CSF in anaerobic condition of growth. Strains SFB2, SF106, SF151, SF152, SF154 and SF195 were able to grow anaerobically and produce CSF (not shown).

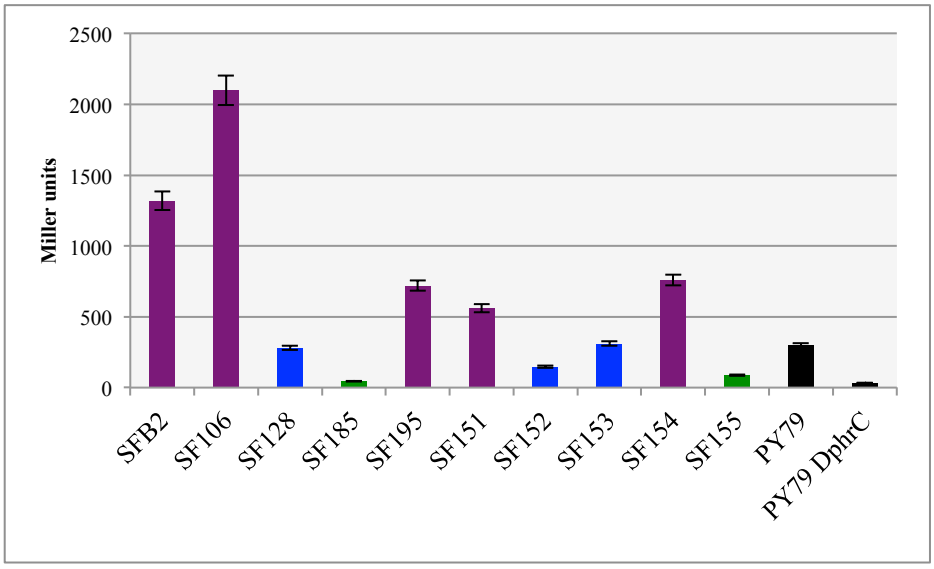

Fig. 1. Beta-galactosidase production in response to aerobically produced CSF. *β-galactosidase activity (Miller units) induced by cell-free supernatants of the various strains to the recipient strain (*srfA::lacZ comQ phrC*). Black bars correspond to the laboratory strain PY79 (positive control) and the isogenic mutant PY79* ΔphrC *(negative control). Purple bars indicate the intestinal isolates producing much more CSF than the laboratory strain PY79; blue bars indicate the intestinal isolates producing less CSF than the laboratory strain PY79; green bars indicate the intestinal isolates that do not produce CSF.*

2.3.2 CSF- induction of heat shock protein 27 (hsp27) by isolates of *Bacillus subtilis* in HT29 intestinal epithelial cells.

The conditioned medium of all strains used for the experiment of Fig. 1 was also tested for the ability to induce heat shock in human colon adenocarcinoma HT29 cells. It's well-known that CSF, produced by *Bacillus subtilis* laboratory strain, is able to induce Hsp27 in $Caco2_{bbe}$ intestinal epithelial cells, in a dose-dependent fashion and that it's transported into mammalian intestinal epithelia through a cell membrane transporter isotype 2 (OCTN2) (Fujiya et al., 2007). Firstly, we observed the same induction of hsp27 in HT29 intestinal cell line by adding to the colture PY79 CM and the synthetic CSF peptide (ERGMT) as shown in Fig 2A. The isogenic mutant PY79 *ΔphrC* is not able to produce CSF and so its CM does not induce Hsp27. As expected all CMs positive to the test of Fig. 1 were also able to induce Hsp27 to levels similar to those observed with PY79 and after heat shock (Fig. 2B).

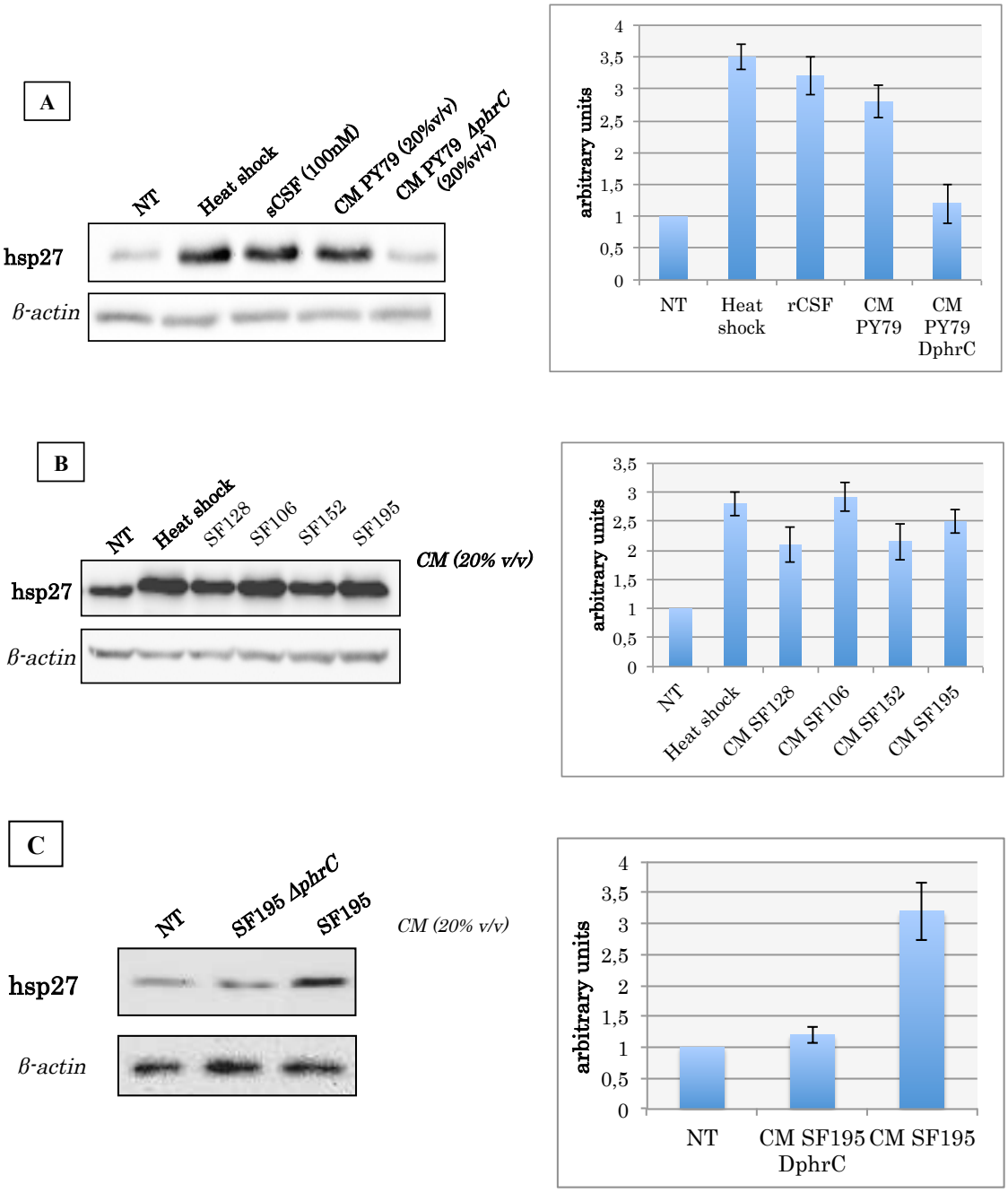

Fig.2 Heat shock protein 27 (Hsp27) induction in HT29 intestinal epithelial cells. *(A) Conditioned-medium (20% v/v) of laboratory strain of* Bacillus subtilis *(PY79) induces Hsp27 in HT29 intestinal epithelial cells as well as the syntethic CSF (100 nM) and the heat-shocked control sample (30min at 45°C). (B) All intestinal isolates of Bacillus subtilis, positive to β-galactosidase assay, are able to induce Hsp27 in HT29 cells. (C) The supernatants of isogenic* ComQ-phrC *null mutant strains lost their biological activity, as expected. After the treatments cells were collected, lysed and protein concentration determined. Equal amount of cell lysates were fractionated on SDS-PAGE and analyzed by western blotting with antibodies against Hsp27. Actin was used as a loading control.*

To verify that HSP induction was due to CSF we obtained by chromosomal DNA mediated transformation *phrC* null mutants of the intestinal strains and tested them for HSP induction (Fig. 2C).

2.3.3 Analysis of *phrC* gene in SF185 strain and preliminary characterization of active molecule secreted inducing Hsp27 in HT29 cells.

SF155 and SF185 are intestinal isolates of *B. subtilis* unable to produce CSF (Fig. 1). However, when tested for HSP induction, only SF185 was able to induce Hsp27 in HT29 (Fig. 3). To rule out the possibility that SF185 produces CSF at very low levels, too low to activate *srfA::lacZ* (Fig. 1) but enough to induce HSP (Fig. 3) we analyzed the strain for the presence and expression of CSF.

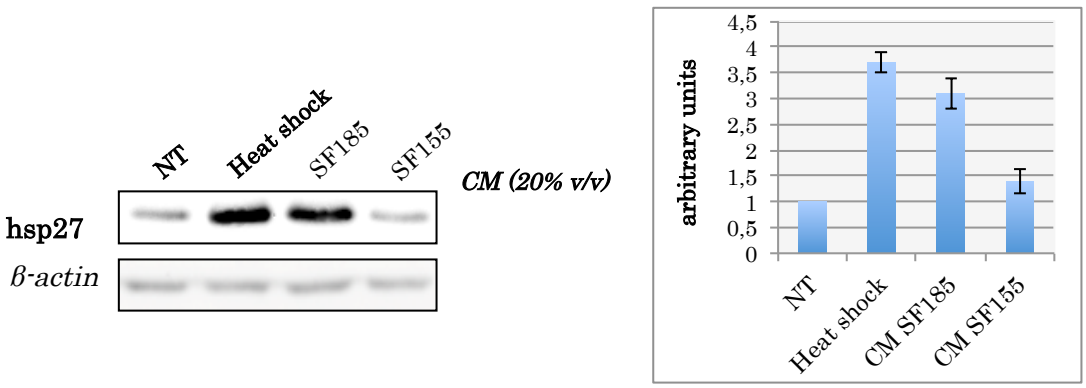

Fig.3 SF185 and SF155 strains not-producing CSF are tested for hsp27 induction in intestinal epithelial cells (HT29)*. The panel clearly shows the induction hsp27 after stimulation of HT29 cells with conditioned media of SF185 and SF155 strains. After the treatments cells were collected, lysed and protein concentration determined. Equal amount of cell lysates were fractionated on SDS-PAGE and analyzed by western blotting with antibodies against hsp27. Actin was used as a loading control.*

A PCR analysis showed that both SF155 and SF185 have a copy of *phrC* gene in their genome (Fig. 4A) while a semi-quantitative RT-PCR analysis showed that *phrC* of both strains is not expressed (Fig. 4B). However, this result does not totally exclude the possibility that *phrC* is weakly transcribed (below the RT-PCR resolution limit). Therefore, we moved by chromosomal DNA mediated transformation the *phrC*-null

carried by the laboratory collection strain into SF185. CM of the resulting strain was still able to induce Hsp27 in HT29 cells (Fig. 4C). Results of Fig. 4A-B-C then indicate that a molecule other than CSF is produced and secreted by SF185 and is able to induce HSP in HT29 cells.

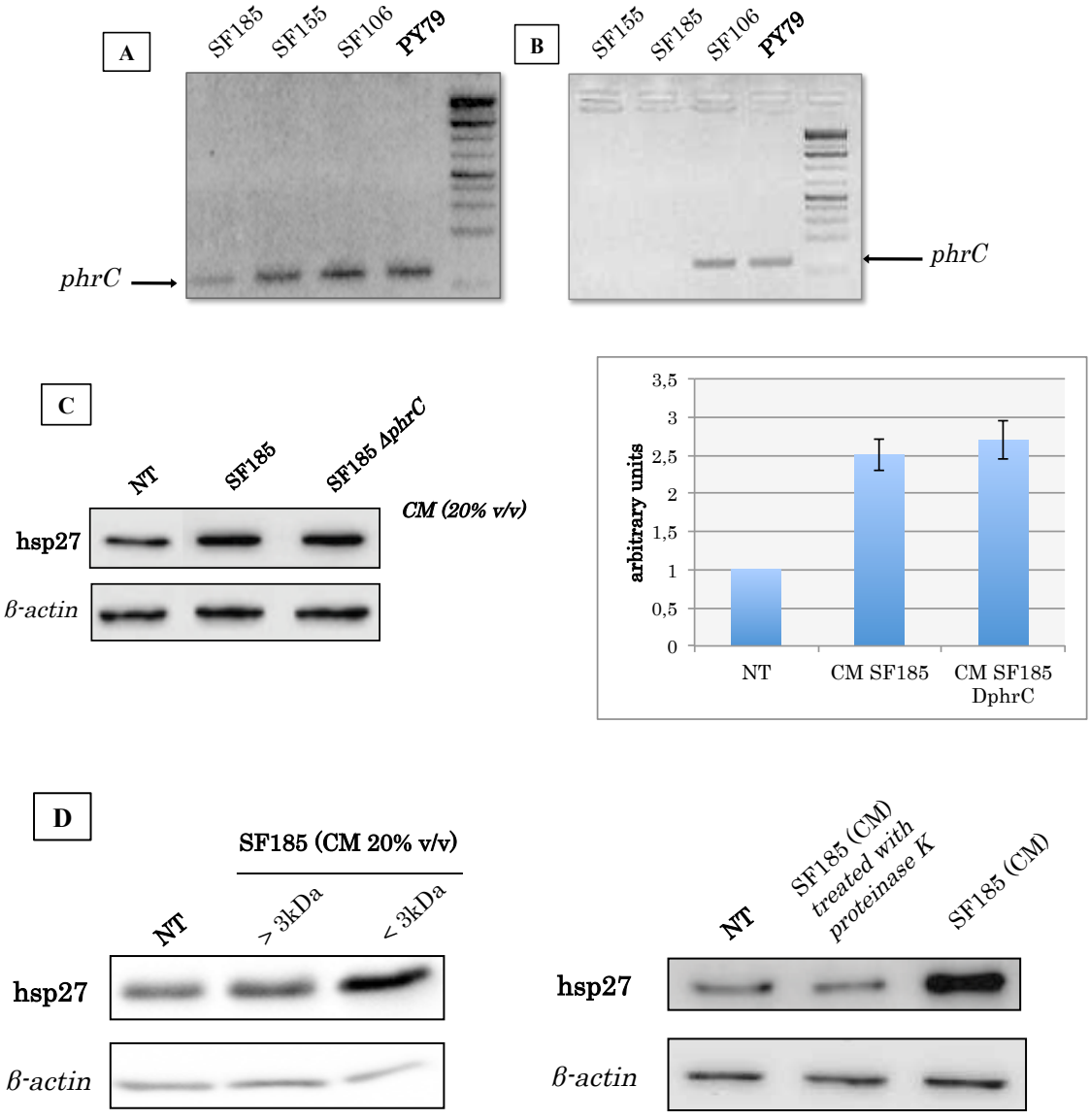

Fig.4 SF185 strain. *PCR (A) and RT-PCR (B) analysis of the phrC locus in various intestinal isolates. (C) HSP induction with CM of SF185 and of its isogenic phrC null mutant. Panel on the right reports the densitometric analysis of the western blot shown on the left. (D) Biochemical characterization of the CM of SF185.*

A preliminary characterization of this molecule has been made. As shown in Fig. 4D, the conditioned-medium was size-separated by using a 3 kDa molecular mass cut-off filter and the bioactivity was still observed in the lower fraction suggesting a small molecular mass for the effector molecule. Moreover, the supernatant was also treated with the proteinase- K (see Materials and Methods) and when added to HT29 cell culture after the enzymatic treatment, it was unable to induce HSP, suggesting its proteinaceous nature. Further characterization of the molecule by mass-spectrometry analysis is currently in progress.

2.3.4 Analysis of proteome changes in HT29 cells treated with synthetic CSF (100nM).

Although CSF is known to induce Hsp27 and to stimulate the phosphorilation of Akt and p38 MAPK, two additional survival pathway of intestinal epithelial cells (Fujiya et al., 2007), it's not yet clear the molecular mechanisms by which it affects cellular methabolism. We thus decided to look at cell proteome changes of HT29 treated with CSF (100nM). Protein extracts from untreated (Control, NT) or CSF-treated (CSF) HT29 cells were fractionated by 2D-GE and stained with colloidal Blue Coomassie (fig. 5). The gels were run in triplicate and compared using the ImageMaster 2D Platinum 6.0 software. A few initial reference points (landmarks) were affixed for gels alignment in the first step of the images analysis. The spots were detected on the gels and the software 'matched' the gels and the corresponding spots. The different 2DE images were compared by synchronized 3-D spots view. Among the spots corresponding to CSF-sensitive proteins clearly detected in repeated trials, 24 were selected for proteomic analysis. The image analysis enabled the identification of 15 spots that were

present either in higher or lower amount in the CSF-treated sample, thereby indicating that they were induced by the treatment.

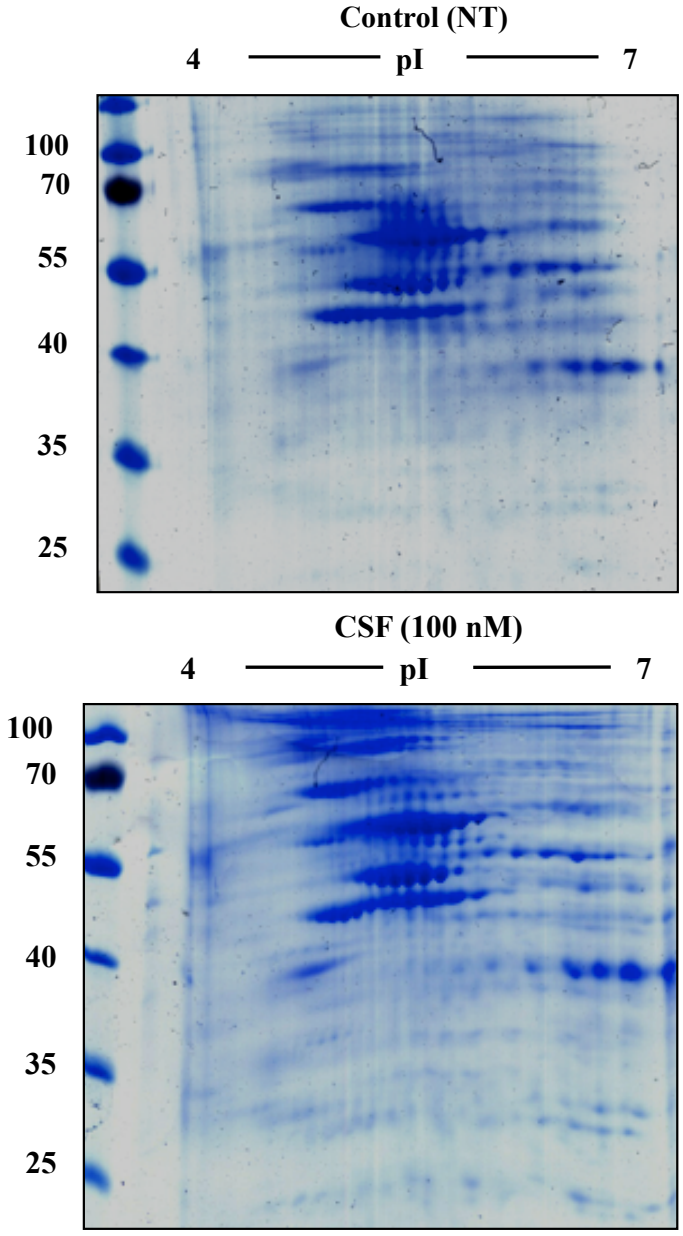

Fig.5 2D-GE of cell lysates of not-treated (control, NT) and CSF-treated HT29. *Panels show different amounts and separation of not-treated and CSF-treated HT29 total proteic extract. The spots that showed a different trend (increase/decrease or present/absent) in the two analyzed samples were then selected for mass spectral identification.*

These spots were selected for mass spectral identification by the merging of images analyses. Proteins excised from the gel were reduced, alkylated, and, in situ digested

with trypsin. The resulting peptide mixtures were analysed by nanoLC/MS/MS experiments. The peptide mixtures were fractionated by nanoHPLC and sequenced by MS/MS, generating sequence information on individual peptides. MSMS spectra were used to search for a non-redundant sequence using the in-house MASCOT software, thus taking advantage of the specificity of trypsin and of the taxonomic category of the samples. The number of measured masses that matched within the given mass accuracy was recorded, and the proteins that had the highest number of peptide matches were examined leading to the identification of the protein components. As further selection criteria, only the proteins, identified by MASCOT search with at least two peptides and found exclusively in the replicates, were selected. The list of proteins identified by this approach is illustrated in Table 1. Among the identified proteins, the signal corresponding to enolase-1 showed a decrease in the treated sample as well as that of phosphoglycerate kinase 1 (PGK1) while the signal corresponding to glyceraldehyde-3-phosphate dehydrogenase (GAPDH) showed an increment. All these enzymes are involved in the glycolytic methabolism and more precisely, PGK1 and enolase-1 catalyze the sixth and eighth reactions of the pathway, respectively, while GADPH is immediately upstream (fifth reaction). Interestingly, although the increase of GADPH, the downstream enzymes didn't show the same trend suggesting that, in this condition, GADPH is involved in other mechanism besides the primary metabolism. Validation of proteomic data by western blot is currently in progress.

Table 1 List of proteins differentially represented in CSF-treated or control HT29 cells identified by mass spectrometry.

Spot	Protein	CSF/Ctr
1	GAPDH	+
2	GAPDH; Annexin A2	+
3	Annexin A2	+
4	HNRNPK; HSPA8	+
5	HSP60	+
6	Keratin-8	-
7	Tubulin beta-4B chain	+
8	Keratin-18	+
9	Actin; SERPINB1; CCT2	-
10	Actin; PGK1; SERPINB1	-
11	PGK1	-
12	Keratin-20	-
13	Enolase 1	-
14	HSPB1	+
15	NPM1; C protein	-

2.4 Discussion

Although the gram positive *Bacillus subtilis* is commonly found in soil, more recent evidence suggests that it inhabits the GIT and should be considered as a normal gut commensal (Hong, et al., 2009; Fakhry et al., 2008). Moreover, a laboratory strain of *B. subtilis* (PY79) is known to produce and secrete a bioactive pentapeptide (CSF), generally involved in the gram-positive *quorum-sensing* mechanism, that exerts cytoprotective effects on intestinal epithelial cells inducing the heat-shock protein 27, as described before (Fujiya et al., 2007). However, the molecular mechanisms underlying this cross-kingdom quorum-sensing and the associated effects are not yet well-understood. Starting from all these evidences, this study reports a characterization of *Bacillus subtilis spp,* isolated from human intestinal biopsies, with the purpose to

investigate the induced metabolic changes on intestinal epithelial cells (HT29), using a molecular approach. Focusing on their capacity to produce and secrete the CSF and thus to exert cytoprotective effects, it is observed that all the strains, positive for the production of the pentapeptide, are also able to induce the hsp27 in HT29 cell-line, as expected. Interestingly, strain SF185 that does not produce CSF is still able to induce Hsp27. PCR and RT-PCR analyses showed that the gene is present but not expressed, suggesting that SF185 is able to produce and secrete another bioactive molecule different from CSF but exerting very similar functions on epithelial cells. A preliminary characterization of this secreted factor shows that it is smaller than 3kDa and has a proteinaceus nature. To define the chemical nature of this molecule affecting intestinal epithelial cells and identify its cellular and molecular targets is a challenging task, actually in progress.

We also focused on the study of metabolic changes induced by CSF stimulation, using a proteomic approach. Interestingly, the MS/MS analysis performed on cell lysates of treated and not-treated HT29 shows changes in the amount of enzymes involved in the glycolitic methabolism. More precisely, it's observed an increase in GADPH levels and a related decrease in phosphoglycerate kinase 1 (PGK1) and enolase-1 in the treated sample compared to the not-treated. Since PGK1 and enolase-1 catalyze the sixth and eighth reactions of the pathway, respectively, and GADPH is immediately upstream (fifth reaction), these results suggest that GAPDH could have other fuctions other than being part of the glycolytic pathway. Recent studies showed that an increase in GAPDH levels, but not in PGK1 or enolase-1 levels, protects cells from cell-death (Jaquin et al., 2013). In addition, when overexpressed GAPDH binds to active Akt limiting its dephosphorylation (Jaquin et al., 2013). Phosphorylated-Akt increase leads to Bcl-xL overexpression that is able to protect a subset of mitochondria from permeabilization

that are required for cellular survival from caspase-independent cell death (CICD). Moreover, in CSF-treated sample we also observed a concomitant increase of Hsp60, a known mitochondrial heat-shock protein involved in apoptosis regulation, indirectly supporting the pro-proliferative role of CSF. Recent studies have suggested that Hsp60 also occurs in the cytosol and plays a key role in preventing apoptosis (Kurt et al., 2000; Ghosh et al., 2007). Experiments are in progress to validate MS/MS results by western blot and to clarify the involvement of these stress-response proteins in the pro-survival mechanism activated by CSF in epithelial cells. In particular, vitality assays (MTS) and cytofluorimetric analyses are in progress to check if primary methabolism and cell-cycle regulation are affected as well.

2.5 Materials and Methods

2.5.1 Construction of the reporter strain ED5

Chromosomal DNA from strain JH11300 (carrying a functional *phrC::Cm*^{r} gene fusion) BD2876 (carrying a functional *sfrA::lacZ* (Tet^r) gene fusion) *B. subtilis* were isolated as described elsewhere (Cutting S, Vander Horn PB 1990) and were used to transform competent cells of laboratory strain PY79, yielding strain ED1 and ED2 respectively. Then, the chromosomal DNA from strain BD2876 was also used to transform competent cells of ED2 (*sfrA::lacZ* (Tet^r)) to yield isogenic ED4 strain carrying another functional gene fusion *comQ::Kan*^{r}. Finally, the chromosomal DNA of ED1 (*phrC::Cm*^{r}) strain was used to transform ED4 competent cells to yield ED5 strain (*phrC::Cm*^{r}*, comQ::Kan*^{r}, *sfrA::lacZ* (Tet^r)).

2.5.2 PCR and RT-PCR of *phrC* gene

The primers for *phrC* gene amplification were designed using the bioinformatic tool Primer3web version 4.0.0 (http://primer3.ut.ee/): phrC For 5'-

TGAAATTGAAATCTAAGTTGTTTGTT-3' and phrC Rev 5'-ACATGAAAGTCGAGTGCTTCC-3'. They amplified a 100bp fragment of *phrC* gene corresponding from position 2 to 101 of *phrC* gene of *Bacillus subtilis.* PCR was performed using 100ng of chromosomal DNA of SF185, SF155, SF106 and wild-type strain PY79 as template and the following condition of reaction: 5minutes at 95°C and 30 cycles including 30seconds at 95°C, and 30 seconds at 52°C and 20 seconds at 72°C. The PCR products were analyzed and checked for their length on 2% agarose gel with ethidium-bromide staining.

Total RNA was extracted from the isolated strains SF185, SF155, SF106 and the wild-type strain PY79 using the Qiagen minikit (Qiagen, Milan, Italy) according to the manufacturer's instructions. Total RNAs were dissolved in 50 μl of RNase-free water and stored at -80°C. The final concentration and quality of the RNA samples were estimated spectrophotometrically and by agarose gel electrophoresis with ethidium bromide staining. Total RNAs were treated with RNase free DNase (1 U/μg of total RNA; Fermentas) for 30 min at 37°C, and the reaction was stopped with DNase inactivation reagent. For reverse transcription-PCR (RT-PCR) analysis a sample containing 2 μg of DNase-treated RNA was incubated with *phrC* Rev at 65°C for 5 min and slowly cooled to room temperature to allow the primer annealing. The mixture was incubated at 50°C for 1 h in the presence of 1 μl AffinityScript multiple-temperature reverse transcriptase (Stratagene), 4 mM dNTPs, reaction buffer (Stratagene), and 10 mM dithiothreitol (DTT). The enzyme was inactivated at 70°C for 15 min. One-tenth of the reaction mix was used as a template in PCRs using oligonucleotide *phrC* For and Rev. The PCR products were analyzed on on 2% agarose gel with ethidium-bromide staining. For a control, PCRs were carried out with RNA alone to exclude the

possibility that the amplification products could derive from contaminating genomic DNA.

2.5.3 Bacterial growth and preparation of conditioned medium

Intestinal isolates of *Bacillus subtilis spp* (Fakhry S. et al., 2008) were grown in LB broth (for 1 l: 10 g Bacto-Tryptone, 5 g Bacto-yeast extract, 10 g NaCl, pH 7.0) to reach 0.6- 0.8 OD_{600nm} at 37°C in aerobic condition and the culture diluted and used to inoculate minimal S7 medium (50mM MOPS, 10mM $(NH_4)_2SO_4$, 5mM potassium phosphate pH 7.0, 2mM $MgCl_2$, 0.9 mM $CaCl_2$,50 μM $MnCl_2$, 10 μM $ZnCl_2$, 5 μM $FeCl_3$, 2 μM thiamine hydrochloride, 20mM sodium glutamate, 1% glucose, 0.1 mg/ml phenylalanine, 0.1 mg/ml tryptophan). Cells were then grown aerobically for 16 hours at 37°C. The culture was centrifuged (3000 rpm for 10 min at RT) and the supernatant (conditioned medium, CM) was filtered-sterilized through a 0.22 μm low-protein binding filter (Millex; Millipore, Bedford, MA). The SF185 CM was size fractionated (3-kDa cutoff spin column; Centricon, Millipore) and treated with proteinase-K (Invitrogen) at a final 100 ug/ml concentration for 60 min at 37°C. After the enzymatic treatments CM was fractionated as described to remove the enzymes. For the preparation of conditioned medium in anaerobic conditions, intestinal isolates of *Bacillus subtilis spp* were grown anaerobically in LB broth (for 1 l: 10 g Bacto-Tryptone, 5 g Bacto-yeast extract, 10 g NaCl, pH 7.0) at 37°C and then used to inoculate Difco-Sporulation-inducing (DS) medium. Cells were grown in anaerobic conditions for 72 hours at 37°C.

2.5.4 Cell culture and treatment with bacterial CM

HT29 cells (ATCC HTB-38) derived from a poorly-differentiated colonic adenocarcinoma and were maintained in Dulbecco's Modified Eagle's Medium (DMEM) supplemented with 10% fetal bovine serum and 1% penicillin-streptomycin. Cells were cultured at 37°C in humidified atmosphere of 5% CO_2. The bacterial CMs were employed for the treatment at 20% v/v concentration in complete growth medium. After incubation of 24 hours with CM (20% v/v) or synthetic CSF (100 nM, PRIMM srl, Milan, IT) cells were harvested, lysed and cell extracts prepared for Western blot analysis, as described below.

2.5.5 SDS-PAGE and Western Immunoblot analysis

Cells were harvested in lysis buffer (50 mM Tris-HCl pH 7.5, 5 mM EDTA, 150 mM NaCl, 1% NP-40, 1 mM phenylmethylsulfonyl fluoride, 0.5% sodium deoxycholate, and protease inhibitors) and total protein extracts prepared. Briefly, cell lysates were incubated on ice for 40 minutes, and the extracts were centrifuged at 13200 rpm for 15 minutes to remove cell debris. Protein concentration was determined by the Bio-Rad protein assay (Bio-Rad). After the addition of 2x Laemmli buffer (SIGMA), samples were boiled at 100°C for 5 minutes and resolved by SDS-polyacrylamide gel electrophoresis (10% or 12%). Proteins were transferred to polyvinylidenedifluoride (PVDF) membranes (Millipore). The membranes were blocked in 5% w/v milk buffer (5% w/v non-fat dried milk, 50 mM Tris, 200 mM NaCl, 0,2% Tween 20) and incubated with primary antibody diluted in 5% w/v milk or bovine serum albumine buffer for 2 hours at room temperature or overnight at 4°C. Primary antibodies were anti-mouse Hsp27 (Cell Signalling), anti-rabbit β-actin (Santa-Cruz Biotechnology). Data were visualized by enhanced chemiluminescence method (ECL, GE-Healthcare)

using HRP-conjugated secondary antibody (Santa-Cruz Biotechnology) incubated 1 hour at room temperature, and analysed by Quantity One ®software of ChemiDoc ^{TM}XRS system (Bio-Rad). Hsp27 band intensity was evaluated by ImageQuant analysis on at least two different expositions to assure the linearity of each acquisition. Values expressed as ratio with the corresponding actin values and normalized to the reference point (not-treated, NT).

2.5.6 Beta-galactosidase assay

ComQ-phrC null mutant (ED5) cells were inoculated in isolated *Bacillus subtilis* conditioned media and incubated at 37°C in aerobic conditions until stationary phase of growth. 1ml of these cultures was harvested and centrifuged at 4000 rpm for 5minutes and the pellet frozen at -80°C. Then, the pellets were resuspended in 1 ml of buffer Z (0.06 M Na_2HPO_4, 0.04 M NaH_2PO_4, 0.01 M KCl, 0.001 M $MgSO_4$ and 0.05M β-mercaptoethanol) and 10 ul of toluene were added. After a brief mixing with vortex, the tubes were incubated for 5 minutes in a 30°C waterbath. Then, the reaction was started by adding 0.2 ml of ONPG solution (0.4 mg/ml ONPG in Z buffer without β-mercaptoethanol). The tubes were mixed and incubated at 30°C until the color at A_{420nm} is approximately 0.3 (clearly yellow). The reaction was stopped by adding 0.5 ml of Na_2CO_3 (1M) and the reaction time was recorded. The tubes were centrifuged for 5minutes and read A_{420nm} and OD_{550nm} immediately. The activity of β-galactosidase was calculated using the following formula: β-galactosidase (Miller units) = ((A_{420nm} – (1.75 x OD_{550nm})/ (reaction time (min) x OD_{595nm})) x 1000.

2.5.7 Two-dimensional electrophoresis (2DE).

The first dimensional electrophoresis (isoelectric focusing, IEF) was carried out on non-linear wide-range immobilized pH gradients (pH 4–7; 7 cm long IPG strips; GE Healthcare, Uppsala, Sweden) and achieved using the Ettan IPGphor system (GEHealthcare,Uppsala, Sweden). 200 mg ofprotein extracts was precipitated with methanol/chloroform according to (Wessel and Flugge, 1984) and solubilized in 125 ml of rehydratation buffer and 0.2% (v/v) carrier ampholyte for 12 h, at 50 mA, at 20°C. The strips were then focused according to the following electrical conditions at 20°C: 500 V for 30 min, 1000 V for 30 min, 5000 V for 10h, until a total of 15000 Vt was reached. After focusing, analytical and preparative IPGstrips were equilibrated for 15 min in 6 M urea, 30% (V/V) glycerol, 2% (w/V) SDS, 0.05 M Tris–HCl, pH 6.8, 1% (w/V) dithiothreitol (DTT), and subsequently for 15 min in the same urea/SDS/Tris buffer solution but substituting the 1% (w/V) DTT with 2.5% (w/V) iodoacetamide. The second dimension was carried out on 12.5% (w/w) polyacrylamide gels (10 cm x 8 cm x 0.75 mm) at 25 mA/gel constant current and 10°C until the dye front reached the bottom of the gel, according to (Laemmli, 1970; Hochstrasser et al., 1988). MS-preparative gels were stained overnight with colloidal Coomassie Brilliant Blue and destained with MilliQ grade water.

2.5.8 Image analysis.

Gels images were acquired with an Epson expression 1680 PRO scanner. Computer-aided 2-D image analysis was carried out using the ImageMasterTM 2D Platinum software. Relative spot volumes (%V) (V = integration of OD over the spot area; %V=V single spot/V total spot) were used for quantitative analysis in order to decrease experimental errors.

2.5.9 In situ digestion.

Trypsin, DTT, iodoacetamide, and R-cyano-4-hydroxycinnamic acid were purchased from Sigma. NH4HCO3 was from Fluka. Trifluoroacetic acidhigh- performance liquid chromatography (HPLC) grade was from Carlo Erba. All other reagents and solvents were of the highest purity available from Baker. Analysis was performed on the Coomassie blue-stained spots excised from the gels. The spots were excised from the gel and destained by repetitive washes with 0.1 M NH4HCO3, pH 7.5, and acetonitrile. Samples were reduced by incubation with 50 ml of 10 mM DTT in 0.1 M NH4HCO3 buffer, pH 7.5 and carboxyamidomethylated with 50 ml of 55 mM iodoacetamide in the same buffer. Enzymatic digestion was carried out with trypsin (12.5 ng/ml) in 10 mM ammonium bicarbonate buffer, pH 7.8. Gel pieces were incubated at 4°C for 2 h. Trypsin solution was then removed, and a new aliquot of the same solution was added; samples were incubatedfor 16 h at 37°C. A minimum reaction volume was used as to obtain the complete rehydration of the gel. Peptides were then extracted by washing the gel particles with 10mM ammonium bicarbonate and 1% formic acid in 50%acetonitrile at room temperature. The resulting peptide mixtures were filtrated using 0.22 μm PDVF filter from Millipore, following the recommended procedure.

2.5.10 NanoHPLC-chip MS/MS analysis.

The peptide mixtures were analysed using a CHIP MS 6520 QTOF equipped with a capillary 1200 HPLC system and a chip cube (Agilent Technologies, Palo Alto, Ca). After loading, the peptide mixture (8 ul in 0.1% formic acid) was first concentrated and washed at 4 ul min-1 in 40 nl enrichment column (Agilent Technologies chip), with 0.1% formic acid in 2% acetonitrile as eluent. The sample was then fractionated on a

C18 reverse-phase capillary column (75 um x 43 mm in the Agilent Technologies chip) at flow rate of 400 nl min-1 with a linear gradient of eluent B (0.1% formic acid in 95% acetonitrile) in A (0.1% formic acid in 2% acetonitrile) from 7 to 60% in 50 min. Peptide analysis was performed using data-dependent acquisition of one MS scan (mass range from 400 to 2000 m/z) followed by MS/MS scans of the three most abundant ions in each MS scan. The acquired MS/MS spectra were transformed in Mascot generic file format and used for peptides identification with a licensed version of MASCOT 2.1, in a local database (Swiss Pro).

2.5.11 Protein identification.

Raw data from nano-LC–MS/MS were analysed using Qualitative Analysis software, and MSMS spectra were searched against non-redundant protein databases (NCBInr 20090924, 9760158 sequences) and UniprotSwissprot (2011, 167910 sequences), with the taxonomy restriction to Homo sapiens, using in-house MASCOT 2.1 software (Matrix Science, Boston, USA). The Mascot search parameters were:'trypsin' as enzyme allowing up to three missed cleavages, carbamidomethyl on as fixed modification, oxidation of M, pyroGlu N-term Q, as variable modifications, 20 ppm MSMS tolerance, and 0.6 Da peptide tolerance. The score used to evaluate quality of matches for MSMS data was higher than 32.

2.6 References

Bassler BL (2002). Small talk: Cell-to-cell communication in bacteria. *Cell* **109**, 421-424.

Berg, R. D. 1996. The indigenous gastrointestinal microflora. *Trends Microbiol*. **4**:430–435.

Borrellio, S. P. 2002. The normal flora of the gastrointestinal tract, p. 1–12. In M. A. Kamm (ed.), *Gut ecology*. Martin Dunitz, Ltd., London, United Kingdom.

Cutting S, Vander Horn PB (1990) Genetic analysis In: C. Harwood and S. Cutting (Eds.), *Molecular Biological Methods for Bacillus*. John Wiley and Sons, Chichester, UK. 27–74.

D'Souza, C., M. M. Nakano, and P. Zuber. (1994). Identification of comS, a gene of the *srfA* operon that regulates the establishment of genetic competence in *Bacillus subtilis*. *Proc. Natl. Acad. Sci. USA* **91**:9397–9401.

Fakhry S, Sorrentini I, Ricca E, De Felice M, Baccigalupi L. (2008) Characterization of spore forming Bacilli isolated from the human gastrointestinal tract. *J Appl Microbiol*.**105**(6):2178-86.

Fujiya, M., Musch, M. W., Nakagawa, Y., Hu, S., Alverdy, J., Kohgo, Y., Scheneewind, O., Jabri, B. & Chang, E. B. (2007). The *Bacillus subtilis* quorum-sensing molecule CSF contributes to intestinal homeostasis via OCTN2, a host cell membrane transporter. *Cell Host & Microbe* **1**,299–308.

Ghosh JC, Dohi T, Kang BH, Altieri DC (2008). Hsp60 regulation of tumor cell apoptosis. *J Biol Chem.* Feb 22;283(8):5188-94.

Hochstrasser DF, Patchornik A, Merril CR. 1988. Development of polyacrylamide gels that improve the separation of proteins and their detection by silver staining. *Anal Biochem* **173**(2): 412–23.

Jacquin MA, Chiche J, Zunino B, Bénéteau M, Meynet O,Pradelli LA, Marchetti S, Cornille A, Carles M and Ricci J-E (2013). GAPDH binds to active Akt, leading to Bcl-xL increase and escape from caspase-independent cell death. *Cell Death and Differentiation* 20, 1043–1054; doi:10.1038/cdd.2013.32;

Kaper JB and Sperandio V (2005). Bacterial cell-to-cell signaling in the gastrointestinal tract. *Infection and Immunity* **73**,6: 3197-3209.

Laemmli UK. (1970). Cleavage of structural proteins during the assembly of the head of bacteriophage T4. *Nature* **227**: 680–685.

Lazazzera BA, Kurtser GI, McQuade RS and Grossman AD (1999). An autoregulatory circuit affecting peptide signaling in *Bacillus subtilis. J. of Bacteriology* **181**,17: 5193-5200.

Lazazzera, B. A., and A. D. Grossman. (1998). The ins and outs of peptide signaling. *Trends Microbiol*. **6**:288–294.

Magnuson R. J. Solomon and A. D. Grossman. (1994). Biochemical and genetic characterization of a competence pheromone from *B. subtilis*. *Cell* **77**:207–216.

Morimoto, R.I. (1993). Cells in stress: Transcriptional activation of heat shock genes. *Science* **259**, 1409–1410.

Morimoto, R.I. (2002). Dynamic remodeling of transcription complexes by molecular chaperones. *Cell* **110**, 281–284.

Nakano, M. M., L. Xia, and P. Zuber. (1991). Transcription initiation region of the *srfA* operon, which is controlled by the ComP-ComA signal transduction system in *Bacillus subtilis. J. Bacteriol*. **173**:5487–5493.

Nakano M. M., and P. Zuber. (1991). The primary role of ComA in establishment of the competent state in *Bacillus subtilis* is to activate expression of *srfA*. *J. Bacteriol*. **173**:7269–7274.

Pritchard, D. I. (2006). Immune modulation by *Pseudomonas aeruginosa* quorum-sensing signal molecules. *Int J Med Microbiol* **296**, 111–116.

Rakoff-Nahoum, S., Paglino, J., Eslami-Varzaneh, F., Edberg, S., and Medzhitov, R. (2004). Recognition of commensal microflora by toll-like receptors is required for intestinal homeostasis. *Cell* **118**, 229–241.

Solomon, J. M., B. A. Lazazzera, and A. D. Grossman. 1996. Purification and characterization of an extracellular peptide factor that affects two different developmental pathways in *Bacillus subtilis*. *Genes Dev*. **10**:2014–2024.

Wessel D, Flugge UI. (1984). A method for the quantitative recovery of protein in dilute solution in the presence of detergents and lipids. *Anal Biochem* **138**(1): 141–143.

Williams P. (2007). Quorum-sensing, communication and cross-kingdom signaling in the bacterial world. *Microbiology* **153**: 3923-3938.

CHAPTER 3

A Biochemical and Cellular Approach to Explore the Antiproliferative and Prodifferentiative Activity of Aloe Arborescens Leaf Extract

*Blanda Di Luccia[1], Nicola Manzo[1], Maria Vivo[1], Eugenio Galano[2], Angela Amoresano[2], Elvira Crescenzi [4], Alessandra Pollice[1] *, Raffaella Tudisco[3], Federico Infascelli[3], Viola Calabrò[1]*

[1] Dipartimento di Biologia Strutturale e Funzionale, Università di Napoli "Federico II", Naples, Italy.

[2] Dipartimento di Chimica Organica e Biochimica, Università di Napoli "Federico II", Naples, Italy.

[3] Dipartimento di Scienze Zootecniche e Ispezione degli Alimenti, Università di Napoli "Federico II", Naples, Italy.

[4] Istituto di Endocrinologia ed Oncologia Sperimentale, CNR, via S. Pansini, 5, 80131 Naples, Italy,

Published in February 2013 on *Phytotherapy Research* doi: 10.1002/ptr.4939

3.1 Abstract

Aloe arborescens Miller, belonging to the Aloe genus (Liliaceae family), is one of the main varieties of Aloe used worldwide. Although less characterized than the commonest *Aloe vera*, *Aloe arborescens* is known to be richer in beneficial phytotherapeutic, anticancer, and radio-protective properties. It is commonly used as a pharmaceutical ingredient for its effect in burn treatment and ability to increase skin wound healing properties. However, very few studies have addressed the biological effects of *Aloe* at molecular level. The aim of the research is to provide evidences for the anti-proliferative properties of *Aloe arborescens* crude leaf extract using an integrated proteomic and cellular biological approach. We analysed the composition of an *Aloe arborescens* leaf extract by GC-MS analysis. We found it rich in Aloe-emodin, a hydroxylanthraquinone with known antitumoral activity and in several compounds with anti-oxidant properties. Accordingly, we show that the *Aloe* extract has antiproliferative effects on several human transformed cell lines and exhibits prodifferentiative effects on both primary and immortalised human keratinocyte. Proteomic analysis of whole cell extracts revealed the presence of proteins with a strong antiproliferative and antimicrobial activity specifically induced in human keratinocytes by *Aloe* treatment supporting its application as a therapeutical agent.

3.2 Introduction

Plants and their extracts are appreciated for their specific aroma, nutraceutical and therapeutical properties, such as antimicrobial, antiproliferative, anti-inflammatory, immunostimulant, and antioxidative (Greathead, 2003). *Aloe arborescens Miller,* belonging to the Aloe genus (Liliaceae family), is one of the main varieties of Aloe

used worldwide. It is commercially grown in South America (Brazil and Uruguay), South Africa and some Asian countries. The concentrated active extract from *Aloe arborescens* shares some therapeutical properties with the well known and studied *Aloe vera* and is commonly used in medicinal applications to treat burn wounds and help accelerating the healing process of the skin. Recent studies have demonstrated that *Aloe arborescens* has immunostimulating activity in animal trials (Infascelli, 2010) and it was found to have beneficial phytotherapeutic and anticancer properties (Lissoni, 2009). It is known that the anticancer properties of *Aloe arborescens* depend not only on its immuno-modulatory effect, but also on a direct inhibition of cancer cell proliferation (Bedini, 2009). Immunostimulatory effects are due to acemannan while antiproliferative effects have been ascribed to anthracenic, antraquinonic and aloenin-like compounds (Lissoni, 2009). *Aloe arborescens* is also known for its effective burn treatment and ability to increase skin wound healing properties. Furthermore, it has been shown to be useful in reducing microbial growth and to kill a broad range of viruses and fungi, thereby providing extraordinary support for the gastrointestinal tract, mucous membranes and connective tissue (Falcetti A., personal communications).

To determine the therapeutic effects of *Aloe arborescens*, a considerable number of clinical investigations have been done; however, very few studies have addressed the biological effects of *Aloe* at molecular level. The aim of the present study is to analyze the cellular response to treatment with *Aloe arborescens* crude leaf extract through a biochemical and cellular approach in order to support its application as a therapeutical agent.

3.3 Materials and Methods

3.3.1 Preparation of the whole-leaf extract. Plants from Italian farms (Marsala, Sicily) certified for organic systems were cultivated in natural habitat and were harvested when they were older than 4 years. The leaves were washed in tanks, laid in plastic bags and successively washed at 25°C and brushed in order to eliminate external impurity. After air-drying the leaves were submitted to a "cold method" provided by HDR sas (Caserta, Italy) which allows to extract the active principles either from the inner part or from the cuticle. Commercial preparation of *Aloe* extract was stabilized by potassium sorbate and citric acid. Successively, the extract were stored in stainless still containers which were sealed to avoid air contact.

3.3.2 Cell culture and *Aloe arborescens* treatment. NHEK primary cells, derived from neonatal foreskin, were from Clonetics (San Diego, California).The HaCaT (human spontaneously immortalized keratinocyte), MDA-MB231 (human breast adenocarcinoma) cell lines were maintained in Dulbecco's Modified Eagle's Medium (DMEM) supplemented with 10% fetal bovine serum and 1% penicillin-streptomycin. The keratinocyte-derived squamous carcinoma cell lines (SCC011 and SCC012) were previously described (Lefort et al., 2007). The A431 (human epidermoid carcinoma) cell line was maintained in RPMI 1640 supplemented with 10% fetal bovine serum and 1% penicillin-streptomycin. All cell lines were cultured at 37°C in humidified atmosphere of 5% CO_2. Aliquots of *Aloe arborescens* fresh leaf extract were centrifuged at 10000 rpm for 10 min and sterilized using disposable Millex syringe filter units, pore size 0.22 mm (Millipore). Sterile extract was employed for the treatment at 10, 20 and 50% v/v, as indicated, in cell culture medium. Equal amounts of Aloe preservation medium were added to control

samples. *Aloe*-treated and untreated cells were photographed and harvested for Western-blot analysis as described below.

3.3.3 Cell growth analysis. HaCaT spontaneously immortalized human keratinocytes, MDA-MB231 metastatic breast adenocarcinoma, A431 human epidermoid carcinoma, CaCo2 human epithelial colorectal adenocarcinoma cells, SCC011 and SCC022 squamous cell carcinoma were plated in 35mm dishes, at the cell density of 1 x 10^5 cells/plate. Cells were cultured in complete growth media supplemented or not with aliquots of fresh *Aloe arborescence* extract (10% v/v) for 6, 24, 30, 48 and 54 hrs, collected, and counted in a Burker chamber. Cell extracts from treated and untreated cells were prepared and subjected to SDS-PAGE and immunoblot for gene-expression analysis.

3.3.4 Flow cytometry analysis. After treatments, cells were washed twice with PBS and harvested with 0.05% trypsin in 0.15% Na_2EDTA. Cells were then centrifuged, washed in PBS, fixed with ice-cold 70% ethanol, and stored overnight at 4°C. Fixed cells were washed in PBS and then incubated with propidium iodide (50 mg/ml) and RNAse A (10 mg/ml) for 30 min at room temperature. Data acquisition was performed using a CyAn ADP Flow Cytometer (Beckman Coulter, Inc., Milano, Italy) and Summit Software.

3.3.5 Keratinocyte differentiation. Non tumorigenic HaCaT cells were chosen because they retain the ability to differentiate upon Ca2+ treatment thus representing an intermediary between normal and cancerous keratinocytes. HaCaT cells were grown to confluence in complete growth medium and switched into differentiation

medium (serum-free DMEM) with 1.2 mM $CaCl_2$ with or without *Aloe extract* (10% v/v) for 6 days according to (Vivo et al., 2009), with the exception that the medium was changed every 48 hours. Differentiated cells treated or not with *Aloe* were photographed and harvested for SDS-PAGE and immunoblot analysis as described below. NHEK cells were propagated in serum-free keratinocyte growth medium containing 0.05 mM calcium. NHEK cells with 70%–80% cell confluency were switched to high-calcium medium (1.2 mM) to induce differentiation. Extracts from *Aloe*-treated or untreated NHEK cells were then subjected to SDS-PAGE and immunoblot analysis as described below.

3.3.6 SDS-PAGE and immunoblot analysis. *Aloe arborescens* treated and untreated cells were harvested in lysis buffer (50 mM Tris-HCl pH 7.5, 5 mM EDTA, 150 mM NaCl, 1% NP-40, 1 mM phenylmethylsulfonyl fluoride, 0.5% sodium deoxycholate, and protease inhibitors). Cell lysates were incubated on ice for 40 minutes, and the extracts were centrifuged at 13200 rpm for 15 minutes to remove cell debris. Protein concentrations were determined by the Bio-Rad protein assay (Bio-Rad). After the addition of 2x Laemmli buffer (SIGMA), the samples were boiled at 100°C for 5 minutes and resolved by SDS-polyacrylamide gel electrophoresis. Proteins were transferred to a polyvinylidene difluoride membrane (Millipore). The PVDF membrane was blocked in 5% w/v milk buffer (5% w/v non-fat dried milk, 50 mM Tris, 200 mM NaCl, 0,2% Tween 20) and incubated with primary antibodies diluted in 5% w/v milk or bovine serum albumine buffer for 2 hours at room temperature or overnight at 4°C. Primary antibodies were anti-mouse p63-4A4 (Calbiochem), anti-mouse involucrin (Abcam antibody), anti-mouse cytokeratin 1 (Santa-Cruz biotechnology), anti-rabbit transglutaminase type 2

(Abcam antibody), anti-rabbit pErks 42/44 (Cell signalling), anti-rabbit p21 (Santa-Cruz biotechnology), anti-rabbit cyclin D1 (Cell Signalling), anti-rabbit PARP-1 (Cell Signalling), anti-goat β-actin (Santa-Cruz biotechnology). Data were visualized by enhanced chemiluminescence method (ECL, GE-Healthcare) using HRP-conjugated secondary antibodies (Santa-Cruz biotechnology) incubated for 1 hour at room temeperature, and analysed by Quantity One ®software of ChemiDoc ^{TM}XRS system (Bio-Rad).

3.3.7 Cell fluorescent staining. SCC011 and SCC022 cells were seeded on sterile coverslips, and treated or not with Aloe arborescens extract (10% v/v) for 48hrs. After the treatment three washes with PBS were performed and cells were fixed with 4% paraformaldehyde at RT for 15 minutes. Then, cells were incubated with WGA (Wheat Germ Agglutinin) membrane fluorescent stain (1:200) for 1h at 37°C. After three washes with PBS cells were permeabilized with 0.5% Triton-X100 (Sigma-Aldrich, Selze/Germany) at room temperature for 5 minutes. Following permeabilization cells were incubated with DAPI (1:10000) for 3 minutes at RT. After three washes with 0.05% PBS-Tween, slides were mounted and analyzed.

3.3.8 Metabolite analysis. Aliquots of commercial preparation of aloe extract were submitted to liquid-liquid extraction procedure by using equal amount of chloroform (1:1 v/v). The extraction step was performed three times and the organic extracts were collected and dried. Analyte mixtures were finally trimethylsilylated in 200 µl of N, O-bis(trimethylsilyl) acetamide (TMSA) at 80°C for 45 min. The sample was dried down under nitrogen, dissolved in 50 µl of hexane and centrifuged to remove

the excess of solid reagents. The hexane supernatant (1/50) was used for the GC-MS analysis.

3.3.9 GCMS analysis. GC-MS analyses were performed on a 5390 MSD quadrupole mass spectrometer (Agilent technologies) equipped with a gas chromatograph by using a DB-5MS fused silica capillary column (30 m, 0.5 mm ID, 0.25 μm ft) from G&W. The injection temperature was 250°C. For lipid analyses the oven temperature was increased from 25°C to 90°C in 1 min and held at 90°C for 1 min before increasing to 140°C at 25°C/min, to 200°C at 5°C/min and finally to 300°C at 10°C/min.. Electron Ionisation (EI) mass spectra were recorded by continuous quadrupole scanning at 70eV ionisation energy. Each species was interpreted on the basis of electron impact spectra (NIST library and Analyst Software).

3.3.10 Two dimensional electrophoresis (2DE). The first dimensional electrophoresis (isoelectric focusing, IEF) was carried out on non-linear wide-range immobilized pH gradients (pH 4-7; 7 cm long IPG strips; GE Healthcare, Uppsala, Sweden) and achieved using the Ettan IPGphor system (GE Healthcare, Uppsala, Sweden). 200 mg of protein extracts were precipitated with methanol/chloroform according to (Wessel et al., 1984) and solubilized in 125 μl of rehydratation buffer and 0,2% (v/v) carrier ampholyte for 12h, at 50 mA, at 20° C. The strips were then focused according to the following electrical conditions at 20°C: 500 V for 30 min, 1000 V for 30 min, 5000 V for 10h, until a total of 15000 Vt was reached. After focusing, analytical and preparative IPG strips were equilibrated for 15 min in 6 M urea, 30% (V/V) glycerol, 2% (w/V) SDS, 0.05 M Tris-HCl, pH 6.8, 1% (w/V) DTT, and subsequently for 15 min in the same urea/SDS/Tris buffer solution but

substituting the 1% (w/V) DTT with 2.5% (w/V) iodoacetamide. The second dimension was carried out on 12.5% (w/w) polyacrylamide gels (10 cm x 8 cm x 0.75 mm) at 25 mA/gel constant current and 10°C until the dye front reached the bottom of the gel, according to (Laemmli et al., 1970; Hochstrasser et al., 1988). MS-preparative gels were stained overnight with colloidal Coomassie Brilliant Blue and destained with MilliQ grade water.

3.3.11 Image analysis. Gels images were acquired with an Epson expression 1680 PRO scanner. Computer-aided 2-D image analysis was carried out using the ImageMasterTM 2D Platinum software. Relative spot volumes (%V) (V=integration of OD over the spot area; %V = V single spot/V total spot) were used for quantitative analysis in order to decrease experimental errors.

3.3.12 In situ digestion. Trypsin, dithiothreitol (DTT), iodoacetamide and R-cyano-4-hydroxycinnamic acid were purchased from Sigma. NH_4HCO_3 was from Fluka. Trifluoroacetic acid (TFA)-HPLC grade was from Carlo Erba. All other reagents and solvents were of the highest purity available from Baker. Analysis was performed on the Coomassie blue-stained spots excised from the gels. The spots were excised from the gel and destained by repetitive washes with 0.1 M NH_4HCO_3, pH 7.5, and acetonitrile. Samples were reduced by incubation with 50 µL of 10 mM DTT in 0.1 M NH_4HCO_3 buffer, pH 7.5 and carboxyamidomethylated with 50 µL of 55 mM iodoacetamide in the same buffer. Enzymatic digestion was carried out with trypsin (12.5 ng/µL) in 10 mM ammonium bicarbonate buffer, pH 7.8. Gel pieces were incubated at 4 °C for 2 h. Trypsin solution was then removed and a new aliquot of the same solution was added; samples were incubated for 16 h at 37 °C. A minimum

reaction volume was used as to obtain the complete rehydratation of the gel. Peptides were then extracted by washing the gel particles with 10 mM ammonium bicarbonate and 1% formic acid in 50% acetonitrile at room temperature. The resulting peptide mixtures were filtrated using 0.22 um PDVF filter from Millipore, following the recommended procedure.

3.3.13 NanoHPLC-chip MS/MS Analysis. The peptide mixtures were analysed using a CHIP MS 6520 QTOF equipped with a capillary 1200 HPLC system and a chip cube (Agilent Technologies, Palo Alto, Ca). After loading, the peptide mixture (8 μL in 0.1 % formic acid) was first concentrated and washed at 4 μL min^{-1} in 40 nl enrichment column (Agilent Technologies chip), with 0.1 % formic acid in 2 % acetonitrile as eluent. The sample was then fractionated on a C18 reverse-phase capillary column (75 μm x 43 mm in the Agilent Technologies chip) at flow rate of 400 nl min^{-1} with a linear gradient of eluent B (0.1% formic acid in 95% acetonitrile) in A (0.1% formic acid in 2% acetonitrile) from 7 to 60 % in 50 min.

Peptide analysis was performed using data-dependent acquisition of one MS scan (mass range from 400 to 2000 m/z) followed by MS/MS scans of the three most abundant ions in each MS scan. The acquired MS/MS spectra were transformed in Mascot generic file format and used for peptides identification with a licensed version of MASCOT 2.1, in a local database (Swiss Pro).

3.3.14 Protein Identification. Raw data from nano-LC–MS/MS were analyzed using Qualitative Analysis software and MSMS spectra were searched against non-redundant protein databases (NCBInr 20090924, 9760158 sequences) and UniprotSwissprot (2011, 167910 sequences), with the taxonomy restriction to Homo sapiens, using in

house MASCOT 2.1 software (Matrix Science, Boston, USA).

The Mascot search parameters were: "trypsin" as enzyme allowing up to 3 missed cleavages, carbamidomethyl on as fixed modification, oxidation of M, pyroGlu N-term Q, as variable modifications, 20 ppm MSMS tolerance and 0.6 Da peptide tolerance. The score used to evaluate quality of matches for MSMS data was higher than 32.

3.3.15 Phase-contrast microscopy. HaCaT and A431 cells were grown and (HaCaT) induced to differentiate on glass coverslips in 6-well plates, washed with phosphate-buffered saline (PBS) and fixed with cold methanol for 10 minutes. Treated and not-treated cells were photographed (40x) with Olympus BX51 microscope.

3.3.16 Bacterial strains and growth conditions. Bacterial strains used in this study were *Bacillus cereus* (*6A2*) (Naclerio et al., 1993), *Staphylococcus aureus* (ATCC 6538), *Listeria monocitogenes* (ATCC 7644), *Salmonella typhimurium* (ATCC 14028), *Shigella sonnei* (ATCC25931), *Escherichia coli* (DH5α), *Bacillus subtilis* (PY79) (Youngman et al., 1984) , *Lactobacillus mucosae* (SF1031) and *Lactobacillus gasseri* (SF1109) (Fakhry et al., 2009). Lactobacilli cultures were cultured in MRS broth (Difco) at 37°C in microaerophilic conditions, while for all other strains, LB medium (8 g/l NaCl, 10 g/l tryptone, 5 g/l yeast extract) and aerobic conditions at 37°C were used. *Aloe*-containing liquid media, obtained by adding 2 ml of an aqueous *Aloe* leaf extract to 8 ml of LB or MRS media, were inoculated with 0.1 ml of an overnight culture and growth at 37°C followed for 8-12 hours by spectrophotometer (OD_{600}) analysis.

3.3.17 Plate antibacterial assays. For each indicator strain utilized, 100 µl aliquots of exponential growth cultures were mixed with 10 ml of LB or MRS soft agar (0.7%). Plates were then spotted with 10µl of *Aloe arborescens* extract, incubated at 37°C and the inhibition halo measured as previously reported (Baccigalupi et al., 2005). The effects of *Aloe arborescens* extracts on bacterial growth were also measured on LB and MRS agar plates prepared by adding various dilutions of *Aloe* extract (1:1, 1:5, 1:10) to the media and then spotting on the solidified plates aliquots (10 µl) of each bacterial culture in stationary growth phase. *Aloe*-containing plates were then incubated 37°C and checked for bacterial growth after 24 and 48 hours.

3.4 Results and Discussion

3.4.1 GC-MS analysis

The composition of the *Aloe arborescens* preparation was determined by GC-MS analyses following liquid-liquid extraction of different analytes from the extract. The extracted mixture of species was derivatised to TMS-derivatives and directly analysed by GC-MS by monitoring the total ion current as a function of time. Each species was univocally identified on the basis of the electron impact fragmentation spectra. All the analyses were performed as triplicates. The chromatograms of organic phase extracted in chloroform essentially revealed the presence of hesenoic ($C_6H_{12}O_2$), sorbic ($C_6H_8O_2$), and benzoic acid ($C_6H_8O_7$). In the aqueous phase 22 predominant species were identified and are listed in TABLE 1. Aloin, one of the main component of Aloe species with known pharmacological activities, was not detected while a significant amount of Aloe-emodin, a hydroxylanthraquinone having specific antineuroectodermal tumor activity (Pecere, 2000), was present (14%).

Peak N°	Retention time (min)	Compound	Molecular formula	% of total
1	**4.28**	**Sorbic acid**	**$C_6H_8O_2$**	**3.88**
2	5.00	Benzoic acid	$C_7H_6O_2$	10.95
3	5.16	Phosphoric acid	H_3PO_4	9.27
4	5.76	Succinic acid	$C_4H_6O_4$	11.67
5	6.17	Itaconic acid	$C_5H_6O_4$	0.27
6	7.54	Octanoic acid	$C_8H_{16}O_2$	0.10
7	8.68	Malic acid	$C_4H_6O_5$	0.06
8	9.19	4-hydroxycyclohexylcarboxylic acid	$C_7H_{12}O_3$	1.76
9	10.08	Rythronic acid	$C_{16}H_{40}O_5Si_4$	0.08
10	10.58	α-hydroxycinnamic acid	$C_9H_{10}O_3$	0.11
11	12.01	Pimelic acid	$C_7H_{12}O_4$	0.35
12	13.17	Isocitric acid lactone	$C_6H_6O_6$	0.39
13	13.50	Cyclooctene-1,2-diol	$C_8H_{14}O_2$	0.21
14	13.71	Tricarballylic acid	C_6H_8O6	0.96
15	14.21	para-Coumaric acid	$C_9H_8O_3$	0.38
16	14.72	Terephtalic acid	$C_8H_6O_4$	0.08
17	**15.27**	**Citric acid**	**$C_6H_8O_7$**	**44.74**
18	16.37	Ferulic acid	$C_{10}H_{10}O_4$	0.15
19	17.11	2,4,6-tri-tert-butylphenol	$C_{18}H_{30}O$	0.24
20	18.34	Palmitic acid	$C_{16}H_{32}O_2$	0.10
21	19.92	1H-Indole-2,3-dione-6-ethoxy	$C_{22}H_{22}N_2O_5$	0.08
22	22.26	1,8-Dihydroxy-3-(hydroxymethyl)-9,10-anthracenedione (Aloe-emodin)	$C_{15}H_{10}O_5$	14.01

***TABLE 1**. List of species identified by GC-MS in the* Aloe arborescens *commercial preparation. The relative abundance is expressed as percentage of total volume injected. Preservatives are indicated in bold.*

3.4.2 Aloe arborescens affects cancer cell proliferation

It is already known that *Aloe arborescens* has anti-proliferative and anti cancer effects (Lissoni, 2009; Bedini, 2009), however the molecular mechanisms underlying the cellular response to *Aloe* treatment remains to be defined. This prompted us to analyze the effect of an *Aloe arborescens* leaf extract on cell proliferation at cellular and molecular level, by comparing the rate of cell proliferation, the cell-cycle distribution and the expression of cell cycle-related molecular markers in *Aloe*-treated and untreated human cells. These analyses were performed in A431 (epidermoid skin carcinoma), MDA-MB231 (metastatic breast cancer), CaCo-2 (epithelial colorectal adenocarcinoma) and HaCaT spontaneously immortalized keratinocytes. As shown in Figure 1, we reproducibly found that *Aloe* extract reduces the cell proliferation rate in all cell lines tested. At 54 hrs of exposure to *Aloe*, a 30 to 40% reduction in the number of cells was observed in MDA-MB231, CaCo2 and HaCaT cells while A431 cells, stopped to proliferate and underwent massive cell death (Figure 1D).

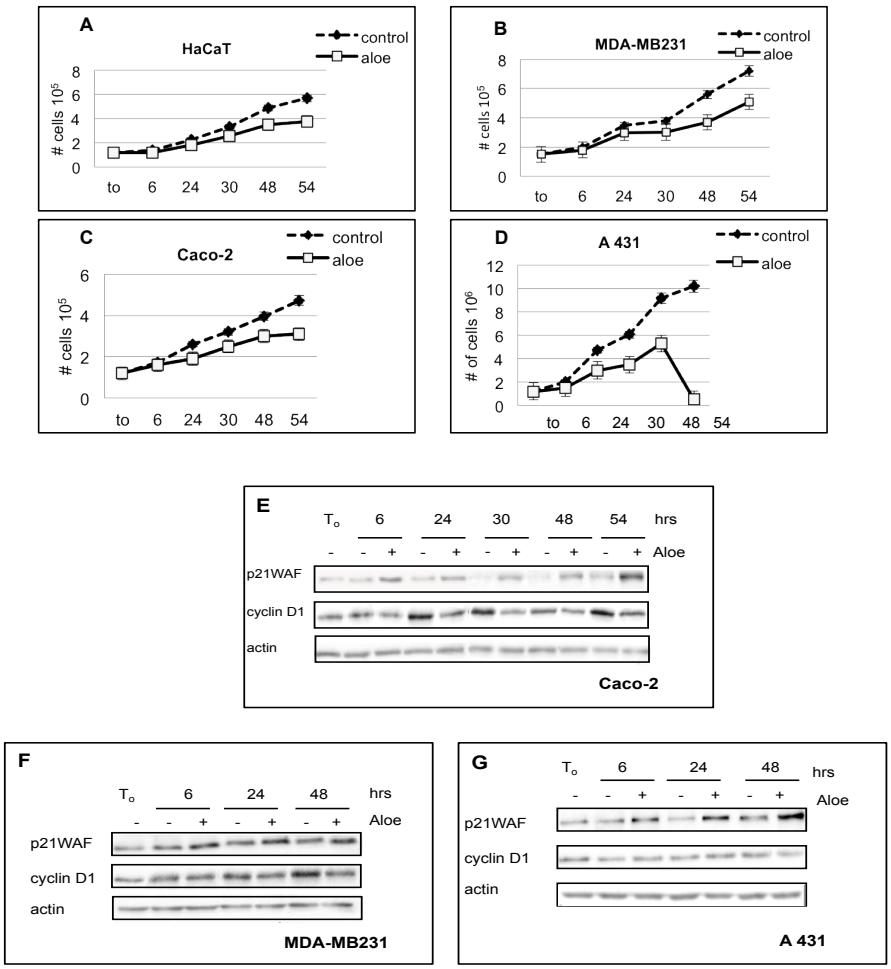

Figure 1. *(A) Proliferating HaCaT, (B) MDA-MB231, (C) CaCo-2, (D) A431 cells were incubated in complete cell culture medium supplemented or not with Aloe extract (1:10 v/v). Control and Aloe-treated cells were collected at 6, 24, 30, 48 and 54 hours and counted in a Burker chamber. (E) Proliferating CaCo-2, (F) MDA-231, (G) A431 cells were incubated in complete cell culture medium supplemented or not Aloe extract (1:10 v/v). Control and Aloe-treated cells were harvested at indicated different times (hrs). Equal amount of cell lysates were subjected to immunoblot analysis with antibodies against cyclin D1 and p21WAF. Actin was used as a loading control.*

The cell cycle distribution of control and *Aloe*-treated cells by flow cytometry show that HaCaT cells display only a slight increase (3%) in the percentage of G2/M cells after 48 hrs of *Aloe* treatment (Figure 2), while the other cell lines tested display an increase of cells in S and/or G2/M phase with a compensatory decrease of G0/G1 phase population indicating that cells were unable to resume the cell cycle at normal phase transit rate. Moreover, except for HaCaT keratinocytes, *Aloe* treatment also caused a significant increase in sub-G1 cell population.

Expression of the cell cycle markers p21WAF and Cyclin D1 was also investigated to explore *Aloe* effect at the molecular level. Immunoblots with the appropriate antibodies show that *Aloe* treatment significantly induced p21WAF in all tumor cells tested while Cyclin D1 expression was inhibited in CaCo-2 and MDA-MB231 cells (Figure 1E and F). Cyclin D1 is a labile factor required at high level for progression through the G1 phase of the cell cycle. Mitogenic pathways directly up-regulate the expression of Cyclin D1, therefore, impaired induction of Cyclin D1 with the concomitant increase of p21WAF is perfectly in line with the ineffectiveness of *Aloe*-treated cells to efficiently resume the cell cycle. Unexpectedly, A431 cells seemed to be unable to regulate Cyclin D1 expression (Figure 1G). We can speculate that the delay or failure of Cyclin D1 induction with the concomitant increase of p21WAF might be responsible, at least in part, for the massive A431 cell detachment at 54 hrs of Aloe treatment. Importantly, although we observed an increase of sub-G1 cells upon *Aloe* treatment (Figure 2), we were unable to observe PARP-1 cleavage by western blot analyses (data not shown) thereby indicating that *Aloe* treatment was not inducing apoptosis.

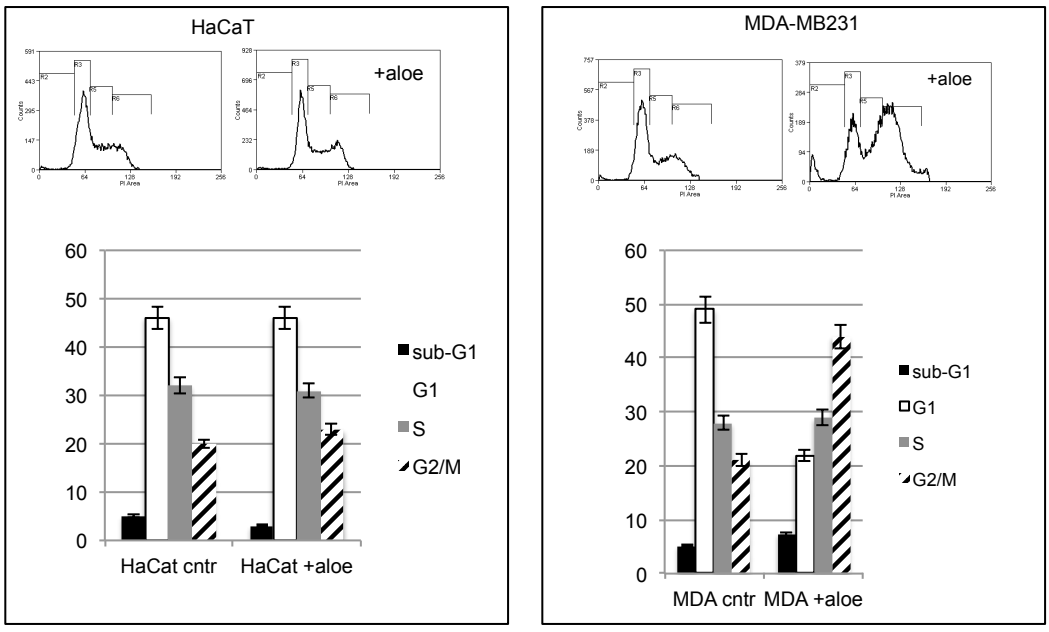

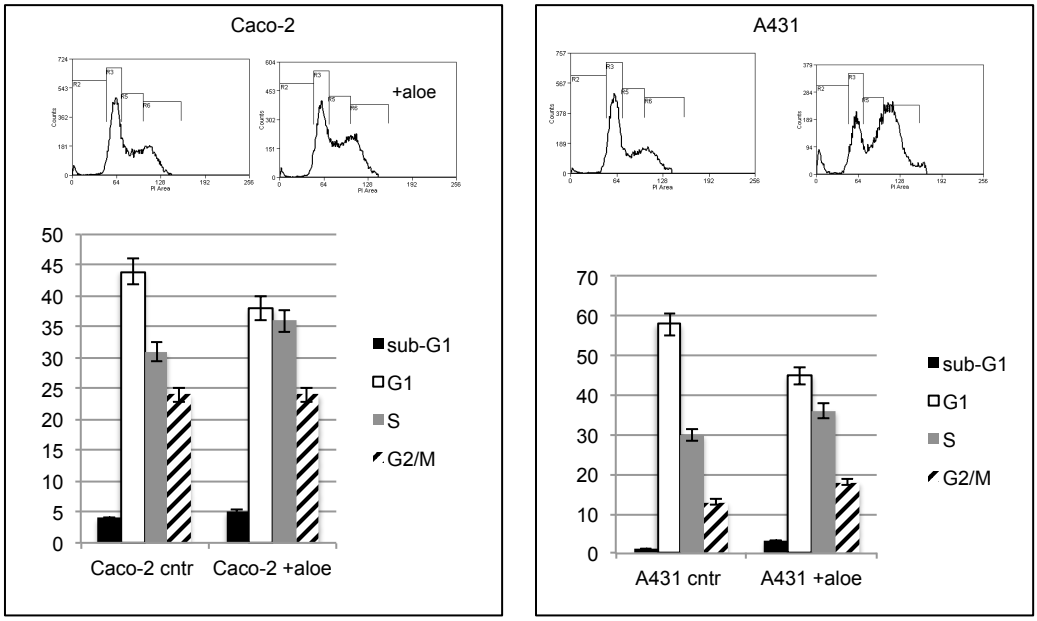

Figure 2. *Representative data obtained from flow-cytometric analysis of cell cycle of HaCat, MDA-MB231, CaCo-2 and A-431cells incubated with or without Aloe for 48 hours.*

3.4.3 Aloe arborescens induces keratinocyte differentiation

The concentrated leaf extract from *Aloe arborescens* plants has been used for hundreds of years in medicinal applications to help accelerating the healing process of the skin. Therefore, we decided to analyze the effect of *Aloe arborescens* on differentiation of human keratinocytes. We decided to compare the behavior of HaCaT cells (spontaneously immortalized human keratinocytes) that retain the ability to differentiate upon Ca^{2+} treatment with that of human primary keratinocytes. Addition of calcium to keratinocyte cultures is the most physiological stimulus to elicit a rather complete differentiation program, inducing not only biochemical markers but also many of the structural changes occurring *in vivo* (Dotto, 1999). To check whether the differentiation profile is altered by *Aloe* treatment, HaCaT cells were induced to terminally differentiate by adding 1.2 mM calcium in a serum-free medium, supplemented or not with *Aloe* extract. After 6 days of culture, *Aloe* treated cells became shrunken and pluristratified (Figure 3A). To provide molecular evidence that differentiation was

anticipated by *Aloe*-treatment, we performed immunoblot analyses on extracts derived from treated and untreated cells. In particular, we observed that Involucrin and Transglutaminase, two well characterized differentiation markers (Paramio, 1997) were expressed at higher levels in *Aloe*-treated cells. Conversely, DNp63a that is associated with the proliferative potential of epithelial cells and disappears in terminally differentiated keratinocytes (Di Costanzo, 2009), was down-regulated earlier upon *Aloe* treatment (Figure 3B).

In human primary keratinocytes (NHEK), *Aloe* treatment caused a dramatic increase of Involucrin gene expression that was already evident after 1 day of treatment. Similarly to what we have observed in HaCaT cells, DNp63a level decreased faster in *Aloe*-treated keratinocytes compared with control cells (Figure 3C).

We then looked more deeply into the effect of *Aloe* treatment during the early phases of HaCaT cell differentiation. To this purpose, HaCaT cells were seeded at medium density ($2.5x10^5$) in complete medium supplemented or not with *Aloe* extract (1:10 v/v) and collected before *Aloe* addition (t0) or after 6, 24, 30, 48 and 54 hours after *Aloe* treatment (Figure 3D). Equal amounts of cell lysates were subjected to immunoblot analysis to detect endogenous p21WAF and Cyclin D1. DNp63a and Cytokeratin 1 (CK1) were also monitored as early differentiation markers. As shown in Figure 3D, we initially observed an increase of Cyclin D1 protein levels both in *Aloe*-treated and untreated keratinocytes. However, according to what observed in tumor cells, Cyclin D1 tended to be down-regulated faster in *Aloe*-treated HaCaT cells while the p21WAF protein was up-regulated only in *Aloe*-treated cells. At 54 hrs of *Aloe* treatment, the remarkable decrease of Cyclin D1 along with sustained expression of p21WAF indicate that keratinocytes were anticipating cell cycle withdrawal. p21WAF-depleted keratinocytes exhibit an increased proliferative potential and a drastic down-modulation

of keratinocyte differentiation markers (Di Cunto, 1998) pointing to an essential involvement of p21WAF in the control of keratinocyte terminal differentiation. In line with these observations, compared to control cells, *Aloe*-treated keratinocytes exhibited higher levels of p21WAF and CK1, in agreement with the induction of a differentiation program. However, the persistence of DNp63a protein expression indicates that both treated and untreated keratinocytes were not fully differentiated (Figure 3D).

Cyclin D1 protein is known to increase under mitogenic signals, through activation of the ERK's pathway. Remarkably, immunoblot analysis of lysates from proliferating HaCaT keratinocytes treated for 24 hrs with increasing amounts of *Aloe arborescens* extract (20% or 50% v/v) show that the reduction of Cyclin D1 and phosphorylated ERKs, as well as the induction of p21WAF and CK1, was dose-dependent. Moreover, the signal corresponding to the cleavage of PARP1 was not enhanced, thus indicating that cells were not undergoing apoptosis (Figure 3E). We then decided to look at the effect of *Aloe* treatment on squamous carcinoma cell lines (SCC011 and SCC022). Squamous cell carcinoma (SCC) is an uncontrolled growth of abnormal cells arising in the squamous layer, which composes most of the skin's upper layers. SCC cells retain high levels of DNp63a that is absolutely required for the survival of early stages of the squamous carcinoma. We first determined the rate of cell proliferation in control and *Aloe*-treated SCC011 and SCC022 cells. As shown in Figure 4A and B, in *Aloe* containing medium both SCC011 and SCC022 cells stop growing. The cell cycle profile of *Aloe*-treated SCC022 cells reveals a dramatic increase in percentage of sub-G1 cells at the expenses of G1 and G2/M cells (Figure 4C).

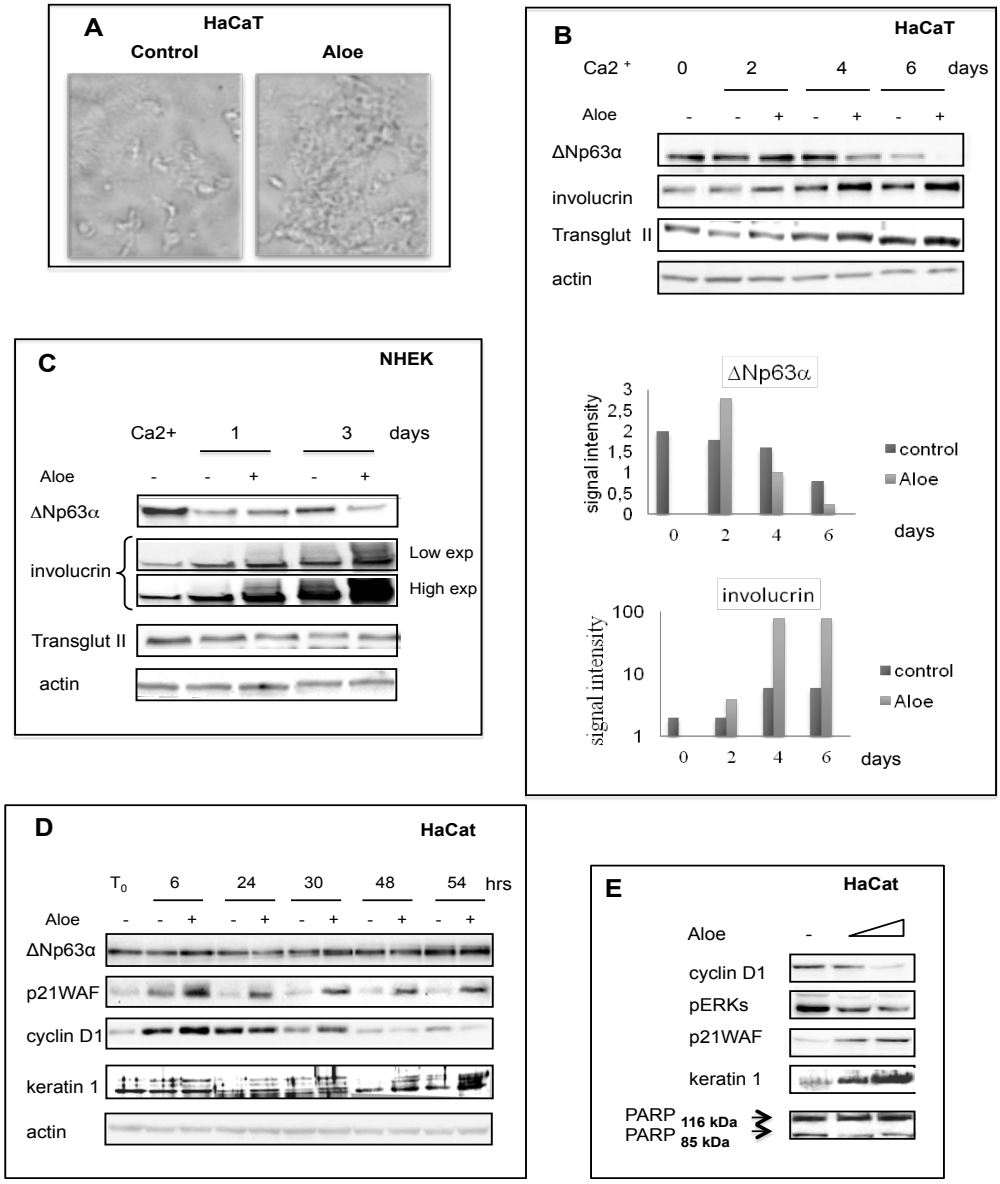

Figure 3. *(A) Confluent HaCaT cells were induced to terminally differentiate by serum withdrawal and calcium addition (1,2 mM) in DMEM cell culture media supplemented or not with Aloe extract (1:10 v/v). After 6 days of culture treated and not-treated cells were fixed with cold methanol and analyzed by phase-contrast microscopy. (B) Differentiated HaCaT and (C) NHEK cells in presence or absence of Aloe extract (1:10 v/v) were collected at different indicated times. Equal amount of cell lysates were subjected to immunoblot analysis with antibodies against DNp63a, involucrin and transglutaminase type II. Actin was used as a loading control. (D) Proliferating HaCaT cells were incubated in DMEM or DMEM Aloe extract containing medium (1:10 v/v). Control and Aloe-treated cells were collected at 6, 24, 30, 48 and 54 hours. Equal amount of cell lysates were subjected to immunoblot analysis with antibodies against DNp63a, cyclin D1, p21WAF and Keratin 1, an early differentiation marker. Actin was used as a loading control. (E) Proliferating HaCaT cells were incubated in DMEM or DMEM Aloe extract containing medium (20% or 50% v/v). Control and Aloe-treated cells were collected at 24 hours. Equal amount of cell lysates were subjected to immunoblot analysis with antibodies against cyclin D1, p21WAF, Keratin 1 an early differentiation marker and PARP-1. Actin was used as a loading control.*

In SCC011 the increase of subG1 cells was less dramatic although the S phase arrest was evident (Figure 4D). Growth arrest was associated with a characteristic enlarged and flattened cell morphology as shown by fluorescence microscopy in SCC011 cells (Figure 4E). Interestingly, compared to SCC022, SCC011 cells display a stronger activation of the Akt survival marker (data not shown) suggesting that Akt may, indeed, counteract *Aloe*-induced cell death. Western blot analysis of control and *Aloe* treated SCC011 shows a dramatic decrease of DNp63a and a concomitant increase of p21WAF and CK1 polymers (Figure 4F). Importantly, since it has been shown that SCC011 and SCC022 proliferation is strictly dependent on DNp63a (Rocco, 2006), the dramatic reduction of DNp63a induced by *Aloe* in these tumor cells may account for the cell death observed.

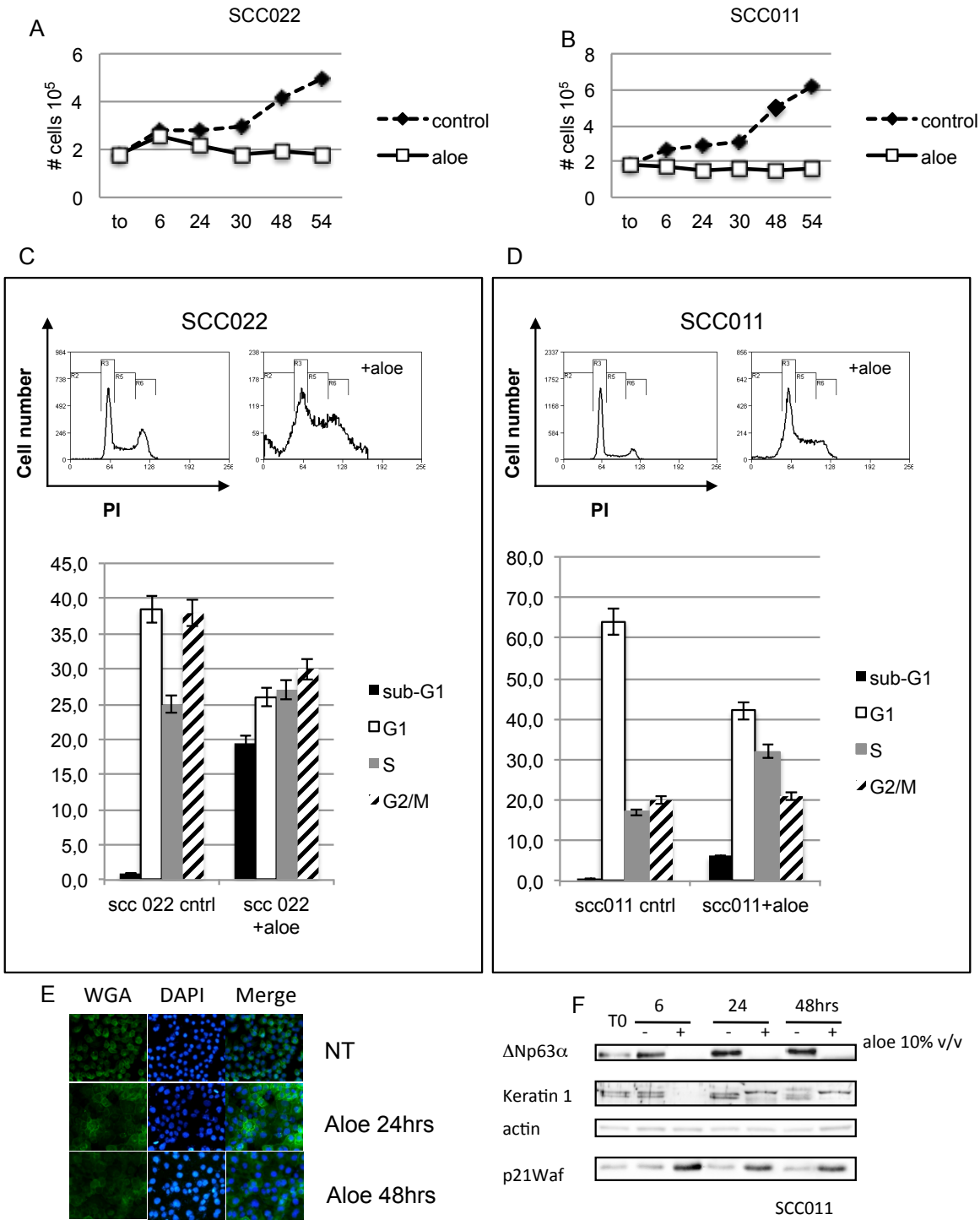

Figure 4. *(A) Proliferating SCC022 and (B) SCC011 cells were incubated in complete cell culture medium supplemented or not with Aloe extract (1:10 v/v). Control and Aloe-treated cells were collected at 6, 24, 30, 48 and 54 hours and counted in a Burker chamber. (C) and (D) Representative data obtained from flow-cytometric analysis of cell cycle of SCC022 and SCC011 cells incubated with or without Aloe for 48 hours. (E) Representative images of SCC011 cells fluorescently stained with WGA (labeling membrane glycoproteins) or DAPI (F) Equal amount of cell lysates were subjected to immunoblot analysis with indicated antibodies. Actin was used as a loading control.*

3.4.4 Antibacterial tests

Inner-leaf extract from *Aloe vera* was shown to inhibit growth of Streptococcus and Shigella species in vitro (Arunkumar, 2009). Aloe-emodin, has been proposed to have direct antimicrobial activity. To assess whether the *Aloe* aqueous extract had antibacterial effects, two different plate antibacterial assays were performed with a panel of nine bacterial strains. As a first assay, LB or MRS plates were disseminated with each of the bacterial strain and spotted with the aliquots of *Aloe* extract. As a second assay, LB or MRS solid media containing various amounts of *Aloe* extract were spotted with aliquots of bacterial cells previously grown in liquid media. With both assays no inhibition of bacterial growth was observed for any of the nine bacterial strains analyzed (data not shown).

3.4.5 Proteomic analysis

Although *Aloe arborescens* extract has been largely used for its immunostimulating and anticancer properties, little is known of its impact at the proteome level. We thus decided to look at cell proteome changes of HaCaT keratinocytes induced by *Aloe* treatment. Protein extracts from untreated (Control) or *Aloe* treated (Sample) HaCaT cells were fractionated by 2D-GE and stained with colloidal Blue Coomassie. The gels were run in triplicate and compared using the ImageMaster 2D Platinum 6.0 software. A few initial reference points (landmarks) were affixed for gels alignment in the first step of the images analysis. The spots were detected on the gels and the software "matched" the gels and the corresponding spots. The spots representing the same protein in different gels were paired. Pairs were automatically determined using ImageMaster powerful gel matching algorithm. The different 2DE images were compared by synchronized 3-D spots view. Among the spots corresponding to *Aloe*

sensitive proteins clearly detected in repeated trials, 17 were selected for proteomic analysis. The image analysis enabled the identification of 8 spots that were present either in higher amount or exclusively in the *Aloe*-treated sample, thereby indicating that they were induced by *Aloe* treatment. In the control sample, instead, 9 spots that were undetectable or whose signal decreased after *Aloe* treatment were detected. These spots were selected for mass spectral identification by the merging of images analyses. Proteins excised from the gel were reduced, alkylated and, in situ, digested with trypsin. The resulting peptide mixtures were analyzed by nanoLC/MS/MS experiments. The peptide mixtures were fractionated by nanoHPLC and sequenced by tandem mass spectrometry, generating sequence information on individual peptides. MSMS spectra were used to search for a non-redundant sequence using the in-house MASCOT software, thus taking advantage of the specificity of trypsin and of the taxonomic category of the samples. The number of measured masses that matched within the given mass accuracy was recorded and the proteins that had the highest number of peptide matches were examined leading to the identification of the protein components. As further selection criteria, only the proteins, identified by MASCOT search with at least 2 peptides, and found exclusively in the replicates were selected. The list of proteins identified by this approach is illustrated in Table 2.

Among the identified proteins, a signal corresponding to **Tubulin** showed an increment in the treated sample as well as that of a powerful antimicrobial peptide known as **Dermcidin**. This observation was particularly intriguing as we failed to detect a direct antimicrobial activity of *Aloe arborescens* against several bacterial strains (see above). Dermcidin (DCD) is constitutively expressed in eccrine sweat glands and is part of the constitutive innate defence of human skin and stimulates keratinocytes to produce cytokines and chemokines (Niyonsaba, 2009). So far, no Dermcidin expression was

found, neither at RNA nor at protein level, in primary keratinocytes, fibroblasts and melanocytes both in normal conditions, or in cells stimulated by LPS, TNFα or TPA. Although the *Aloe* ability to stimulate Dermcidin production by keratinocytes needs further investigations, our observation provides a novel insight for the *Aloe* implication in microbicidal ability and skin immunity. *Aloe* treatment also induced the expression of molecules involved in several aspects of keratinocyte proliferation and differentiation such as **GRP78**, **Prohibitin** and **Stathmin**. Prohibitin is a potential tumor suppressor protein that exhibits growth suppressor ability by repressing E2F-mediated gene transcription (Joshi, 2003). Stathmin is a microtubule-destabilizing protein and, in association with Tubulin and HSP70, was reported to be functionally relevant in the control of numerous regulatory pathways that require a reorganization of the entire cytoskeleton. GRP78 (also known as HSRPA5) was found to be increased in the suprabasal layers of normal epidermis and can work as a molecular chaperone in cooperation with other Heat Shock Proteins being part of the unfolded protein response (UPR) activated in differentiating epidermal keratinocytes (Sugiura, 2009). In *Aloe*-treated HaCaT cells, heat shock proteins, essential for the survival of malignant cells, were under-represented. However, heat-shock proteins also occur under non-stressful conditions, simply "monitoring" the cell's recycling or folding. Further experiments are needed to clarify this phenomenon.

Remarkably, Calmodulin and Keratin 1 signals were detected only in the control sample and disappeared following the *Aloe* treatment. The remaining proteins exhibited a sensitive decrement in the *Aloe*-treated sample.

Aloe-treated Spot	MW	Score	Protein	Swissprot code	Peptides	Sequence coverage
1	72402	186	78 kDa glucose-regulated protein	P11021	8	20%
2	50095	325	Tubulin beta chain	P07437	11	34%
3	11391	37	Dermcidin	P81605	3	30%
4	29843	60	Prohibitin	P35232	6	25%
5	22826	175	Heat shock protein beta-1	P04792	4	33%
6	22436	53	UMP-CMP kinase	P30085	4	42%
7	23569	47	Glutathione S-transferase P	P09211	6	42%
8	17292	60	Stathmin	P16949	2	18%
Control Spot	MW	Score	Protein	Swissprot Code	Peptides	Sequence coverage
9	62255	83	Keratin, type I cytoskeletal 9	P35527	5	10%
10	71082	224	Heat shock cognate 71 kDa protein	P11142	13	23%
11	73920	49	Stress-70 protein, mitochondrial	P38646	7	12%
12	70294	68	Heat shock 70 kDa protein 1A/1B	P08107	4	8%
13	61187	492	60 kDa heat shock protein, mitochondrial	P10809	24	50%
14	42052	156	Actin, cytoplasmic 1	P60709	9	34%
15	32726	267	Nucleophosmin	P06748	10	26%
16	27871	189	14-3-3 protein sigma	P31947	9	37%
17	16827	101	Calmodulin	P62158	2	29%

Table 2. *List of proteins differentially represented in Aloe-treated or control HaCaT cells identified by Mass Spectrometry.*

3.5 Conclusions

The results presented in this study indicate a clear antiproliferative effect of an Aloe extract on several tumor cells and a prodifferentiative effect both on primary and immortalized human keratynocytes.

For a medicinal application perspective, our study supports the use of *Aloe arborescens* extract for topic treatment of hyperproliferative skin diseases or skin squamous cell carcinoma. *In vivo* animal experimentation will be necessary to further confirm the proposed health benefit of the extract.

3.6 References

Arunkumar S, Muthuselvam M, 2009. Analysis of phytochemical constituents and antimicrobial activities of Aloe vera L. against Clinical Pathogens. World Journal of Agricultural Sciences, **5**(5):572-576.

Baccigalupi L, Di Donato A, Parlato M, Luongo D, Carbone, V, Rossi M, Ricca E, De Felice M, 2005. Small surface-associated factors mediate adhesion of a food-

isolated strain of Lactobacillus fermentum to Caco-2 cells. Res. Microbiol., **156**:830-8365

Bedini C, Caccia R, Triggiani D, Mazzucato A, Soressi GP, Tiezzi A, 2009. Micropropagation of Aloe arborescens Mill: A step towards efficient production of its valuable leaf extracts showing antiproliferative activity on murine myeloma cells. Plant Biosystems-an International Journal Dealing with all Aspects of Plant Biology, **143** (2): 233.

Botes L, van der Westhuizen FH, Du Toit L, 2008. Phytochemical contents and antioxidant capacities of two Aloe greatheadii var, davyana extracts. *Molecules* **13**:2169-2180.

Di Costanzo, A.; Festa, L.; Duverger, O.; Vivo, M.; Guerrini, L.; La Mantia, G.; Calabrò V., 2009. Homeodomain protein Dlx3 induces phosphorylation-dependent p63 degradation. Cell Cycle 8(8),1185-95.

Di Cunto F.; Topley, G.; Calautti, E.; Hsiao, J.; Ong, L.; Seth, P.K.; Dotto, G.P., 1998. Inhibitory function of p21Cip/Waf1 in differentiation of primary mouse keratinocytes independent of cell cycle control. Science, 280:1069-72.

Dotto P, 1999. Signal Transduction Pathway controlling the switch between keratinocyte growth and differentiation. Critical reviews in oral biology and medicine,**10**: 442-457

Fanali S, Aturki Z, D'Orazio G, Rocco A, Ferranti A, Mercolini L, Raggi MA, 2010 Analysis of Aloe-based phytotherapeutic products by using nano-LC-MS. Journal of Separation Science **33**(17):2663-2670.

Fakhry S, Manzo N, D'Apuzzo E, Pietrini L, Sorrentini I, Ricca E, De Felice M, Baccigalupi L, 2009. Characterization of intestinal bacteria tightly bound to the human ileal epithelium. Research in Microbiology, **160**(10):817-823.

Greathead H, 2003. Plants and plants extracts for improving animal productivity. Proceedings of the Nutrition Society, **62**: 279–290

Hochstrasser DF, Patchornik A, Merril CR. 1988. Development of polyacrylamide gels that improve the separation of proteins and their detection by silver staining. Anal Biochem Sep;**173**(2):412-23

Infascelli F, Tudisco R, Mastellone V, Cutrignelli MI, Lombardi P, Calabrò, S, Gonzalez OJ, Pelagalli A, Grossi M, d'Angelo D, Avallone L. 2010. Diet Aloe supplementation in pregnant buffalo cows improves colostrum immunoglobulin content. Revista Veterinaria **21** (Suppl. 1): 151-153.

Joshi B, Ko D Ordonez-Ercan, Chellappan SP, 2003. A putative coiled-coil domain of prohibitin is sufficient to repress E2F1-mediated transcription and induce apoptosis. Biochem. Biophys. Res. Commun., **312**(2):459-6.

Kampa M, Alexaki VI, Notas G, Nifli AP, Nistikaki A, Hatzoglou A, Bakogeorgou E, Kouimtzoglou E, Blekas G, Boskou D, Gravanis A, Castanas E. 2004. Antiproliferative and apoptotic effects of selective phenolic acids on T47D human breast cancer cells: potential mechanisms of action. Breast Cancer Res., **6** (2): 63-74.

Laemmli UK. 1970. Cleavage of structural proteins during the assembly of the head of bacteriophage T4. Nature, **227**, 680-685.

Lefort K, Mandinova A, Ostano P, Kolev V, Calpini V, Kolfschoten I, Lieb J, Raffoul W, Hohl D, Neel V, Garlick J, Chiorino G, Dotto GP. Notch1 is a p53 target gene involved in human keratinocyte tumor suppression through negative regulation of ROCK1/2 and MRCKα kinases. Genes & Dev. 2007, 21, 562-577.

Lesca P. 1983. Protective effects of ellagic acid and other plant phenols on benzo[a]pyrene-induced neoplasia in mice. Carcinogenesis, 4(12): 1651-3.

Lissoni P, Rovelli F, Brivio F, Zago R, Colciago M, Messina G, Mora A, Porro G. 2009 A randomized study of chemotherapy versus biochemotherapy with chemotherapy plus Aloe arborescens in patients with metastatic cancer. In vivo **23**(1):171-5.

Liu L, Hudgins WR, Shack S, Yin MQ, Samid D. 1995. Cinnamic acid: A natural product with potential use in cancer intervention. Int J Cancer , **62**: 345–350.

Mori, H., Kawabata, K.; Yoshimi, N.; Tanaka, T., Murakami, T.; Okada, T.; Murai, H.; 1999, Chemopreventive effects of ferulic acid on oral and rice germ on large bowel carcinogenesis. Anticancer Res, **19**(5): 3775-8.

Naclerio G, Ricca E, Sacco M, De Felice M. 1993. Antimicrobial activity of a newly identified bacteriocin of B. cereus. Appl. Environ. Microbiol., **59**: 4313-4316

Niyonsaba F, Suzuki A, Ushio H, Nagaoka I, Ogawa H, Okumura K. 2009. The human antimicrobial peptide dermicin activates normal human keratinocytes. British Journal of Dermatology, **160**(2):243-249.

Paramio JM, Jorcano JL. 1997. Role of protein kinases in the in vitro differentiation of human epidermal HaCaT cells. Br. J. Dermatol., **137**(1):44-50.

Pecere T, Gazzola V, Mucignat C, Parolin C, Dalla Vecchia F, Cavaggioni A, Basso G, Diaspro A, Salvato B, Carli M, Palù G. 2000. Aloe-emodin is a new type of anticancer agent with selective activity against neuroectodermal tumors. Cancer Research, **60**:2800-2804.

Rocco JW, Leong CO, Kuperwasser N, DeYoung MP, Ellisen LW. p63 mediates survival in squamous cell carcinoma by suppression of p73-dependent apoptosis. Cancer Cell. 2006 Jan; **9**(1):45-56.

Srinivas G, Babykutty S, Sathiadevan PP, Srinivas P. 2007. Molecular mechanism of emodin action: transition from laxative ingredient to an antitumor agent. Med. Res. Rev., **27**(5): 591-608.

Sugiura K, Muro Y, Futamura K, Matsumoto K, Hashimoto N, Nishizawa Y, Nagasaka T, Saito H, Tomita Y, Usukura J, 2009. The unfolded protein response is activated in differentiating epidermal keratinocytes. J. Invest. Dermatol., 129(9):2126-35.

Vivo M, Di Costanzo A, Fortugno P, Pollice A, Calabrò V, La Mantia G. 2009. Downregulation of ΔNp63α in keratinocytes by p14ARF-mediated SUMO-conjugation and degradation. Cell Cycle, **31**; 8(21).

Wessel D, Flugge UI. 1984. A method for the quantitative recovery of protein in dilute solution in the presence of detergents and lipids. Analytical Biochemistry, **138(**1): 141-143.

Youngman P, Perkins JB, Sandman K. 1984. New genetic methods, molecular cloning strategies and gene fusion techniques for /Bacillus subtilis/ which take advantage of Tn/917/ insertional mutagenesis. In Hoch, J.A. and Ganesan, A.T. (eds), Genetics and Biotechnology of Bacilli. Academic Press, NY, pp. 103-111.

3.7 Acknowledgement

This work was funded by MIUR (PRIN 2009KFS94X_003) to V. Calabrò.

This work was also supported by Aloe-Beta-HDR sas Capriati a Volturno - ITALY.

3.8 Supporting information

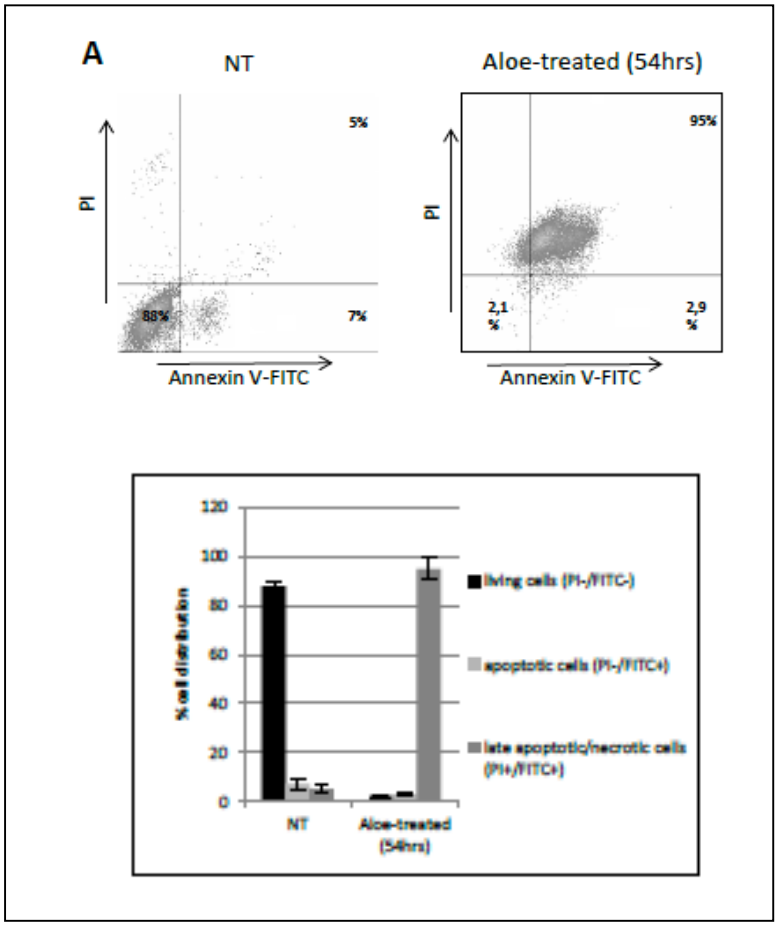

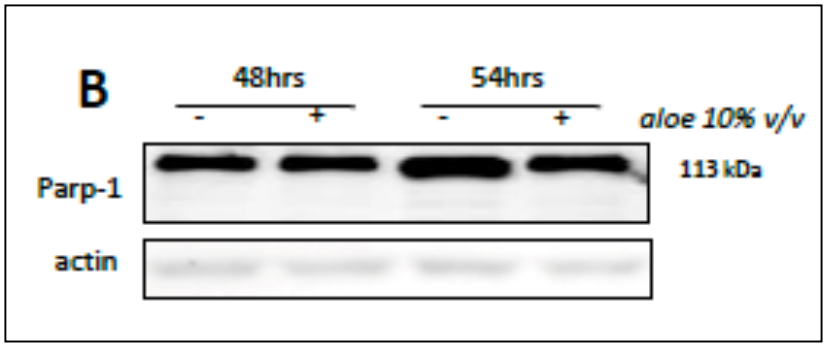

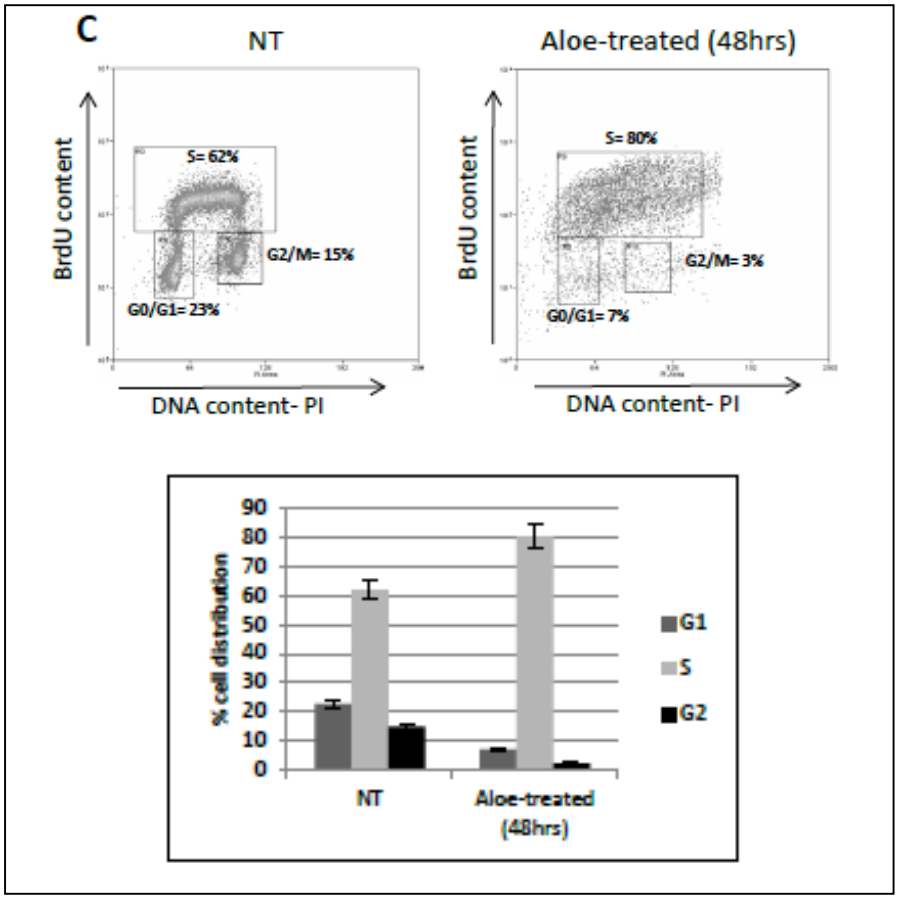

Fig. 1. *A431 cell response after Aloe- extract treatment. (A) Cell death was evaluated after treating A431 cells with 10% v/v Aloe-extract for 54hrs, and staining with Annexin-V. Flow cytometry profile represents Annexin-V-FITC staining in x axis and PI in y axis. Numbers represent the percentage of living or dead cells (B) Apoptosis (after 48 and 54 hrs of treatment) was assessed by Immuno-blotting of cellular total extract with anti-PARP1 antibody. (C) Cell proliferation was evaluated after treating A431 cells with 10% v/v Aloe-extract for 48hrs, and staining with BrdU reagent. Flow cytometry profile represents DNA content- PI staining in x axis and BrdU incorporation in y axis. The number represents the percentage of cell distribution during the cell cycle.*

8.1 Materials and Methods

Annexin V staining. After Aloe extract treatment (10% v/v for 54hrs), cells were washed twice with PBS and harvested with 0.05% trypsin in 0.15% Na2EDTA. Cells were centrifuged and washed twice in PBS. Then the cell pellet were resuspended in Annexin V-FLUOS (Roche) labelling solution (10mM Hepes/NaOH pH 7.4, 140 mM NaCl, 5mM CaCl2, Annexin V labelling reagent and 1ug/ml PI reagent) and incubated for 10 minutes at RT. Data acquisition was performed using a CyAn ADP Flow Cytometer (BeckmanCoulter, Inc., Milano, Italy) and Summit Software.

BrdU staining. After Aloe extract treatment (10% v/v for 48hrs) or not, cells were incubated with 30uM BrdU reagent (BectonDickinson kit) for 30 minutes at 37°C. Then cells were washed twice with PBS and harvested with 0.05% trypsin in 0.15%

Na2EDTA. Cells were centrifuged, washed in PBS, fixed with ice-cold 70% ethanol, and stored overnight at 4°C. Then fixed cells were washed in PBS and incubated with HCl 4M for 30 minutes at room temperature. Then cells were washed twice with PBS-Tween 0,1% and centrifuged at 1200 rpm for 5min 4°C. The cell pellet were resuspended in anti- BrdU-FITC labeling solution and incubated for 1hr at RT. After incubation, cells were washed twice with PBS-Tween 0,1% and centrifuged at 1200 rpm for 5min 4°C. The cell pellet were incubated with propidium iodide (50 μg/ml) and RNAse A (5 μg/ml) for 20 min at room temperature. Data acquisition was performed using a CyAn ADP Flow Cytometer (BeckmanCoulter, Inc., Milano, Italy) and Summit Software.

CHAPTER 4

Rescue of fructose-induced metabolic syndrome by antibiotics or faecal transplantation in a rat model of obesity

Blanda Di Luccia [1], Raffaella Crescenzo [1*], Arianna Mazzoli [1], Luisa Cigliano [1], Paola Venditti [1], Jean-Claude Walser [2], Alex Widmer [3], Loredana Baccigalupi [1], Ezio Ricca [1], Susanna Iossa [1#]*

1Department of Biology, Federico II University of Naples, Italy

2ETH Zurich, Genetic Diversity Centre, Zurich, Switzerland

3 ETH Zurich, Institute of Integrative Biology (IBZ), Zurich, Switzerland

**These authors contributed equally to the work.*

#Correspondence: Prof. Susanna Iossa, Department of Biology, Complesso Universitario Monte S.Angelo, Edificio 7, Via Cinthia - I-80126 Napoli ITALY.

Recently submitted for publication

4.1 Abstract

Background & Aims. A fructose-rich diet is one of the factors inducing the metabolic syndrome, a combination of health disorders significantly increasing the risk of diabetes and cardiovascular disease. The diet is also known to alter the microbial composition of the gut, although it is not clear whether such alteration is a consequence or one of the causes of the diet-induced health disorders. Aim of this work is to assess whether the gut microbiota is linked to the development of the diet-induced metabolic syndrome in rats.

Methods. Rats were either fed a standard or high-fructose diet. Groups of fructose-fed rats were treated with either antibiotics or faecal samples from control rats. Body composition, plasma metabolic parameters and tissue oxidative stress were measured in all the groups. A metagenomic approach was used to evaluate the bacterial composition of the gut of animals under different diets.

Results. The fructose-rich diet strongly altered the microbial composition of the gut and induced markers of metabolic syndrome, inflammation and oxidative stress. Metabolic markers of fructose-fed animals were significantly reduced when the animals were treated with antibiotic or fed faecal samples. The faecal transplant was also able to restore the microbial composition of the gut.

Conclusions. Our data suggest that in rats on a fructose-rich diet the development of the metabolic syndrome is directly correlated with the alteration of the gut microbial population/community. The data might indicat that the manipulation of the gut microbiota can be considered as a possible therapeutic strategy in the treatment of the metabolic syndrome.

4.2 Introduction

It is well established that diets, rich in simple carbohydrates as sucrose and fructose, can induce a wide range of metabolic alterations, including obesity, increased plasma triglyceride concentration, impaired glucose tolerance and insulin resistance[1-3]. However, the contribution of high-fructose diets to the development of obesity remains controversial, since some authors have not observed unequivocal evidence linking fructose consumption with metabolic disorders[2]. To address this issue, studies with animal models have proven particularly informative[4]. A recent study performed with nonhuman primates has shown that even in the absence of weight gain, fructose rapidly causes liver damages and that hepatic steatosis relates to the duration of fructose consumption[5]. In a different study with a rat model of obesity[6,7], a fructose-rich diet has been shown to impair glucose tolerance, to induce an oxidative stress status and to increase plasma non-esterified-fatty-acids (NEFA), considered as a reliable marker of the development of insulin resistance[8].

In the last decade the rapid development of metagenomic approaches has allowed the analysis of microbial communities present for example in the human gut. It is now clear that the microbial community found in the human gut is complex. It not only expands the metabolic properties of the gastrointestinal tract it also contributing to the health status of the host[9]. The role of microbes is now viewed as essential for human health and the gut microbiota as an important metabolic organ[9]. It is also clear now that the composition of the gut microbiota is influenced by changes of environmental factors, including the diet, although little is known about how individual species respond to such changes[9]. It has been reported that the presence of specific nutrient substrates can have an influence on the composition of the microbial community leading to changes in the function of the microbiota[10-12].

In this context it is reasonable to assume that a fructose-rich diet could alter the composition of the gut microbiota. However, whether such alteration really occurs and whether it is related to the adverse effects of a fructose-rich diet on health still remains to be addressed. Only very recent studies have started to address the role of microbiotia in animal models or humans exposed to a fructose-rich diet[3]. Hsieh et al[13] reported that the oral administration of a probiotic strain of *Lactobacillus reuteri* improves insulin resistance and reduces hepatic steatosis in rats fed with a fructose-rich diet, suggesting the probiotic-based approach as a promising therapeutic strategy in the treatment of the metabolic syndrome and of the type 2 diabetes.

Here we show that the detrimental effects caused by fructose-induced obesity in adult rats were abolished by an antibiotic treatment, suggesting a direct involvement of the microbiota in the induction of the metabolic syndrome. Similar, although less marked, beneficial effects were observed when fructose-fed rats were inoculated with faecal samples of rats under standard diet. A metagenomic analysis of the gut microbiota of the various animals was used to evaluate the alteration of the macrobiotic gut community composition in animals under different diets.

4.3 Materials and Methods

4.3.1 Animals and treatments. Male Sprague-Dawley rats (Charles River, Italy), of 100 days of age were caged singly in a temperature-controlled room (23±1°C) with a 12-h light/dark cycle (06.30-18.30). Treatment, housing, and killing of animals met the guidelines set by the Italian Health Ministry. All experimental procedures involving animals were approved by "Comitato Etico-Scientifico per la Sperimentazione Animale" of the University "Federico II" of Naples.

Rats were divided in two groups and were fed a fructose-rich or control diet (Mucedola 4RF21; Settimo Milanese, Milan, Italy) for 8 weeks as previously reported[6, 7, 14]. Rats fed the control diet were divided in two groups of six rats each: one group received water supplemented with antibiotic mix (Ampicillin 1 g/L + neomycin 0.5 g/L) (CA rats), while the second group did not received any further treatment and served as control (C rats). Rats fed the fructose-rich diet were divided in three groups, each composed of six rats: one group received water supplemented with the above antibiotic mix (FA rats), the second group was subjected to microbiota transplantation (FT rats), while the third group did not receive any further treatment (F rats). For microbiota transplantation, fresh faecal pellets (2 pellets for each rat) from all six donor rats (C rats) were collected and placed in transfer buffer (pre-reduced sterile phosphate buffered saline containing 0.05% cysteine HCl, 2 mL/g) on ice. The faecal pellets were homogenized, centrifuged at 800g for 2 min and the supernatant was collected. Diluted faecal supernatant was then orally inoculated to recipient rats (0.5 mL/rat) every third day during the 8 weeks dietary treatment period. During the treatments, body weight, food and water intake were monitored daily.

4.3.2 Metabolic analysis. To perform the glucose tolerance test the day before the sacrifice, rats were fasted for 6 hours from 09.00 a.m. Basal, postabsorptive blood sample was obtained from a small tail clip and placed in EDTA–coated tubes and then glucose (2 g/kg body weight) was injected intraperitoneally. Blood samples were collected after 20, 40, 60, 90, 120 and 150 min and placed in EDTA-coated tubes. The blood samples were centrifuged at $1400xg_{av}$ for 8 min at 4°C. Plasma glucose concentration was measured by colorimetric enzymatic method (Pokler Italia, Genova, Italy).

Plasma NEFA levels were measured by colorimetric enzymatic method (Roche Diagnostics, Mannheim, Germany). Plasma tumor necrosis factor alpha (TNF-α) concentrations were determined using a rat specific enzyme linked immunosorbent assay (R&D Systems, MN, USA) according to manufacturer's instruction. Plasma lipopolysaccharide (LPS) determinations were performed using a kit based upon a *Limulus amaebocyte* extract (LAL kit; Lonza, Basel, Switzerland).

To evaluate body energy and lipid content, sacrificed rats were killed by decapitation and livers and hindleg skeletal muscles were quickly removed. Guts were cleaned of undigested food and the carcasses were then autoclaved. After dilution in distilled water and subsequent homogenisation of the carcasses, duplicate samples of the homogenised carcass were analyzed for energy content by bomb calorimeter[7]. Total body lipid content was measured by the Folch extraction method[15].

4.3.3 Isolation of epididymal adipocytes and measurement of in vitro lypolitic capacity. Adipocytes were isolated from intra-abdominal epididymal white adipose tissue (WAT) as in [14]. Aliquots corresponding to 15000 cells were then incubated in the presence of 1 μM isoproterenol, with or without 0.1 μM insulin, for 2 h at 37 °C in a shaking bath. At the end of the incubation, aliquots were used for the determination of glycerol production, by incubating samples with Sigma glycerol reagent at 37 °C for 15 min and then monitoring absorbance at 540 nm against appropriate standards.

4.3.4 Preparation of whole tissue homogenates from liver and skeletal muscle. Whole tissue homogenates were prepared from liver and skeletal muscle as previously reported[6, 16]. The extent of the peroxidative processes in whole tissue homogenates was

determined by measuring the level of lipid hydroperoxides according to Heath & Tappel[17]. Determination of protein oxidative damage was performed measuring protein-bound carbonyl levels by the procedure of Reznick & Packer[18].

4.3.5 Western blot quantification of p-Akt in skeletal muscle tissue. Skeletal muscle tissue samples were denatured, subjected to electrophoresis and the gels were transferred onto PVDF membranes (Millipore, MA, USA). After preblocking, the membranes were incubated overnight at 4 °C with polyclonal antibody for p-Akt (Cell Signaling, MA, USA, diluted 1:1000 in blocking buffer). After washing, the membranes were incubated 1 hour at room temperature with a anti-rabbit, alkaline phosphatase-conjugated secondary antibody (Promega, WI, USA), and then incubated at room temperature with a chemiluminescent substrate, CDP-Star (Sigma-Aldrich, MO, USA). Data detection was carried out by exposing autoradiography films (Eastman Kodak Company, NY, USA) to the membranes. Quantification of signals was carried out by Un-Scan-It gel software (Silk Scientific, UT, USA). Akt was detected with polyclonal antibody (Cell Signaling, MA, USA, diluted 1:1000 in blocking buffer) and used to normalize the p-Akt signal.

4.3.6 Caecal sample preparation and DNA extraction. The caecal content was collected from 30 rats (six replicates for each of the five different treatment groups). Total genomic DNA was extracted using the QIAamp® DNA Stool Mini Kit (QIAGEN) following the manufacturer's instructions. Briefly, 200mg of each sample were homogenized in buffer ASL and were subjected to 2 x 45s intervals of bead-beating at speed 6.0 in a FastPrep Instrument with zirconia-silica beads (0.1-mm diameter, MP-Biomedicals). The tubes were incubated on ice for 2 min between bead-

beatings. After the bead-beating the samples were incubated at 95 °C for 5 min to lyse bacterial cells. After removal of potential inhibitors by incubation with an InhibitEx tablet, the lysates were treated with proteinase K and buffer AL at 70 °C for 10 min to remove protein and polysaccharides. DNA was precipitated by ethanol, applied to a column provided in the kit followed by two washing steps with buffers AW1 and AW2, and then dissolved in pre-heated sterile ddH2O. Genomic DNA was extracted in triplicate from each sample and the extracts were subsequently pooled in order to eliminate possible bias associated with DNA extraction.

4.3.7 PCR and amplicon preparation. Primers designed by Caporaso et al.[19] (515F: 5'-GTGCCAGCMGCCGCGGTAA-3') and Andersson et al.[20] (1061R: 5'-CRRCACGAGCTGACGAC-3') were used to amplify a ≈ 540nt region of the 16S rRNA gene. The amplicon covers the hyper variable regions V4, V5 and V6. Each 25ul PCR mix contained 2X Phusion Master Mix (BioLabs® Inc., New England), 10uM of each PAGE-purified primer (Microsynth, Switzerland) and 2 ul of template-DNA. The PCR conditions used were 98°C for 30s, 15 cycles of 98°C for 10s, 52°C for 30s and 72°C for 30s, followed by 72°C for 10min using a SensoQuest PCR cycler (Germany). The PCR products were checked for their length on 1,5% agarose gel with GelRed™ Nucleic Acid Gel Stain (Biotium Inc., USA) and purified with DNA clean and concentrator™-5 kit (Zymo Research, U.S.A). The DNA concentration was determined using Qubit® 2.0 Fluorometer and Qubit™ dsDNA HS Assays Kit (Invitrogen, Life Technologies). Equal amounts for each sample within the same group of the six replicates were pooled in order to eliminate possible bias associated with PCR amplification.

4.3.8 Illumina library preparation. Index libraries for the pooled and purified PCR products were prepared using the TruSeq™ DNA Sample Preparation kit following manufacturer's recommended protocols (Illumina, Inc., San Diego, Ca, USA). The quality and the quantity of the different libraries were assessed on a Bioanalyzer 2100 (Agilent, Palo Alto, CA) using a dsDNA HS chip (Agilent, Palo Alto, CA) and by qPCR using the Library Quantification Kit For Illumina sequencing platforms (KAPA Biosystems Inc., USA) respectively. Single read 500 cycle (SR500) sequencing was performed on an Illumina MiSeq at the Genomic Diversity Centre (GDC) at the ETH, Zurich, Switzerland following manufactures run protocols (Illumina, Inc., San Diego, CA, USA). The MiSeq Control Software Version 2.2 including MiSeq Reporter 2.2 was used for the primary analysis and the de-multiplexing of the raw reads.

4.3.9 Amplicon sequencing analyses. The raw reads were quality checked and filtered. Cutadapt version 1.2.1 was used to remove reads with TruSeq adapter sequences[38]. Cutadapt was also used to filter and trim reads of the PCR primer start sequences. The filtered reads were quality checked and quality filtered using PrinSeq Lite version 0.20.3[39]. Reads smaller than 150 nucleotides or containing ambiguous nucleotides (e.g. "N") were removed in this step. The remaining cleaned reads were de-replicated, de-noised (identity threshold 99%) and chimera checked (de-novo and reference based against the 16S gold reference database provided by Qiime) using Usearch[21] version 6. The reads were binned using reference mapping applying the Usearch option as part of QIIME version 1.6.0[40]. The remaining reads were passed to the QIIME pipeline. Uclust[21] was used to define OTUs at 97% sequence identity, which were assigned a taxonomy using the RDP classifier[22]. Representative sequences for each OTU were aligned with PyNast[23] and columns uninformative for phylogeny building were filtered

out using Greengenes[24]. The resulting alignments were used to build a phylogeny using FastTree[25]. The principal coordinates analysis (PCoA) was performed on pairwise unweighted UniFrac distances[26]. The hierarchical cluster tree was built using UPGMA (unweighted pair group method with arithmetic mean) on the UniFrac distance matrix.

4.3.10 Statistical analysis. Data are given as means±SEM of six different rats. Statistical analyses were performed by one-way analysis of variance followed by Tukey post hoc test. Probability values less than 0.05 were considered to indicate a significant difference. All analyses were performed using GraphPad Prism 4 (GraphPad Software, San Diego, CA, USA).

4.4 Results

4.4.1 Experimental set up

Male Sprague-Dawley rats 100 days old were used as a model of diet-induced obesity. Two groups of rats were fed either with control diet (group C, n=6) or with a fructose-rich diet (group F, n=6), known to induce early signs of obesity within 8 weeks of treatment[6, 7, 14]. In order to assess the role of the gut microbiota in diet-induced obesity, additional groups of rats, fed the same fructose-rich diet of group F, were treated with a mixture of two antibiotics (group FA, n=6) or with faecal samples from rats of group C (group FT, n=6). To ensure that each of the FT rats received a bacterial load similar in number and species, stools from all six control animals were pooled and rats of group FT fed with aliquots of the pooled mixture A fifth, control group of rats was fed control diet and treated with the same antibiotics given to rats of group FA (group CA, n=6). A schematic summary of the experimental design is shown in Fig. 1. In all our metabolic analysis no differences were observed between rats of groups C and CA indicating that

the antibiotic treatment did not have any effect on animals under the same diet regimen. For this reason, results from group CA are shown, in comparison with those of group C, as Supplementary Material Fig. 1.

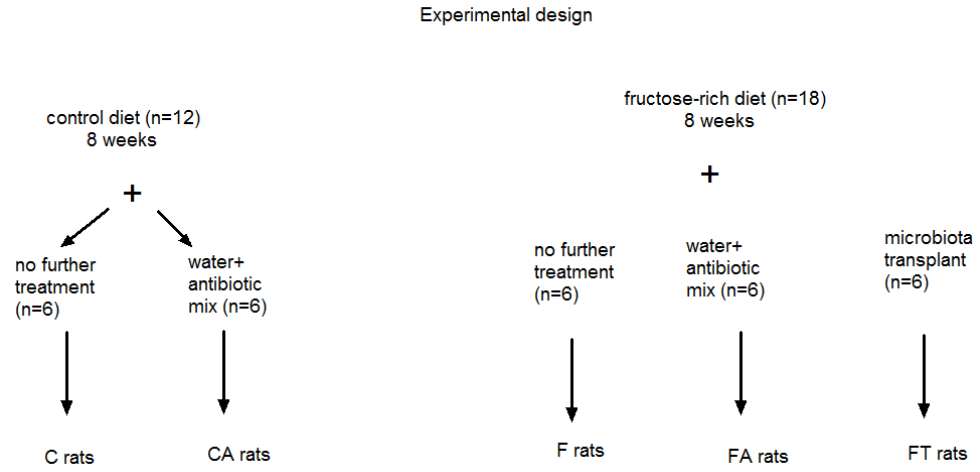

Figure 1. The experimental design. *Five groups of rats (n=6) were kept 8 weeks under different diet regimens. Group C: control diet; CA: control diet plus antibiotic treatment; F: low fat / high-fructose diet; FA: low fat / high-fructose diet plus antibiotic treatment; FT: low fat / high-fructose diet plus faecal samples of rats of group C (see Methods). After 8 weeks all animals were sacrificed for analysis.*

4.4.2 Antibiotics or faecal samples do not affect the fructose-induced increase in body energy and lipid content

A first metabolic characterization was carried out by analyzing the animal whole body composition. As shown in Fig. 2, fructose-fed rats displayed significantly higher body energy (panel A), lipids (panel B) and epididymal fat compared to controls. The treatment with antibiotics or faecal samples did not affect the increase in body energy (Fig.2A) or lipids (Fig.2B, C) due to the diet. Since changes in energy intake are the primary drive of obesity development, metabolisable energy (ME) intake was monitored throughout the experimental period to verify whether the fructose-induce increase in body energy and lipid content was due to an increase of ME. To this aim,

food intake and energy loss through faeces and urines were analyzed (Methods) and indicated that ME intake was similar in all experimental groups (C=19,700±1,200 kJ, CA=19,400±1,050 kJ, F=19,500±1,100 kJ, FA=19,200±990 kJ, FT=19,500±1,000 kJ).

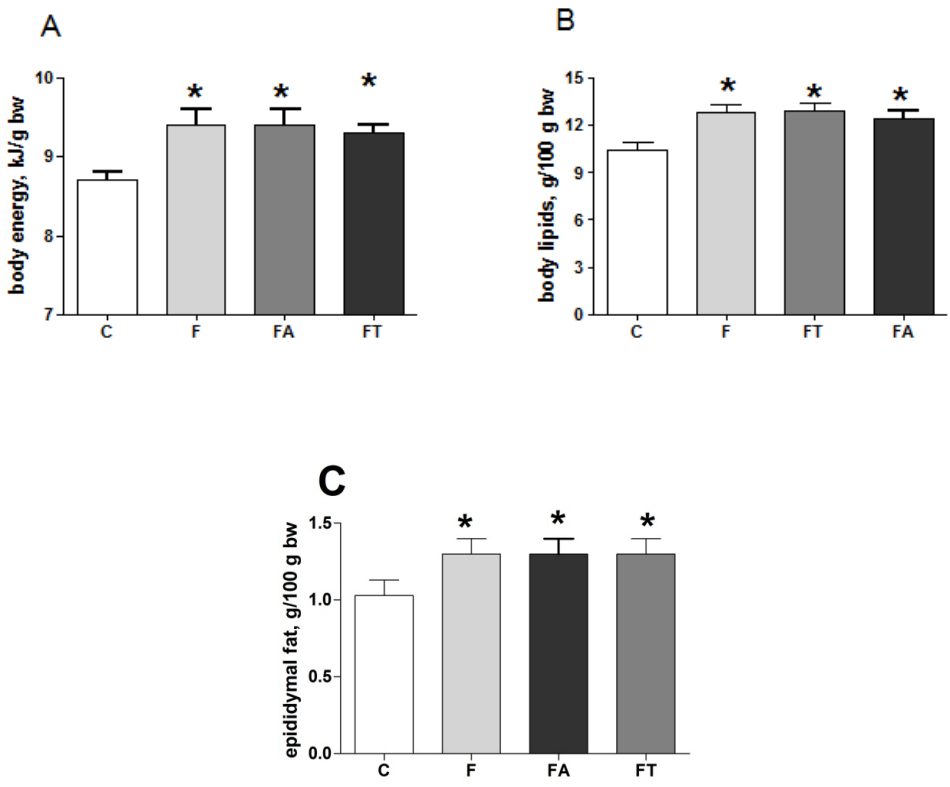

Figure 2. Body energy (A), lipids (B), and epididymal fat (C) *content in control (C), fructose-fed (F), fructose-fed+antibiotic (FA) and fructose-fed+faecal samples (FT) rats. Values are reported as means±SEM of six different rats. * P< .05 compared to C rats, # P< .05 compared to F rats (one-way ANOVA followed by Tukey post-test).*

4.4.3 Antibiotics or faecal samples reduce markers of the fructose-induced metabolic syndrome

The levels of plasma NEFA and glucose intolerance were followed as early markers of the development of metabolic derangement and insulin resistance. The Fig. 3A shows that the significant increase in plasma NEFA found in fructose-fed rats (group F vs C) was almost completely reversed by treatment with antibiotics (group FA) or faecal

samples (group FT). In addition, the inhibitory effect of insulin on lipolysis in epididymal WAT was nearly absent in fructose-fed rats (group F), but was completely restored by treatment with antibiotics (group FA) or faecal samples (group FT) (Fig. 3B). Changes in plasma glucose after the administration of a given dose of glucose were plotted over the time and the area under the curves was calculated and used to estimate glucose tolerance. The significantly higher values observed in fructose-fed rats (group F vs C) indicate that, with the same glucose injection, the increase in plasma glucose levels was more marked in fructose-fed rats (Fig. 3C). This reduced glucose tolerance was abolished by antibiotic treatment (group FA), while the treatment with faecal samples caused only a minor, not statistically relevant, reduction (group FT) (Fig. 3C). To assess the contribution of skeletal muscle to changes in glucose tolerance, we investigated a distal effector of insulin signalling in this tissue, and we found that pAkt levels were significantly lower in fructose-fed (group F) and fructose-fed+faecal samples (group FT) rats, while this decrease was abolished by antibiotic treatment (group FA) (Fig. 3D, S2).

As a third marker of the development of a metabolic syndrome, the plasma concentration of LPS was considered, since metabolic endotoxaemia is associated with obesity, metabolic syndrome and type 2 diabetes[27]. A statistically significant increase in plasma LPS levels were measured in fructose-fed rats and was partly reduced by both treatments, with antibiotic and faecal samples (fig. 3E). In addition, plasma concentrations of TNF-alpha were found four-fold higher in fructose-fed rats than in control animals (Fig. 3F) and both antibiotic treatment and faecal transplant were both able to completely abolish this increase (Fig. 3F).

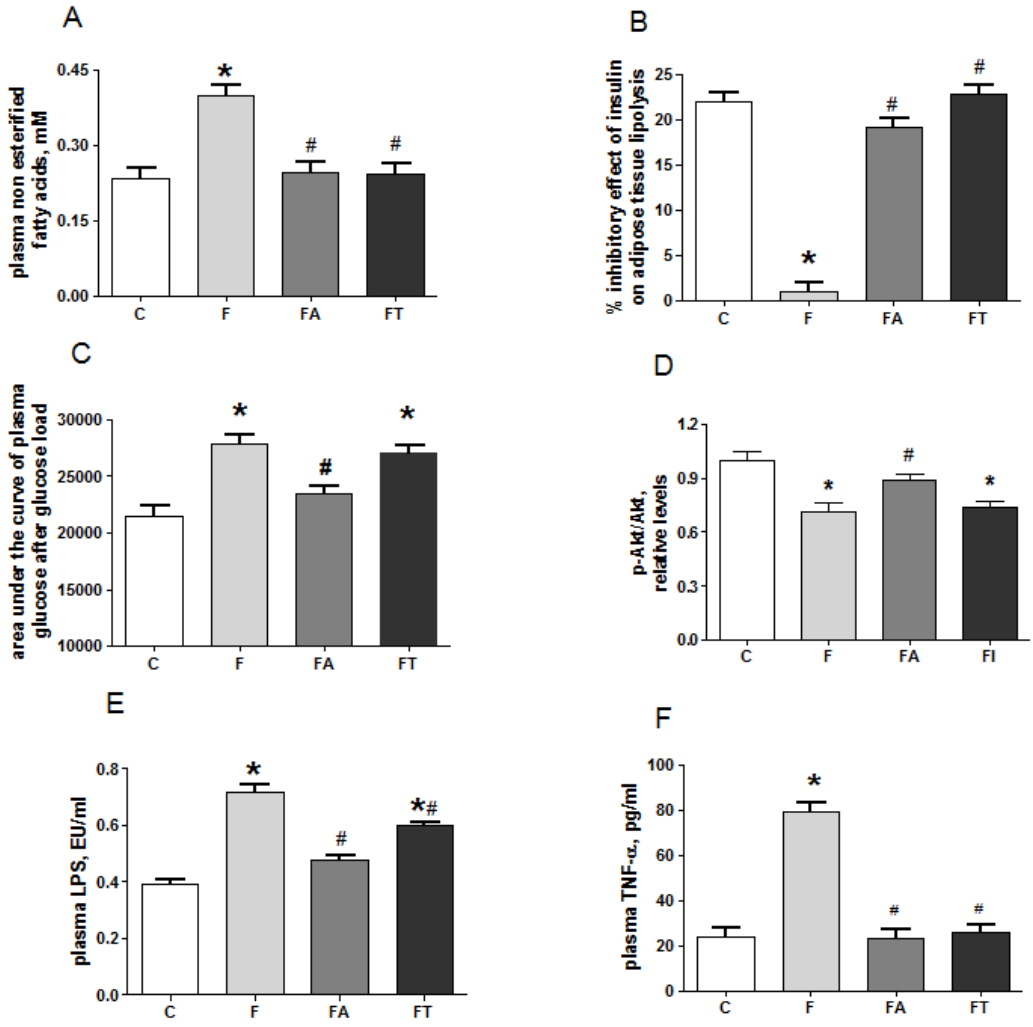

Figure 3. Plasma non esterified fatty acids (A), inhibitory effect of insulin on adipose tissue lipolysis (B), area under the curve of plasma glucose after glucose load (C), pAkt/Akt content in skeletal muscle (D), plasma LPS (E) and plasma TNF-α (F) *in control (C), fructose-fed (F), fructose-fed+antibiotic (FA) and fructose-fed+faecal samples (FT) rats. Values are reported as means±SEM of six different rats. * P< .05 compared to C rats, # P< .05 compared to F rats (one-way ANOVA followed by Tukey post-test). EU=endotoxin unit.*

4.4.4 Antibiotics or faecal samples reduce the fructose-induced tissue oxidative stress.

Oxidative damage in liver and skeletal muscle was evaluated by assessing the levels of damaged lipids (panels A and C of Fig. 4) and proteins (panels B and D of Fig. 4) in both tissues. Fructose-fed rats showed higher levels of oxidative stress than control rats in liver (panels A and B of Fig. 3) and skeletal muscle (panels C and D of Fig. 4).

Treatments with antibiotics or faecal samples totally or partially reversed the effect in both tissues, respectively (Fig. 4).

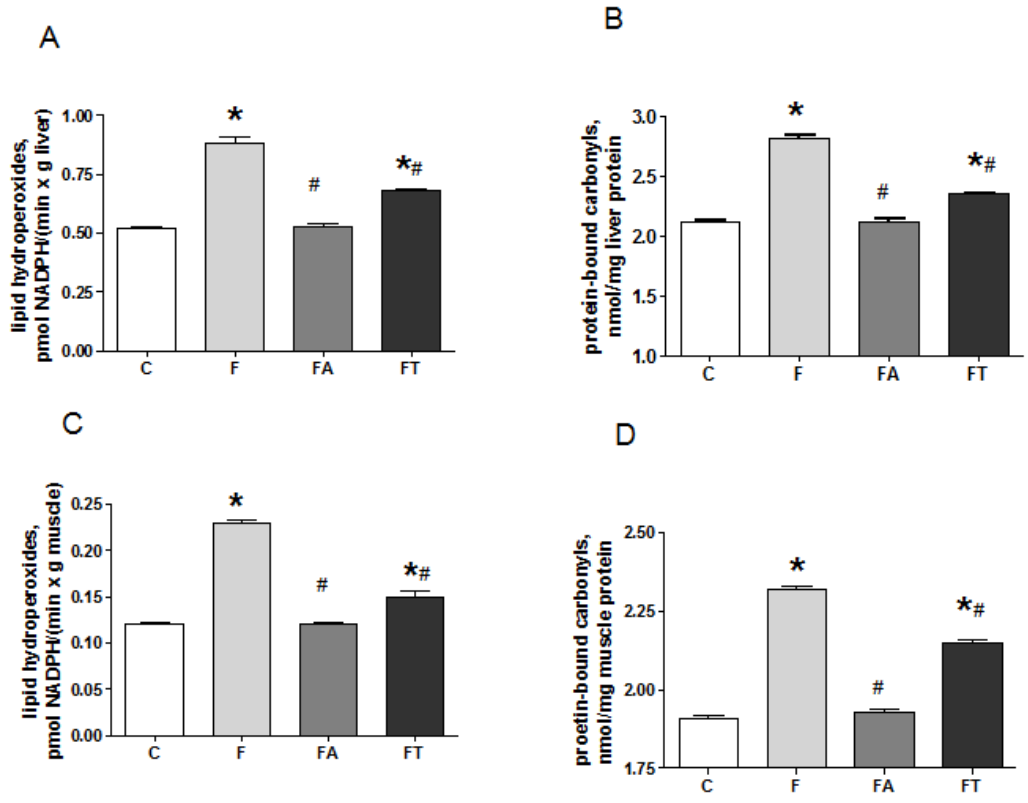

Figure 4 Lipid (A, C) and protein (B, D) oxidative stress in liver (A, B) and skeletal muscle (C, D) *in control (C), fructose-fed (F), fructose-fed+antibiotic (FA) and fructose-fed+faecal samples (FT) rats. Values are reported as means±SEM of six different rats. * P< .05 compared to C rats, # P< .05 compared to F rats (one-way ANOVA followed by Tukey post-test).*

4.4.5 Gut microbial composition

In order to investigate whether the fructose-rich diet affected the gut microbial composition and whether the faecal transplant was able to rescue such effects we used a metagenomic approach. Caecal samples were collected from all rats and used to extract genomic DNA. The V4-V6 hypervariable region of the 16S bacterial gene was then amplified by a low-cycle PCR and the ≈ 500 bp amplicons obtained used for Illumina sequencing. For cost considerations and for the modest variability previously observed

in the gut microbial composition of animals under the same diet regimen[41], the metagenomic analysis was performed by pooling together the DNA of the six replicates of each group as previously reported[42]. As detailed below, the analysis on pooled samples for rats of the control group was in agreement with previous data for rats under standard diet regimen [34] and showed a bacterial richness sufficient to observe significant reshaping of the gut microbiome following both antibiotic and transplantation treatments.

A single run (SR-500) sequencing was performed and 5' reads analysed by using QIIME pipeline[19].

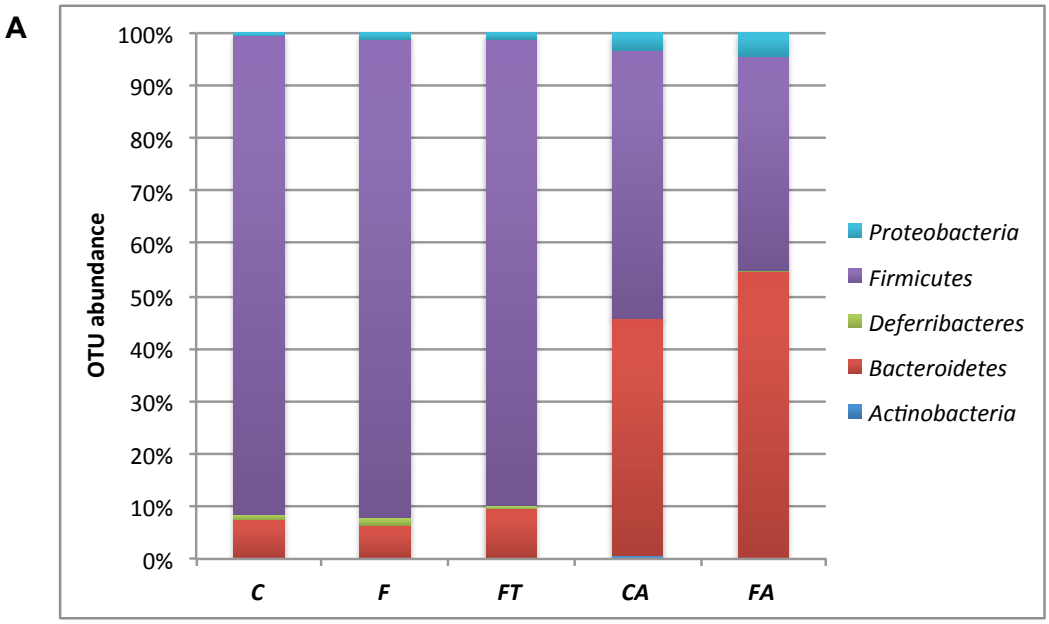

Figure 5A. *Relative OTUs (Operational Taxonomic Units) abundance at the Phylum level. The bar plot shows how the caecal microbiota distribution of each sample changes in rats of the various groups. Samples from animals treated with antibiotics (CA and FA) have very different composition compared to all other samples. (B-C) Variation of bacterial composition in/among the samples.*

The identified phylotypes show that the microbial community harbours two major *phyla* in all the five feeding groups: *Firmicutes* (91-40,6%) and *Bacteroidetes* (54,6- 6,2%) as

shown in Fig. 5A. Group C shows a microbial composition at the phylum level similar to that previously reported for rats under standard diet regimen[28].

The bacterial richness of the samples was estimated by Chao1 algorithm (alpha-diversity metric) and showed an increased microbial complexity in samples C and FT compared to the other three groups (not shown). In order to analyze relationships among samples based on differences in phylogenetic diversity (beta-diversity metric), principle coordinates (PC) were calculated (Fig. 5B) using UniFrac distances[26] between samples. Sample distribution in the PCoA plot (Fig. 5B) clearly shows that while samples CA and FA share a similar microbiota composition, they both strongly differ from the other three groups. This conclusion is in agreement with the taxonomical assignment at *phylum* level of Fig. 5A and is observed also within a phylogenetic tree using UPGMA algorithm (Fig. 5C). Not surprisingly, the microbial composition of the caecum of animals treated with antibiotics completely differs from that of animals not under antibiotic treatment.

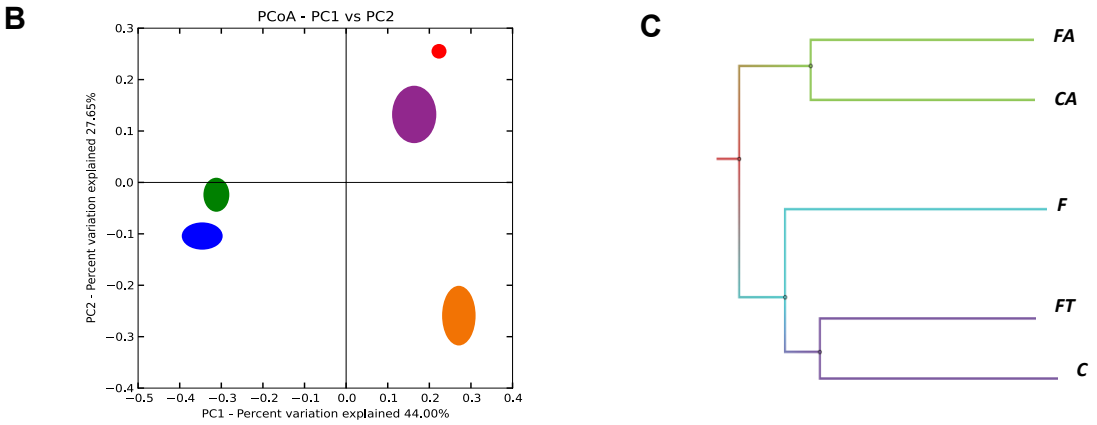

Figure 5B-C. *Beta-diversity is shown by Principal Coordinates Analysis (PCoA), based on UniFrac method: C and FT samples cluster close to each other in the plot, such as CA with FA, while F sample occupies a different area. (C) Clustering of caecal microbiotas of rats, fed with different diets, was obtained by UPGMA algorithm. It shows that samples C and FT have a more similar composition compared to F sample and to CA and FA samples, according to PCoA distribution.*

Because of the strong alterations caused by the antibiotic treatment, only data from C, F and FT groups were considered for the analysis of the variations at the genus taxonomic level.

As shown in Fig. 6, most differences lies in the *Firmicutes* phylum with the *Lactobacillus* genus significantly decreased in fructose-fed animals (46.2%) in comparison with control animals (62,4%). Treatment with faecal samples (group FT) restored *Lactobacillus* representativeness (60,3%). The same trend of rescue of C microbial distribution is observed in other bacterial groups, for example, in the *Erysipelotrichacaee* family (C: 1.7%; F: 5.5%; FT: 1.0%) and the *Ruminococcus* genus (C: 5.8%; F: 17.3%; FT: 8.8%) and other genera listed in Table 1

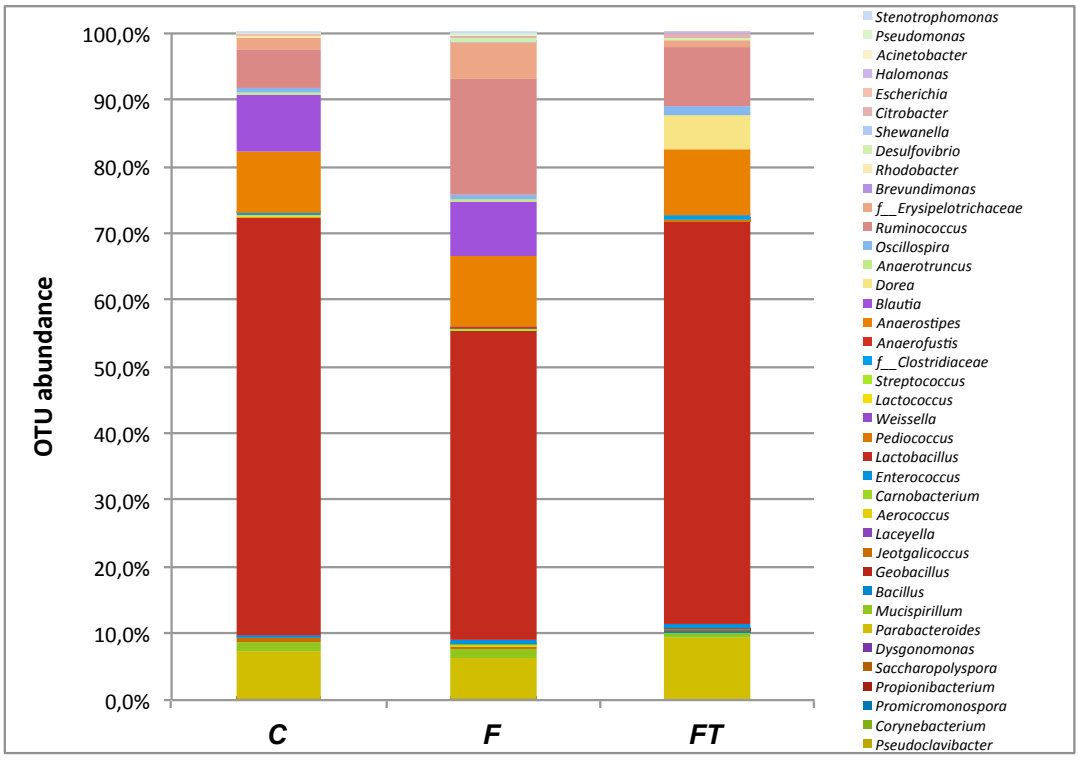

Fig. 6. Relative OTUs (Operational Taxonomic Units) abundance at the Genus level. *Composition of caecal microbiota of rats from different diet groups as revealed by Illumina sequencing of V4-V6 hypervariable region of 16S rRNA gene. Population analyses for each diet group show major genera found.*

It is interesting to observe that an increase in the relative abundance of members of the Erysipelotrichacaee family has been previously associated to a western diet and to obesity development in humanized gnotobiotic mice[29].

The presence of all bacterial genera reported in Table 1 was analyzed also in animals of groups CA and FA, treated with the antibiotic mixture. Interestingly, all genera present only in animals of group F and absent in groups C and FT are also absent in the animals under antibiotic treatment (not shown). Similarly, members of the Shewanella genus, found in groups C and FT but absent in group F (Table 1) were not found in antibiotic treated animals (not shown).

Table 1. Bacteria differentially distributed in the caecum of the different groups of rats.

Phylum	**Class**	**Order**	**Family**	**Genus**	**Group C**[a]	**Group F**[a]	**Group FT**[a]
Actinobacteria	*Actinobacteria*	*Actinomycetales*	*Cellulomonadaceae*	*Pseudoclavibacter*	ND	0.1	ND
			Promicromonosporaceae	*Promicromonospora*	ND	0.1	ND
Firmicutes	*Bacilli*	*Lactobacillales*	*Aerococcaceae*	*Aerococcus*	ND	0.1	ND
			Carnobacteriaceae	*Carnobacterium*	ND	0.1	ND
			Streptococcaceae	*Streptococcus*	ND	0.1	ND
				Lactococcus	0.1	0.2	0.1
			Lactobacillaceae	*Lactobacillus*	62.7	46.3	60.4
	Clostridia	*Clostridiales*	*Ruminococcaceae*	*Ruminococcus*	9.8	17.3	8.9
	Erysipelotrichi	*Erysipelotrichales*	*Erysipelotrichaceae*		1.8	5.6	0.9
Proteobacteria	*Alphaproteobacteria*	*Caulobacterales*	*Caulobacteraceae*	*Brevundimonas*	ND	0.1	ND
	Gammaproteobacteria	*Pseudomonales*	*Pseudomonaceae*	*Pseudomonas*	ND	0.1	ND
		Alteromonadales	*Shewanellaceae*	*Shewanella*	0.1	ND	0.1

[a] Percentage of OTU abundance in the sample; ND: not detectable.

4.5 Discussion

Main result of this study is that in fructose-fed rats the development of the metabolic syndrome directly correlates with the alteration of the microbial composition of the gut. Markers of metabolic syndrome, increased in fructose-fed rats, are reversed by treatment with an antibiotic mixture and partly by faecal transplant of rats under standard diet. Both treatments restore the gut microbiota, in terms of composition at the genus level and of overall diversity.

It has been recently reported that microbiota transplantation through surgical extraction of donor caecal content and administration to the recipient rats by oral gavage was able to reshape indigenous gut microbial community to an extent not previously anticipated[28]. Here we show that a similar reshaping can be obtained without the need of surgical extraction of caecal bacteria, but simply using faecal content, and, more importantly, that the reshaping of gut microbiota occurs in concomitance with metabolic improvement in obese rats.

The animal model used in the present study is represented by adult rats that become obese after long-term feeding with a fructose-rich diet[6, 7, 14]. Fructose-fed obese rats also display increased plasma NEFA, a reliable marker of the development of insulin resistance[8], but this metabolic alteration is fully reversed by treatment with antibiotic or faecal samples. In addition, the inhibition of lipolysis by insulin in WAT is almost completely lost in fructose-fed rats, but treatment with antibiotic or faecal samples is able to restore insulin sensitivity at the level of control rats.

The loss of insulin sensitivity in WAT can be driven by inflammation[30], and here we show that fructose-fed rats exhibit higher plasma LPS and TNF-α, that could therefore contribute to derangements in WAT function. Treatment with antibiotic or faecal samples in fructose-fed rats greatly reduces plasma LPS and completely abolishes the

increase in plasma TNF-α, and these changes could be at the basis of the restored insulin sensitivity in WAT in these rats. The increased plasma LPS in fructose-fed rats and its reversal by antibiotic treatment is in agreement with previous findings obtained in mice made obese by high fat diet or high-fructose diet[31-33]. To our knowledge, for the first time we show that partial reversal of systemic inflammation can be obtained by faecal transplantation.

The glucose intolerance found in fructose-fed rats was abolished by treatment with antibiotic but not by faecal transplant. The lack of effect of faecal transplant on glucose tolerance in the present study is at variance with results obtained in men[34], but it should be taken into account that in the cited experiment the transplant was carried out by duodenal gavage. Skeletal muscle greatly contributes to glucose disposal under the control of insulin[35], so we investigated a distal effector of insulin signalling in skeletal muscle, the kinase Akt. The degree of Akt activation was reduced by fructose-rich diet but significantly increased in fructose-fed rats treated with antibiotic. Since LPS directly induces insulin resistance in skeletal muscle[36], and antibiotic treatment completely abolished the diet-induced increase in plasma LPS, the direct involvement of LPS in high fructose diet-induced glucose intolerance can be hypothesized.

Our present results highlight an increased oxidative damage to lipid and proteins in liver and skeletal muscle of fructose-fed rats, that is fully prevented by antibiotic treatment, and only partly reversed by faecal transplant. This pattern of variation can be explained by modulation of plasma LPS by diet and treatments, since LPS has a well known pro-oxidant effect[37] .

As expected, a fructose-rich diet induces signs of metabolic syndrome in rats and alters the microbial composition of the gut, decreasing the total bacterial diversity. The reduction of all markers of metabolic syndrome, inflammation and tissue oxidative

stress in animals under antibiotic treatment indicates that the metabolic disorders are somehow due to the fructose-induced alteration of the gut microbiota. Consistently, in fructose-fed rats treated with faecal samples of animals under standard diet, the microbial composition of the gut is restored and markers of metabolic syndrome, inflammation and tissue oxidative stress are significantly reduced. The antibiotic treatment strongly alters the gut microbial composition impairing a comparative analysis of the metagenomic data with those of animals not treated with antibiotics. However, as shown in Table 1, members of specific genera differentially represented in the various groups correlates with the metabolic data: genera present in group F and absent in C and FT are also absent in the metabolically similar groups CA and FA. On the same line, members of the Shewanella genus are present in all groups but group F, that is the only group with metabolic disorders.

In conclusion, our data suggest that the alteration of the gut microbial composition correlates with the development of the metabolic syndrome and support the hypothesis that the manipulation of the gut microbiota is a promising therapeutic strategy in the treatment of diet-induced obesity and diabetes.

4.6 Acknowledgements

The authors thank the GDC for the help and support with the library preparation and the MiSeq run.

4.7 References

1. Johnson RJ, Segal MS, Sautin Y, et al. **Potential role of sugar (fructose) in the epidemic of hypertension, obesity and the metabolic syndrome, diabetes, kidney disease, and cardiovascular disease**. *Am J Clin Nutr* 2007;86:899–906.
2. Tappy L, Le KA, Tran C, et al. **Fructose and metabolic diseases: New findings, new questions** *Nutrition* 2010;26**:**1044–1049.
3. Payne AN, Chassard C, Lacroix C. **Gut microbial adaptation to dietary consumption of fructose, artificial sweeteners and sugar alcohols: implications for host–microbe interactions contributing to obesity.** *Obesity* 2012;13**:**799–809.
4. Li S, Zhang HJ, Hu CC, et al. **Assessment of diet-induced obese rats as an obesity model by comparative functional genomics**. *Obesity* 2008;16:811-818.
5. Kavanagh K, Wylie AT, Tucker KL, et al. **Dietary fructose induces endotoxemia and hepatic injury in calorically controlled primates.** *Am J Clin Nutr* 2013;98:349-357.
6. Crescenzo R, Bianco F, Coppola P, et al. **Increased skeletal muscle mitochondrial efficiency in rats with fructose-induced alteration in glucose tolerance**. *Br J Nutr* 2013a; 110:1996-2003.
7. Crescenzo R, Bianco F, Falcone I, et al. **Increased hepatic de novo lipogenesis and mitochondrial efficiency in a model of obesity induced by diets rich in fructose**. *Eur J Nutr* 2013b;52:537-545.
8. Karpe F, Dickmann JR, Frayn KN **Fatty Acids, Obesity, and Insulin Resistance: Time for a Reevaluation.** *Diabetes* 2011;60:2441-2449.
9. McNulty NP, Wu M, Erickson AR, et al. **Effects of Diet on Resource Utilization by a Model Human Gut Microbiota Containing *Bacteroides cellulosilyticus***

WH2, a Symbiont with an Extensive Glycobiome. *PLoS Biol* 2013;11: e1001637. doi:10.1371/journal.pbio.1001637

10. Tilg H, Moschen AR, Kaser A. **Obesity and the Microbiota.** *Gastroenterology* 2009**;**136:1476-1483.
11. Faith JJ, McNulty NP, Rey FE, et al. **Predicting a human gut microbiota's response to diet in gnotobiotic mice.** *Science* 2011;333:101–104.
12. Walker AW, Ince J, Duncan SH, et al. **Dominant and diet-responsive groups of bacteria within the human colonic microbiota.** *ISME J* 2011;5:220–230.
13. Hsieh FC, Lee CL, Chai CY, et al. **Oral administration of *Lactobacillus reuteri* GMNL-263 improves insulin resistance and ameliorates hepatic steatosis in high fructose-fed rats.** *Nutr Metab* 2013;10:35. doi: 10.1186/1743-7075-10-35.
14. Crescenzo R, Bianco F, Coppola P, et al. **Adipose tissue remodeling in rats exhibiting fructose-induced obesity**. *Eur J Nutr* 2013c;10.1007/s00394-013-0538-2
15. Folch J, Lees M, Stanley GHS **A simple method for the isolation and purification of total lipids from animal tissues.** *J Biol Chem* 1957;226:497-510.
16. Crescenzo R., Bianco F., Falcone I, et al. **Alterations in hepatic mitochondrial compartment in a model of obesity and insulin resistance.** *Obesity* 2008;16:958-964.
17. Heath RL, Tappel AL **A new sensitive assay for the measurement of hydroperoxides.** *Anal Biochem* 1976;76:184-191.
18. Reznick AZ, Packer L. **Oxidative damage to proteins: spectrophotometric method for carbonyl assay**. *Meth Enzymol* 1994;233:357–363.
19. Caporaso JG, Lauber CL, Walters WA, et al. **Global patterns of 16S rRNA diversity at a depth of millions of sequences per sample**. *Proc Natl Acad Sci U S*

A 2010;108 Suppl 1:4516-4522.

20. Andersson AF, Lindberg M, Jakobsson H, et al. **Comparative analysis of human gut microbiota by barcoded pyrosequencing**. *PLoS One* 2008;3(7):e2836. doi:10.1371/journal.pone.0002836.
21. Edgar, RC. **Search and clustering orders of magnitude faster than BLAST**. *Bioinformatics* 2010;26(19):2460-2461.
22. Wang Q, Garrity GM, Tiedje JM, et al. **Naive Bayesian classifier for rapid assignment of rRNA sequences into the new bacterial taxonomy**. *Appl Environ Microbiol* 2007;73(16):5261-5267.
23. Caporaso JG, Bittinger K, Bushman FD, et al. **PyNAST: a flexible tool for aligning sequences to a template alignment.** *Bioinformatics* 2010;26(2):266-267.
24. DeSantis TZ, Hugenholtz P, Larsen N, et al. **Greengenes, a chimera-checked 16S rRNA gene database and workbench compatible with ARB.** *Appl Environ Microbiol* 2006;72(7):5069-5072.
25. Price MN, Dehal PS, Arkin AP. **FastTree 2--approximately maximum-likelihood trees for large alignments.** *PLoS One* 2010;5(3):e9490.
26. Lozupone C, Knight R. **UniFrac: a new phylogenetic method for comparing microbial communities**. *Appl Environ Microbiol* 2005;71(12):8228-8235.
27. Piya MK, Harte AL, McTernan PG **Metabolic endotoxaemia: is it more than just a gut feeling?** *Curr Opin Lipidol* 2013;24:78-85.
28. Manichanh C, Reeder J, Gibert P, et al. **Reshaping the gut microbiome with bacterial transplantation and antibiotic intake.** *Genome Res.* 2010;20:1411-1419

29. Turnbaugh PJ, Ridaura RK, Faith JJ, et al. **The Effect of Diet on the Human Gut Microbiome: A Metagenomic Analysis in Humanized Gnotobiotic Mice.** *Sci Transl Med.* 2009; 1(6):6-14.

30. van de Woestijne P, Monajemi H, Kalkhoven E, et al. **Adipose tissue dysfunction and hypertriglyceridemia: mechanisms and management.** *Obes Rev* 2011;12:829–840.

31. Bergheim I, Weber S, Vos M, et al. **Antibiotics protect against fructose-induced hepatic lipid accumulation in mice: role of endotoxin.** *J Hepatol* 2008**;**48: 983-992.

32. Membrez M, Blancher F, Jaquet M, et al. **Gut microbiota modulation with norfloxacin and ampicillin enhances glucose tolerance in mice.** *FASEB J* 2008;22:2416-2426.

33. Carvalho BM, Guadagnini D, Tsukumo DML, et al. **Modulation of gut microbiota by antibiotics improves insulin signaling in high-fat fed mice.** *Diabetologia* 2012;55:2823-2834.

34. Vrieze A,Van Nood E, Holleman F, et al. **Transfer of intestinal microbiota from lean donors increases insulin sensitivity in individuals with metabolic syndrome.** *Gastroenterology* 2012;143: 913–916.

35. Stump CS, Henriksen EJ, Wei Y, et al. **The metabolic syndrome: role of skeletal muscle metabolism**. *Ann Med* 2006;38:389–402.

36. Liang H, Hussey SE, Sanchez-Avila A, et al. **Effect of lipopolysaccharide on inflammation and insulin action in human muscle.** *PLoS One* 2013;8(5):e63983.doi: 10.1371/journal.pone.0063983.

37. Nishio K, Horie M, Akazawa Y, et al. **Attenuation of lipopolysaccharide (LPS)-induced cytotoxicity by tocopherols and tocotrienols**. *Redox Biol* 2013;1(1):97-103.

38. Martin M**. Cutadapt removes adapter sequences from high-throughput sequencing reads.** *EMBnet.journal, [S.l.]***,** v. 17, n. 1, p. pp. 10-12, may. 2011. ISSN 2226-6089.

39. Schmieder R, Edwards R. **Quality control and preprocessing of metagenomic datasets.** *Bioinformatics.* 2011 Mar 15; 27(6): 863-4. doi: 10.1093/bioinformatics/btr026. Epub 2011 Jan 28.

40. Caporaso JG, Kuczynski J, Stombaugh J, Bittinger K, Bushman FD, Costello EK, Fierer N, Peña AG, Goodrich JK, Gordon JI, Huttley GA, Kelley ST, Knights D, Koenig JE, Ley RE, Lozupone CA, McDonald D, Muegge BD, Pirrung M, Reeder J, Sevinsky JR, Turnbaugh PJ, Walters WA, Widmann J, Yatsunenko T, Zaneveld J, Knight R. **QIIME allows analysis of high-throughput community sequencing data.** *Nat Methods.* 2010 May;7(5):335-6. doi:10.1038/nmeth.f.303. Epub 2010 Apr 11.

41. Marie A. Hildebrandt, Christian Hoffman, Scott A. Sherrill-Mix, Sue A. Keilbaugh, Micah Hamady, Ying-Yu Chen, Rob Knight, Rexford S. Ahima, Frederic Bushman, Gary D. Wu. **High Fat Diet Determines the Composition of the Murine Gut Microbiome Independently of Obesity**. *Gastroenterology*. Nov 2009; 137(5): 1716–24

42. Lazarevic V, Whiteson K, Huse S, Hernandez D, Farinelli L, Østerås M, Schrenzel J, François P. **Metagenomic study of the oral microbiota by Illumina high-throughput sequencing.** *J Microbiol Meth* 2009, **79**: 266–271.

4.8 Supporting information

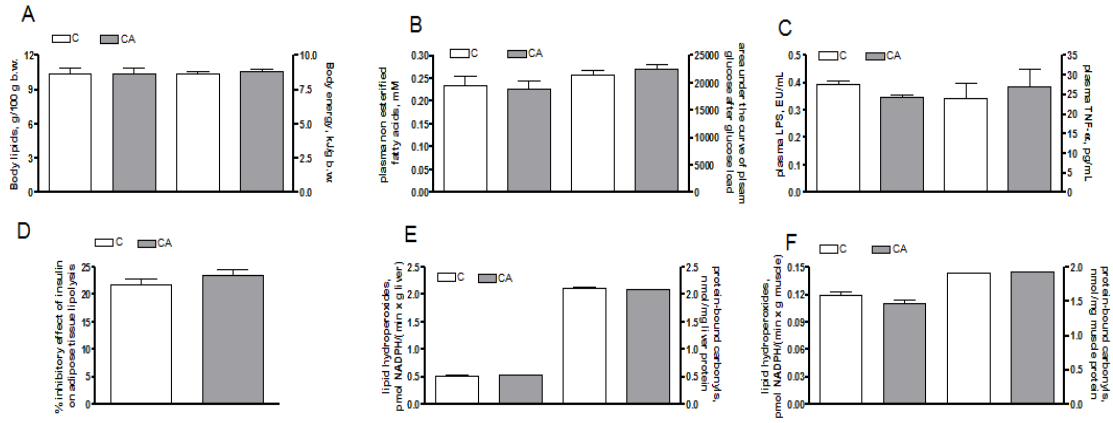

Fig. S1. *Body energy and lipid content (A), plasma non esterified fatty acids and area under the curve of plasma glucose after glucose load (B), plasma LPS and TNF-α (C), epididymal fat weight and inhibitory effect of insulin on adipose tissue lipolysis (D), lipid and protein oxidative stress in liver (E), lipid and protein oxidative stress in skeletal muscle (F), in control (C) and control+antibiotic (CA) rats. Values are reported as means±SEM of six different rats. EU=endotoxin unit.*

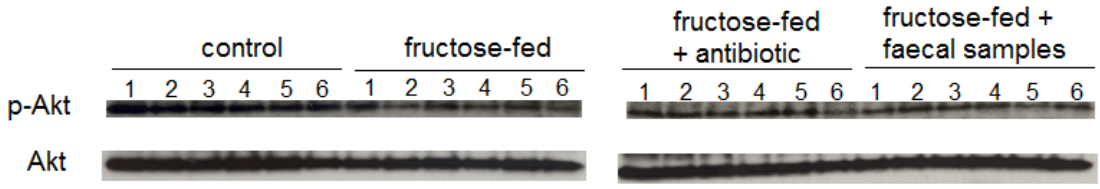

Fig. S2. *Western blot of p-Akt and Akt in skeletal muscle in control, fructose-fed, fructose-fed+antibiotic and fructose-fed+faecal samples rats.*

APPENDIX

OPEN ACCESS Freely available online

PLOS ONE

Pigmentation and Sporulation Are Alternative Cell Fates in *Bacillus pumilus* SF214

Nicola Manzo[9], **Blanda Di Luccia**[9], **Rachele Isticato, Enrica D'Apuzzo, Maurilio De Felice, Ezio Ricca***

Department of Biology, Federico II University, Napoli, Italy

Abstract

Bacillus pumilus SF214 is a spore forming bacterium, isolated from a marine sample, able to produce a matrix and a orange-red, water soluble pigment. Pigmentation is strictly regulated and high pigment production was observed during the late stationary growth phase in a minimal medium and at growth temperatures lower than the optimum. Only a subpopulation of stationary phase cells produced the pigment, indicating that the stationary culture contains a heterogeneous cell population and that pigment synthesis is a bimodal phenomenon. The fraction of cells producing the pigment varied in the different growth conditions and occured only in cells not devoted to sporulation. Only some of the pigmented cells were also able to produce a matrix. Pigment and matrix production in SF214 appear then as two developmental fates both alternative to sporulation. Since the pigment had an essential role in the cell resistance to oxidative stress conditions, we propose that within the heterogeneous population different survival strategies can be followed by the different cells.

Citation: Manzo N, Di Luccia B, Isticato R, D'Apuzzo E, De Felice M, et al. (2013) Pigmentation and Sporulation Are Alternative Cell Fates in *Bacillus pumilus* SF214. PLoS ONE 8(4): e62093. doi:10.1371/journal.pone.0062093

Editor: Riccardo Manganelli, University of Padova Medical School, Italy

Received January 28, 2013; **Accepted** March 15, 2013; **Published** April 25, 2013

Funding: This research was supported by a EU grant (KBBE-2007–207948) from the EU 7th Framework to ER. The funders had no role in study design, data collection and analysis, decision to publish, or preparation of the manuscript.

Competing Interests: The authors have declared that no competing interests exist.

* E-mail: ericca@unina.it

[9] These authors contributed equally to this work.

Introduction

Spore-forming *Bacilli* are Gram positive organisms characterized by the ability to differentiate the endospore (spore), a metabolically quiescent and extremely resistant cell type. The soil is generally indicated as the main habitat of *Bacilli*, however, spores have been found in many diverse environments, including rocks, dust, aquatic environments, and the gut of various insects and animals [1,2]. Such a wide environmental distribution is facilitated by the spore ability to survive long-term absence of water and nutrients and withstand extreme habitats that would kill other cell types [3]. Survival is due to the peculiar structure of the spore that is formed by a dehydrated cytoplasm containing a condensed and inactive chromosome, and by a series of protective layers. An innermost layer is the peptidoglycan-rich cortex that is itself surrounded by additional layers of proteinaceous material, the coat and, in some species, the exosporium [4,5]. Together these components protect the spore from UV radiation, extremes of heat or pH, exposure to solvents, hydrogen peroxide, toxic chemicals and lytic enzymes [3,6]. In the presence of water and appropriate nutrients the spore starts germination, a fast process during which the protective structures are removed and resumption of vegetative cell growth is allowed [3,4].

Spore formation is dependent upon environmental conditions that do not allow cell growth, such as a block of DNA replication and a decline of available nutrients [7]. In *Bacillus subtilis*, the model organism for spore formers, growing cells are mainly single and highly motile. When those dispersed cells reach the end of exponential growth they can follow alternative developmental pathways with some cells forming long chains, producing a polymeric matrix rich in sugars and proteins (matrix) and assembling into multicellular biofilms and others entering the irreversible program of spore formation [8,9,10]. Therefore, in dispersed cell populations matrix and spore production are mutually exclusive cell fates [8,11] and are both bimodal processes in which cells follow either one or the other pathway [12,13]. Both developmental cell fates are governed by a regulatory protein, Spo0A-P, that directly activates genes of the sporulation pathway [14] and indirectly acts on matrix synthesis, relieving the repression of genes for matrix production (*epsA-O* and *yqxM-sipW-tasA* operons) [15,16,17]. Two mechanisms cooperate to make sporulation and matrix production mutually exclusive: a metabolic control mediated by the intracellular levels of SpoOA-P and a chromosome copy number mechanism that prevents cells that have entered the sporulation pathway from expressing matrix genes [10]. Low levels of SpoOA-P induce matrix formation while high levels of the phosphoprotein block matrix formation and activate sporulation. Therefore, in a sporulation-inducing medium, in which SpoOA-P levels rapidly rise, cells enter sporulation instead of forming a biofilm. Conversely, in a medium in which SpoOA-P remains at low levels biofilm formation is promoted [10]. However, extracellular matrix production and sporulation are linked. KinD, a membrane histidine kinase which is part of the Spo0A phosphotransfer network, has been proposed to act as a checkpoint protein able to regulate the onset of sporulation by inhibiting Spo0A activity. KinD would alter its activity, depending on the presence or absence of the extracellular matrix, thus affecting the selective functionality on the master regulator Spo0A to regulate expression of genes involved in matrix production and sporulation [18]. Within a biofilm different cell types coexist and

display a high degree of spatiotemporal organization with matrix-producing cells that ultimately differentiate into spores [8].

Another interesting feature of some *Bacilli* is the production of pigments. Isolates of several *Bacillus* species produce a wide variety of pigments, from spore-associated melanin-like molecules [19] to different types of carotenoids [20,21]. In some cases, those carotenoids have been characterized and proposed to provide resistance to UV irradiation and reactive oxygen species [20,21,22,23]. A pigmented strain of *Bacillus pumilus*, SF214, isolated from a marine sample, has been previously described [21]. SF214 is a moderate halophilic bacterium able to form a matrix and to produce an orange to red water-soluble pigment, i.e. a pigment that can not be partitioned into organic solvents but is retained in the aqueous phase [21]. The inability to partition this pigment into organic solvents, to resolve it by HPLC and to obtain characteristic carotenoid UV/VIS spectra, has precluded its definitive assignment as a carotenoid [21]. However, the spectral peak at 410 nm shown by aqueous extracts of SF214 [21] is likely to represent a protein-associated carotenoid, as previously described for carotenoproteins extracted from crawfishes [24].

Here we report that in SF214 pigment production is a highly regulated process that occurs during the stationary growth phase only in cells not devoted to spore formation. Thus SF214 pigment production appears as a bimodal phenomenon alternative to sporulation, parallel to matrix biosynthesis and essential to grant cell resistance to oxidative stress.

Results

Pigment Production is Dependent on Growth-phase, –temperature and –medium

Synthesis of the water-soluble pigment produced by SF214 is a strictly regulated process as it depends on the growth-phase, -temperature and -medium. Pigment production was shown to be strongly induced only 8–10 hours after that cells have entered the stationary growth phase at 37°C in rich (LB) medium (Fig. 1A). Although SF214 is a mesophilic bacterium and its optimal growth temperature is 37°C, the maximal production of the pigment was observed at 25°C (Fig. 1B). Compared with cells grown at 25°C a slightly decreased production of pigment was observed at 30°C, whereas more than 2-fold and about 6-fold decreased synthesis was observed at 37°C and at 42°C, respectively (Fig. 1B). The absorbance spectrum of cell extracts of SF214 between 300 and 500 nm [20] showed that cells grown at 25°C produced about 4-fold more pigment in a minimal (S7; black symbols in Fig. 1C) than in a rich (LB; gray symbols in Fig. 1C) medium, while in a sporulation-inducing (DS; white symbols in Fig. 1A) medium the synthesis of pigment was almost abolished.

Heterogeneity of Pigment Production

Previous reports have shown that carotenoids produced by the yeast *Phaffia rhodozyma* [25] or the halotolerant green alga *Dunaliella salina* [26] autofluoresce and that such property can be used to follow carotenoid production by fluorescence microscopy. We found that the water-soluble pigment of SF214 is also autofluorescent and that the fluorescence is not localized but rather diffuse in the cell cytoplasm. Interestingly, in the cell culture only some of the cells are fluorescent. Fig. 2 shows a representative microscopy field observed by phase contrast (left) and fluorescent microscopy either following the autofluorescence (middle) or after DAPI-staining (right). The enlarged panels of Fig. 2 clearly show that only some of the DAPI-stained cells were autofluorescent. The number of autofluorescent cells varied with the growth conditions (see below) but ranged between 20% in exponentially growing cells to 80% in stationary cells. Ghost-like cells, negative to DAPI staining and showing some autofluorescence were not considered. It is interesting to observe in Fig. 2 a doublet of cells (white and grey arrows in the enlarged sections). Those two cells seem to be still partially attached and to derive from the same mother cell, following the last round of division before stationary phase. Only one of them (grey arrows) has switched to the "pigment state" and is autofluorescent.

Two lines of evidence support our conclusion that the observed autofluorescence was actually due to the water-soluble pigment: i) unpigmented *Bacilli* (including other isolates of *B. pumilus*) (not shown) and an unpigmented mutant of SF214 (described below) did not show any fluorescence under identical experimental conditions (Fig. 3); ii) the number of autofluorescent cells varied consistently with the variations of pigment production observed at various growth-phase, -temperature and -medium. As shown in Fig. 4, the number of fluorescent cells was higher in a stationary than in an exponential cultures (left panels), in cells grown at 25°C than in cells grown at 37°C (middle panels) and in cells grown in minimal (S7) than in rich medium (LB) (right panels). For each condition considered in Fig. 4, different microscopy fields were analyzed and over 1,000 cells for each condition counted. This analysis indicated that the increased production of pigment observed depending upon growth-phase, -temperature and -medium is not due to a higher production of carotenoid by each producing cell but rather to an increased proportion of cells able to produce the pigment. Restriction of pigment synthesis to a subpopulation of cells indicates that late stationary cultures of SF214 contain a heterogeneous population of cells and that pigment formation is a bimodal process.

Pigment Synthesis Only Occurs in Cells not Devoted to Sporulation

Free spores as well as immature spores still contained within the mother cells are known to autofluoresce [27]. We observed that the fluorescence of sporangia containing an almost mature spore was always limited to the prespore. Fig. 5 shows a representative microscopy field with sporulating cells of SF214 observed by phase contrast (left), autofluorescence (middle) and the merge (right): while only some cells autofluoresced with a fluorescence diffused in the cytoplasm, fluorescence associated to sporangia containing an almost mature spore was confined to the forming spore, as no fluorescence was visible within the cytoplasm. This observation, together with experiments reported in Fig. 1C indicating that when grown in a sporulation-inducing (DS) medium SF214 cells did not produce the pigment, suggests that pigment production in *B. pumilus* SF214 is mutually exclusive with spore formation.

To better address this point we analyzed SF214 cells by pigment-driven autofluorescence (green) and by immunofluorescence due to anti-CotE primary antibody and fluorescent secondary antibody (red). CotE is a spore coat protein [28], produced early during sporulation, known to localize on the spore surface [27]. For our analysis antibody raised against CotE of *B. subtilis* were used [29]. In a preliminary experiment this antibody was shown to specifically react against a protein of *B. pumilus* SF214 corresponding in size to CotE of *B. subtilis* (Fig. S1). Fig. 6 reports representative microscopy fields of fluorescence and immunofluorescence microscopy of SF214 cells grown in LB at 37°C up to the early stationary growth phase. In this analysis we observed that, similarly to what observed in *B. subtilis* [27], *B. pumilus* CotE is localized around the forming spore, and that cells recognized by the anti-CotE antibody were all not autofluorescent. We never observed yellow cells, which would have been indicative of cells producing the pigment (green signal) and the spore-specific

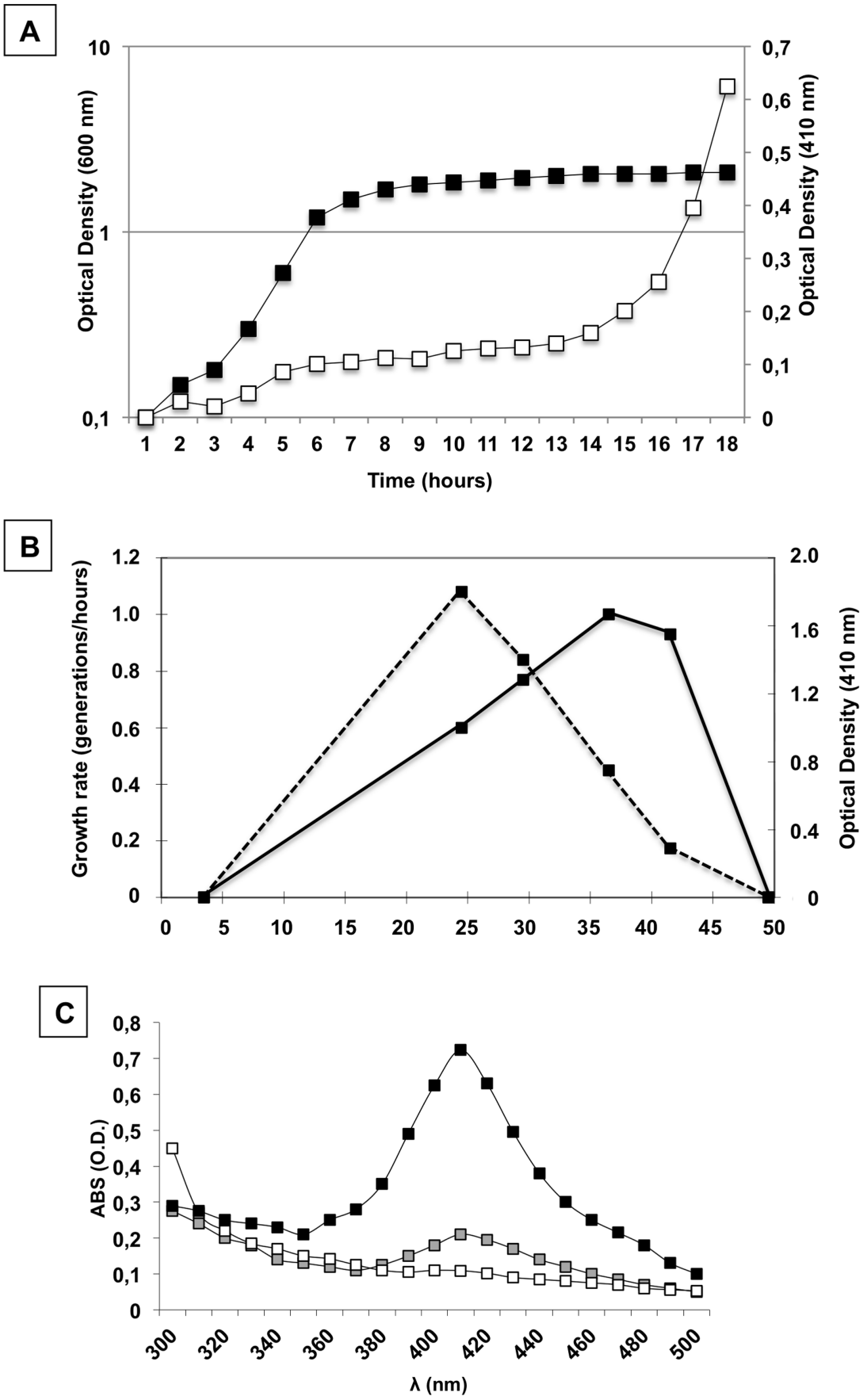
A
Optical Density (600 nm)
Optical Density (410 nm)
Time (hours)
B
Growth rate (generations/hours)
Optical Density (410 nm)
C
ABS (O.D.)
λ (nm)

Figure 1. Characterization of growth and pigment production in *B. pumilus* SF214. (A) Growth curve of *B. pumilus* SF214 at 37°C in rich (LB) medium (black symbols) was determined by following over time the optical density of the culture at 600 nm. Pigment production (white symbols) was determined by measuring over time the optical density of 1 ml of cell-free culture supernatant at 410 nm. (B) Growth rate (continuous line) and pigment production (dashed line) of SF214 at different growth temperatures in rich (LB) medium. Pigment production was evaluated by measuring the optical density of 1 ml of cell-free culture supernatant at 410 nm after 24 hours of growth. (C) Absorbance spectrum between 300 and 500 nm of 360 µg of cell extracts of SF214 grown at 25°C in minimal (S7) (black symbol), rich (LB) (gray symbol) and sporulation-inducing (DS) medium.
doi:10.1371/journal.pone.0062093.g001

protein CotE (red signal) (see the merged panels of Fig. 6 for some examples). Therefore, based on the experiments of Figs. 5 and 6 we conclude that pigment synthesis and sporulation are alternative developmental pathways and occur in different cell subpopulations.

Matrix Synthesis Occurs Only in a Subpopulation of Pigmented Cells

In *B. subtilis* sporulation and matrix formation are alternative developmental programmes [11]. Since SF214 also forms a matrix [21] we verified whether also in this bacterium matrix formation and sporulation are alternative and whether matrix and pigment synthesis can occur in the same cells. To this aim we analyzed SF214 cells by pigment-driven autofluorescence (green) and by immunofluorescence due to anti-TasA primary antibody and fluorescent secondary antibody (red). TasA is a major protein component of the *B. subtilis* biofilm [15], encoded by the third gene of the *yqxM-sipW-tasA* operon [16,30]. For our analysis we used antibody raised against TasA of *B. subtilis* (a gift of A. Driks). Preliminary experiments showed that a protein homologous to TasA of *B. subtilis* can be extracted from spores of strain SF214 and that this protein is recognized by the anti-TasA antibody (Fig. S2). The homology with the protein of SF214 starts at position 24 of TasA, which corresponds to the first amino acid residue of the mature form of TasA after the proteolytic maturation of pre-TasA [30,31] (Fig. S2). Fig. 7 reports representative fields of fluorescence and immunofluorescence microscopy of SF214 cells grown in minimal (S7) medium at 25°C up to the early stationary phase. This analysis showed that: i) cells that were not autofluorescent and therefore devoted to sporulation (indicated by white arrows in Fig. 7A) were never recognized by the anti-TasA antibody, and ii) only about 80% of the autofluorescent cells (from a total of approx. 1500 cells counted in 6 different microscopy fields) were recognized by anti-TasA antibody (yellow cells in Fig. 7). Panel B of Fig. 7 shows some examples of autofluorescent cells that are not recognized by anti-TasA antibody. These results indicate that

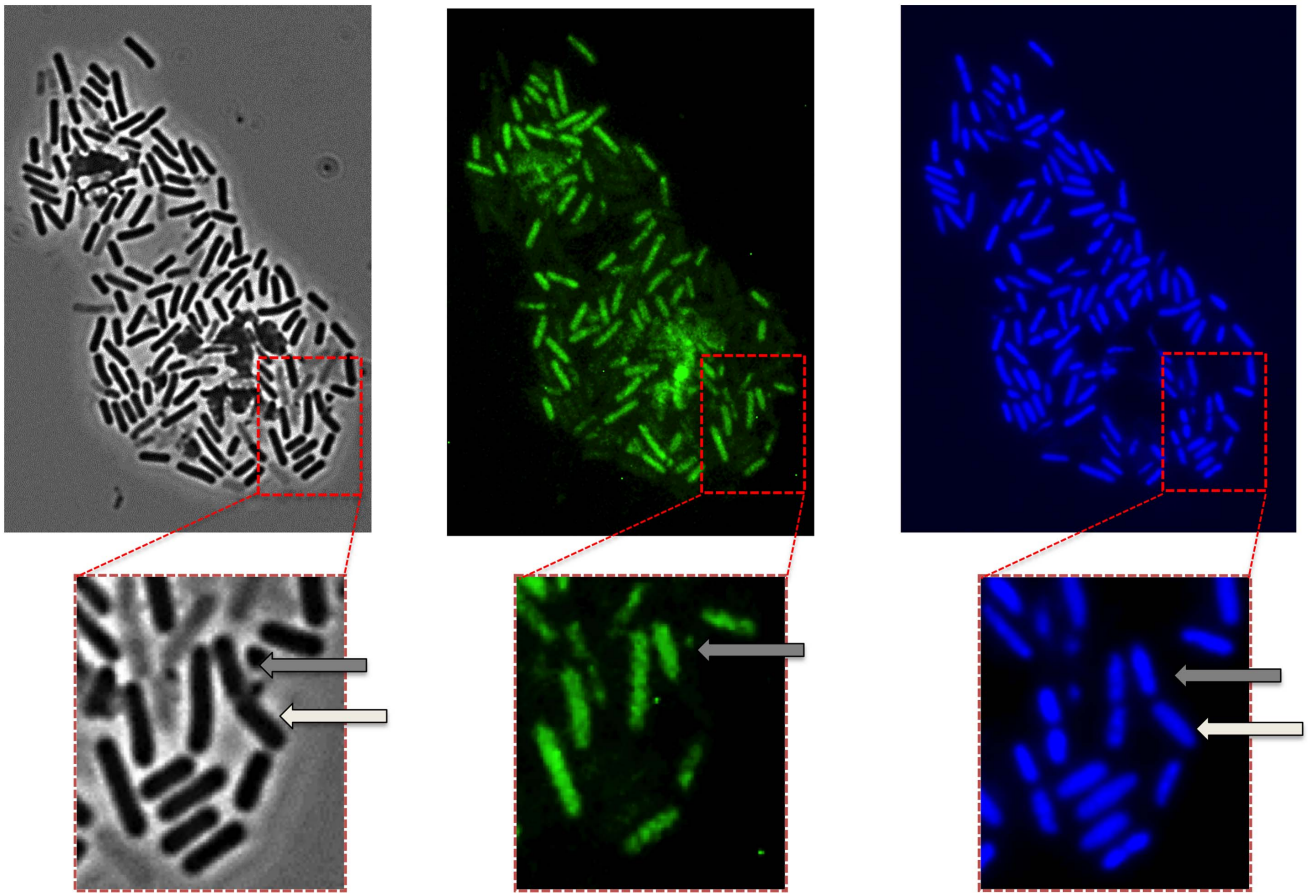

Figure 2. Phase contrast and fluorescence microscopy analysis of SF214. Observation of the same microscopy field by phase contrast (left), autofluorescence (middle) and DAPI staining (right). The same section of each panel is enlarged. The arrows in the enlarged sections point to a doublet of cells, still partially attached and deriving from the same mother cell, in which only one cell (grey arrows) is autofluorescent.
doi:10.1371/journal.pone.0062093.g002

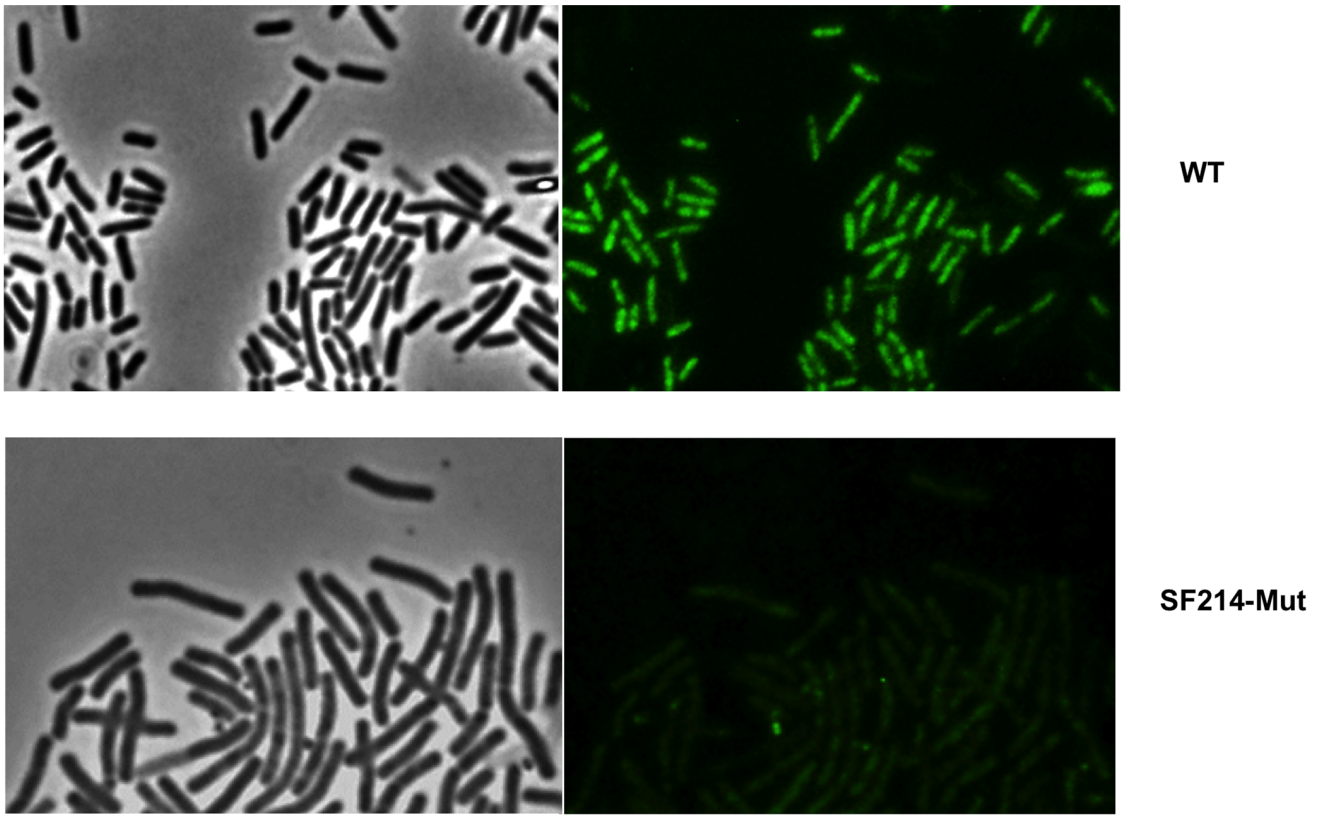

Figure 3. Microscopy analysis of SF214 and of its unpigmented mutant. Microscopy analysis of SF214 and of its unpigmented mutant (SF214-Mut). For each strain the same microscopy field is shown by phase contrast (left) and autofluorescence (right). The same conditions of exposure were used for the two microscopy fields.
doi:10.1371/journal.pone.0062093.g003

as in *B. subtilis* also in *B. pumilus* SF214 sporulation and matrix formation are alternative and that matrix synthesis occurs only in a subpopulation of pigmented cells.

The Pigment of SF214 is Essential for Cell Resistance to Hydrogen Peroxide

In non-photosynthetic organisms pigments have been associated to cell resistance to UV irradiation and reactive oxygen species [21,22,23]. To analyze the role of the SF214 pigment we isolated an unpigmented mutant after nitrosoguanidine (NTG) mutagenesis [32] (Fig. S3). To this aim mid-exponential phase cells were incubated for different times with 10 μg of NTG and the percentage of survival assessed by CFU determination (Fig. S3B). To minimize the possibility to have mutants carrying multiple mutations, we only analyzed cells exposed to NTG for the shortest time. NTG-treated cells were then diluted, plated and checked for pigmentation after 36 hours of incubation at 25°C. One unpigmented mutant, SF214-Mut, was chosen for further analysis. Although we could not isolate the mutation responsible for loss of pigmentation, as several attempts to transform SF214 with either plasmid or chromosomal DNA resulted unsuccessful (not shown), we were able to show that the unpigmented phenotype reverted spontaneously at a frequency of 1 clone out of 10^9, thus suggesting that the NTG treatment had not produced multiple mutations. Analysis of the aqueous extracts showed that the mutant does not produce any molecule able to adsorb at 410 nm (Fig. S4) and, consistently, a fluorescence microscopy analysis showed that no fluorescent cells were present in a stationary phase culture of the unpigmented mutant (Fig. 3).

SF214 and its unpigmented derivative were used to analyze the cell response to hydrogen peroxide. Cells of the two strains were grown at 25°C in minimal (S7) liquid medium and collected 10 hours after the entry into stationary phase. Cells were then incubated with 30 mM hydrogen peroxide and analyzed for viability after various incubation times. While wild type cells were all viable after exposure to hydrogen peroxide for up 30 minutes and showed a reduced viability only after 45, 60 and 90 minutes of treatment, the unpigmented mutant showed a clear decrease of viability at all incubation times (Fig. 8). In a parallel experiment spores of both strains were totally resistant to the hydrogen peroxide treatment at all time points tested (Fig. 8). Results of Fig. 8 confirm that the pigment has a role in the response of vegetative cells to oxidative stress. Spores do not contain the pigment but are totally resistant to hydrogen peroxide due to other, pigment-independent mechanisms [6,33].

Discussion

The main result of this report is the observation that pigment production in SF214, a marine isolate of *B. pumilus*, is a bimodal phenomenon alternative to sporulation. SF214 cells in stationary growth phase form a heterogeneous population able to follow diverse developmental fates. Some cells start the sporulation programme while others produce the pigment. Only a subpopulation of pigmented cells also produces a matrix. This is reminiscent of the situation found in *B. subtilis*. Seminal studies

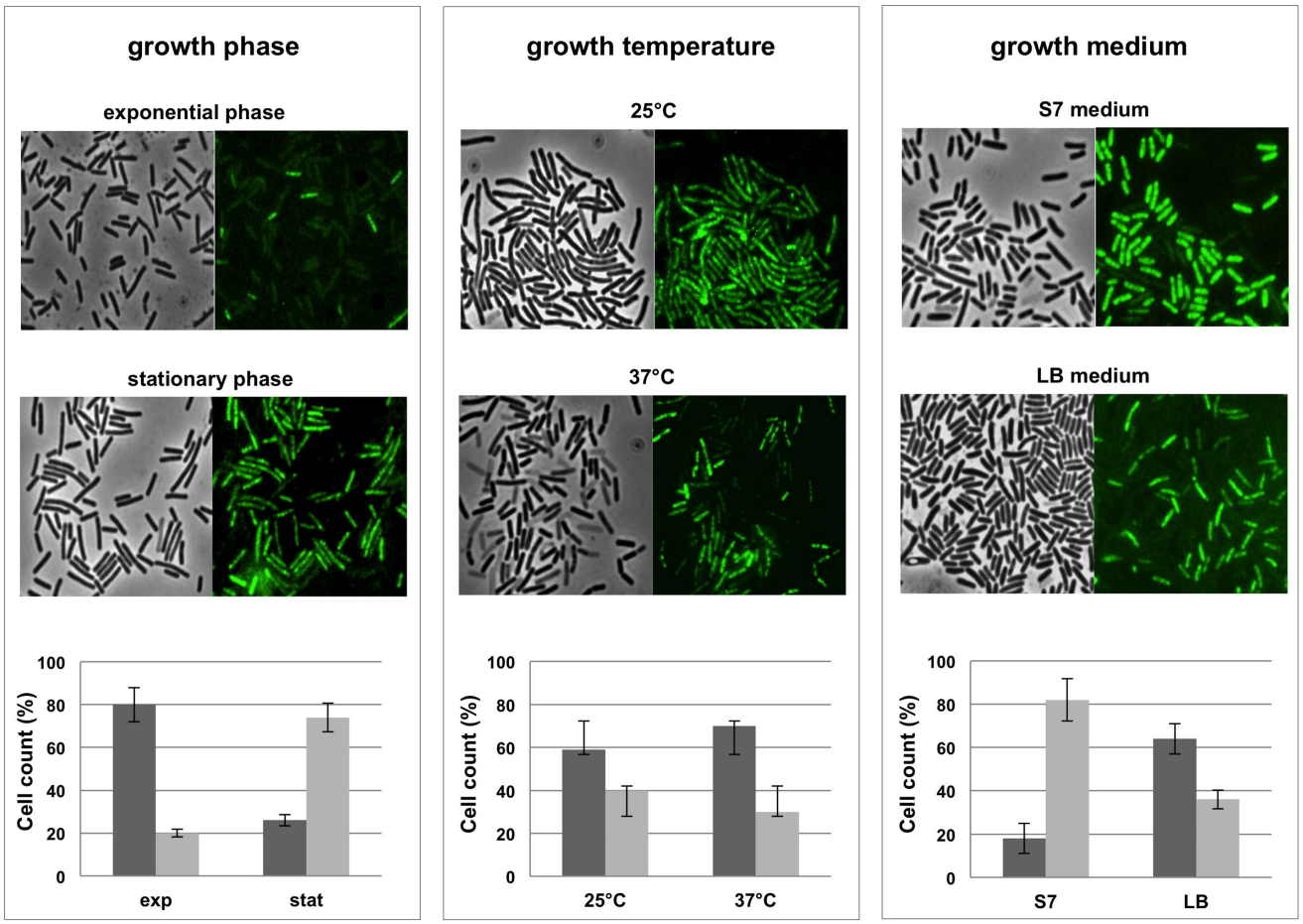

Figure 4. Autofluorescence at different growth conditins. Microscopy fields of SF214 cells grown at different conditions and observed by phase contrast and autofluorescence and compared to assess the proportion of fluorescent vs not fluorescent cells. Left panel: exponential vs. stationary growth phase (in LB medium at 37°C); middle panel: 25°C vs. 37°C as growth temperature (in LB medium for 24 hours); right panel: minimal (S7) vs. rich (LB) growth medium (stationary cells grown at 25°C). For each panel a graph reports the percentage of fluorescent (gray bars) vs. not fluorescent (dark gray bars) cells. For each condition a total of 1.000 cells from five different microscopy fields were counted. Spores and cells containing a prespore were not counted.
doi:10.1371/journal.pone.0062093.g004

performed using *B. subtilis*, the model organism for spore formers, have shown that in dispersed cell populations spore formation, matrix production, competence to acquire external DNA and production of extra-cellular proteases are all bimodal processes [9,10,12]. Spore and matrix formation appear as alternative developmental pathways with some cells producing a matrix and others entering the irreversible program of spore formation [8,9,10]. In addition to those two also other cell fates are alternative in *B. subtilis:* within a biofilm, only a subpopulation of *B. subtilis* cells produce surfactin but, while surfactin-producers do not respond to their own surfactin, other cells do and become matrix producers. In this case, individual *B. subtilis* cells simultaneously expressing genes for both surfactin and matrix synthesis have never been observed [11]. These two subpopulations do not include the entire population and the rest of the cells that do not differentiate as surfactin or matrix producers probably originate the other cell types known to be present in *B. subtilis* populations [13]. In this frame each differentiation fate sets the stage for a subsequent cell type. For example, within biofilms matrix-producing cells are initially predominant and later differentiate and become spores [8]. By analogy, we propose that *B. pumilus* SF214 dispersed stationary cells also form a heterogeneous population able to follow diverse developmental fates. Some cells enter the irreversible sporulation cycle forming the highly resistant but metabolically quiescent spore while other cells follow a different survival strategy and produce a pigment able to protect the cell from oxidative conditions. Cell diversification and the ability to develop different survival strategies in *B. pumilus* SF214 can then be viewed as a risk spreading (or bet hedging) strategy. Such stochastic switches between phenotypic states have been found in diverse organisms ranging from bacteria to humans and are considered among the earliest evolutionary solutions to adapt and facilitate persistence in fluctuating environments [34].

Only a subpopulation of pigment-producing cells forms an extracellular matrix. It is not clear whether matrix-production can also be viewed as a survival strategy in specific environments. However, the existence of more than two developmental cell fates is not surprising but rather expected on the base of the multiple cell types previously observed in *B. subtilis* [7,13].

An additional result of this work is the observation that pigment formation is a highly regulated process. Growth conditions affect pigment synthesis most probably regulating the number of cells that become able to synthesize the pigment. This conclusion is supported by the number of fluorescent vs. not fluorescent cells in

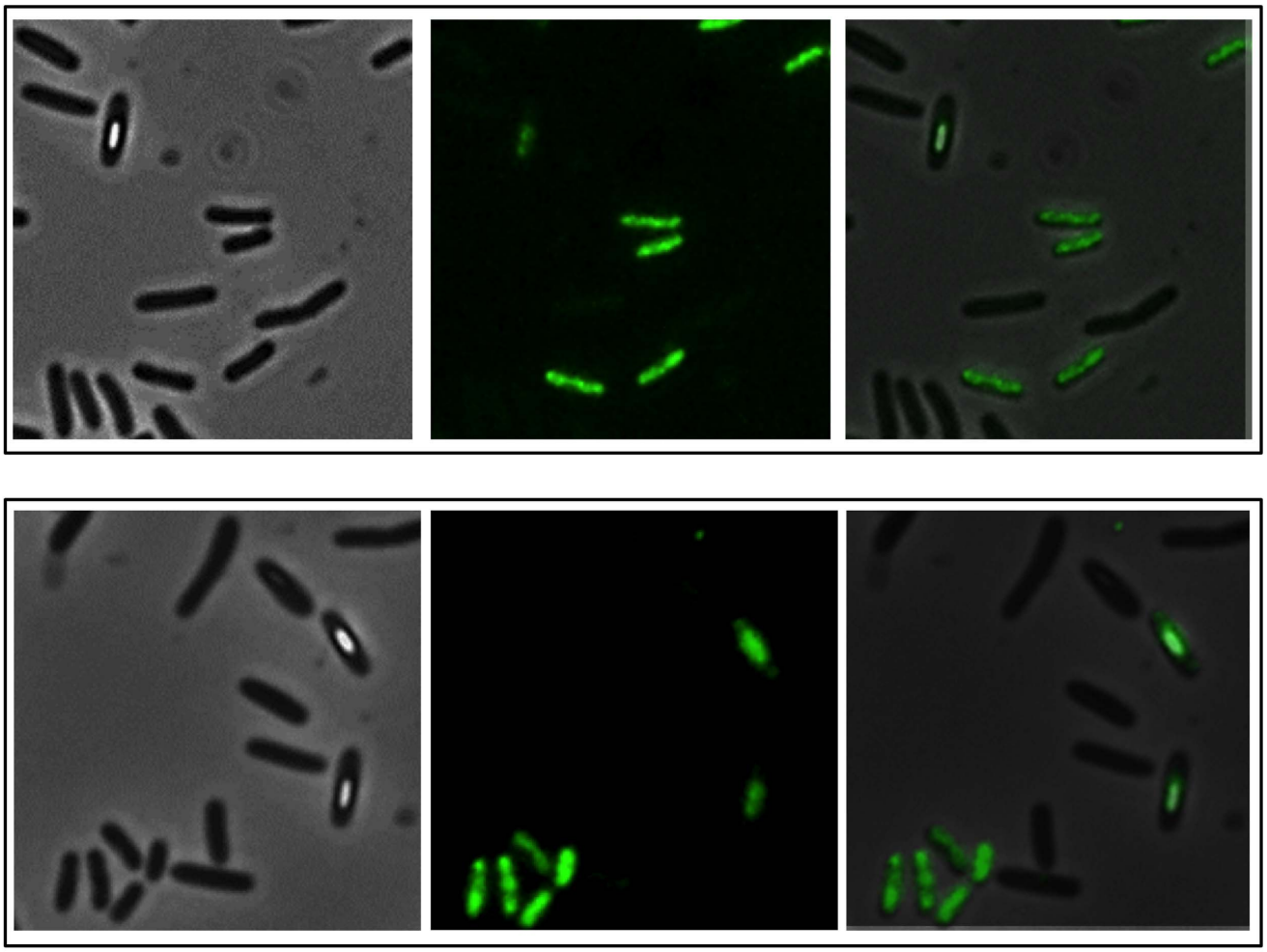

Figure 5. Autofluorescence of sporulating cells. The same microscopy field observed by phase contrast (left), autofluorescence (middle). The right panel reports the merge of phase contrast and autofluorescence images. Cells were grown in rich (LB) medium for 15 hours.
doi:10.1371/journal.pone.0062093.g005

diverse microscopy fields (Fig. 4). Although our analysis does not allow us to assess the amount of pigment synthesized at a single-cell level in the various conditions, it clearly shows that a regulation is exerted when the single stationary cell turns its fate towards either sporulation or pigment synthesis.

Strain SF214 of *B. pumilus* is a field isolate and our attempts to genetically manipulate it have been so far unsuccessful. Several attempts to transform SF214 with chromosomal DNA of an antibiotic-resistant strain of *B. pumilus* or with a non replicative plasmid have all been unsuccessful. SF214 contains a large natural plasmid. We obtained a cured strain which did not show apparent phenotypic differences from SF214 but that was still refractory to transformation. The impossibility to manipulate SF214 has so far impaired a deeper molecular analysis of the various developmental fates of SF214 and of the regulatory proteins involved. A future challenging task will be to verify whether the master regulator Spo0A, known to control matrix formation and sporulation, as well as other cell fate regulators of *B. subtilis* such as ComX and SinI/R, is also involved in pigment development in *B. pumilus*.

Methods

Bacterial Growth Conditions and Spore Induction and Purification

Bacilli were grown either in LB medium (for 1 l: 10 g Bacto-Tryptone, 5 g Bacto-yeast extract, 10 g NaCl, pH 7.0) or in Difco-Sporulation-inducing (DS) medium or in minimal S7 medium (50 mM MOPS, 10 mM $(NH_4)2SO_4$, 5 mM potassium phosphate pH 7.0, 2 mM $MgCl_2$, 0.9 mM $CaCl_2$, 50 µM $MnCl_2$, 10 µM $ZnCl_2$, 5 µM $FeCl_3$, 2 µM thiamine hydrochloride, 20 mM sodium glutamate, 1% glucose, 0.1 mg/ml phenylalanine, 0.1 mg/ml tryptophan) in aerobic conditions. For spore production cells were grown in DS medium in aerobic conditions for 48 hours [32]. Spores were collected by centrifugation and purified by repeated washes and lysozyme treatment, as previously reported [35]. The *B. subtilis* strains used as reference were PY79 (wild type) [36] and the isogenic BZ213 (*cotE::cat*) [28].

Pigment Extraction and Detection

For pigment extraction, cultures were centrifugated at 7000 rpm for 10 minutes. The cell pellet was suspended in a lysis buffer (50 mM Tris-HCl pH 7.5, 1 mM DTT, 0.1 mM PMSF, 10% glycerol) and sonicated at 4°C for 10 min (30 sec. ON and

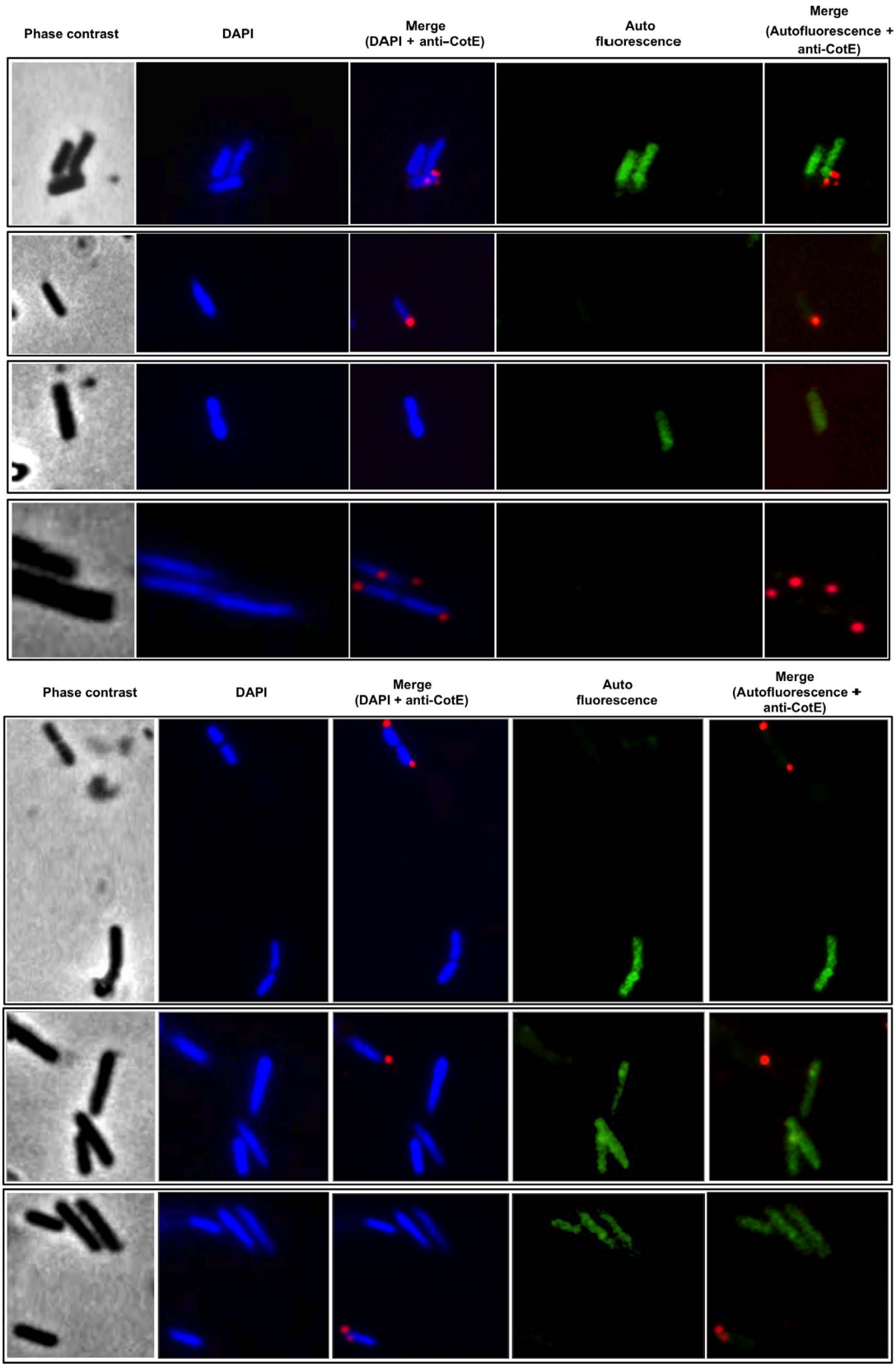

Figure 6. Fluorescence and immunofluorescence microscopy with anti-CotE antibody. Microscopy analysis of cells from different fields observed by phase contrast, DAPI-staining, immunofluorescence with anti-CotE primary antibody and Texas Red conjugated secondary antibody. Merged panels of DAPI-immunofluorescence and autofluorescence-immunofluorescence are shown.
doi:10.1371/journal.pone.0062093.g006

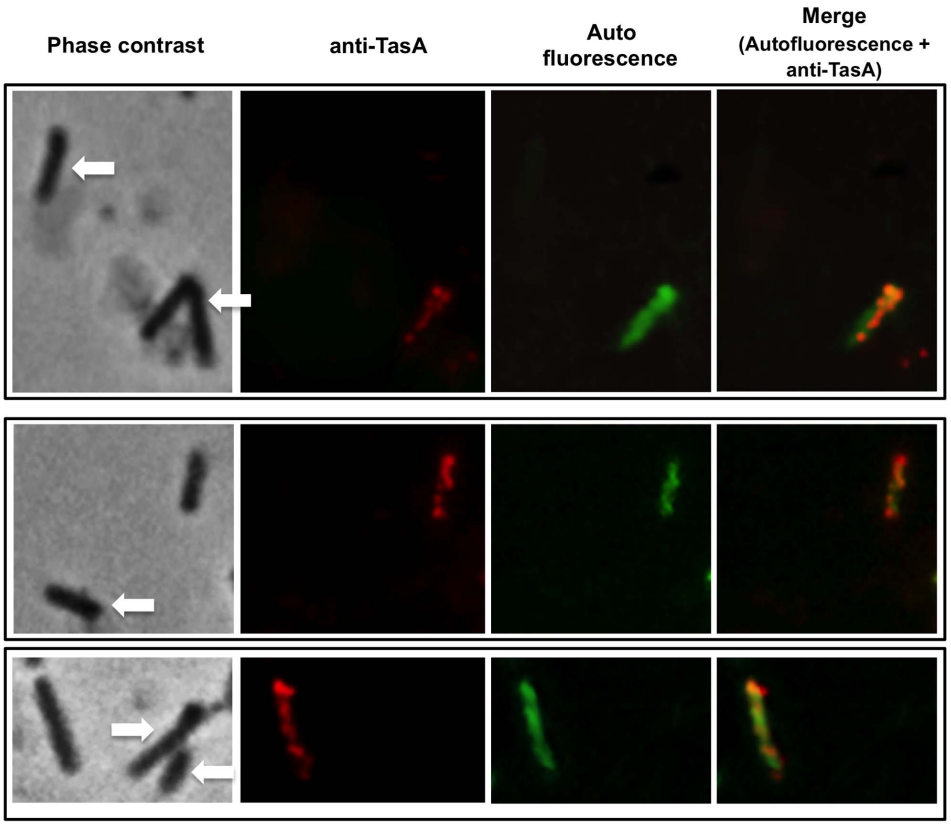
Phase contrast
anti-TasA
Auto fluorescence
Merge (Autofluorescence + anti-TasA)

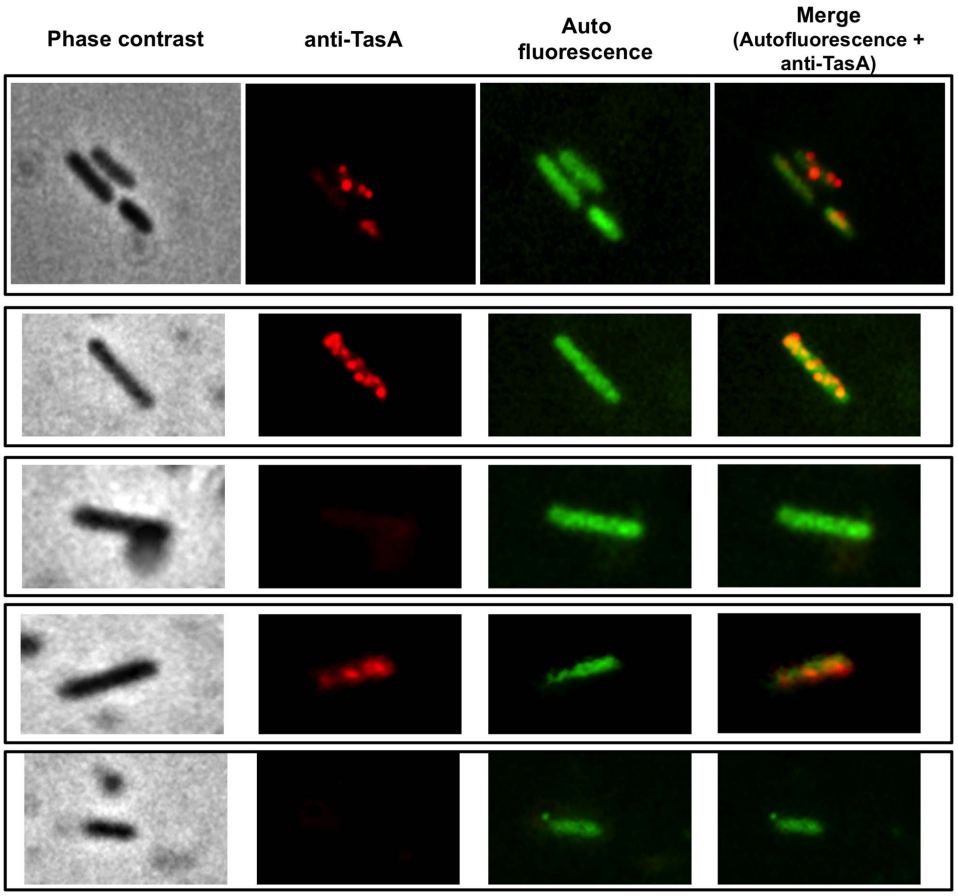
Phase contrast
anti-TasA
Auto fluorescence
Merge (Autofluorescence + anti-TasA)

Figure 7. Fluorescence and immunofluorescence microscopy with anti-TasA antibody. Microscopy analysis of cells from different fields observed by phase contrast, immunofluorescence with anti-TasA primary antibody and Texas Red conjugated secondary antibody and autofluorescence. Merged panels of autofluorescence-immunofluorescence are shown. Panel A reports examples of cells that are not autofluorescent and that are also not recognized by anti-TasA, indicated by arrows. Panel B focuses on examples of autofluorescent cells, with some recognized (yellow in the merge) and some not recognized by anti-TasA antibody.
doi:10.1371/journal.pone.0062093.g007

30 sec. OFF). The pellet was completely removed by centrifugation at 13000 rpm for 15 minutes. Protein concentration of the various extracts was determined spectrophotometrically and aliquots of identical protein concentration used to determine the adsorbance spectrum between 300 and 550 nm, as previously reported [21].

Hydrogen Peroxide Assays

Vegetative cells and spores were diluted to a concentration of approximately 10^8 CFU/ml in PBS, and 1 ml of the cell suspensions placed in a 1.5 ml microcentrifuge tube. 30 mM H_2O_2 (Sigma) was added to the cell suspensions at the concentration of 30 mM. Spores or cell suspensions were incubated at room temperature with continous gentle mixing. After various incubation times 100-µl samples were removed, immediately diluted, plated onto LB agar plate and incubated in order to determine the number of colonies.

Fluorescence and Immunofluorescence Microscopy

For autofluorescence and DAPI staining 200 µl aliquots of cell culture were centrifuged (2 min 6,000 g) and cells resuspended in 20 µl of phosphate-buffered saline (PBS, pH 7.4). Only for the DAPI staining PBS contained 0.1 µg/ml of 4′,6-diamidino-2-phenylindole dihydrochloride (DAPI). Six microliters of each sample were placed on microscope slides and covered with a coverslip previously treated for 30 seconds with poly-L-lysine (Sigma). Samples were observed with an Olympus BX51 fluorescence microscope using a Fluorescein-Isothiocyanate (FITC) or DAPI filters to visualize the fluorescence of the cells. Typical acquisition times were 2000 ms for autofluorescence and 100 ms for DAPI and the Images were captured using a Olympus DP70 digital camera and processed.

Immunofluorescence was performed essentially as described by Azam et al (2000) [37], with a few modifications. Bacteria were fixed for 1 hour at room temperature in 80% methanol, washed, briefly treated with lysozyme and fixed to poly-L-lysine-treated coverslip slides to improve micrographs resolution. The coverslips were air dried and pretreated with 5% (w/v) dried milk in PBS, prior to incubation overnight a 4°C with the primary antibodies. In particular, a 1:400 diluition of anti-CotE (raised in mouse) and a 1:300 dilution for anti-TasA (raised in rabbit) were used. After ten washes, the samples were incubated with a 1000-fold diluted specific secondary antibody conjugates with Tetramethyl Rhodamine, TRITC (Santa Cruz Biotechnology, Inc.) for 2 hours at room temperature in the dark. After ten washes the coverslips were covered with one drop (30 µl) of Component C (Slow Fade: Molecular Probe S-2828) containing 0.1 µg/mL of DAPI. After 5 minutes the liquid was aspirated and the coverslips mounted onto microscope slides adding one drop of Component A (Slow Fade:

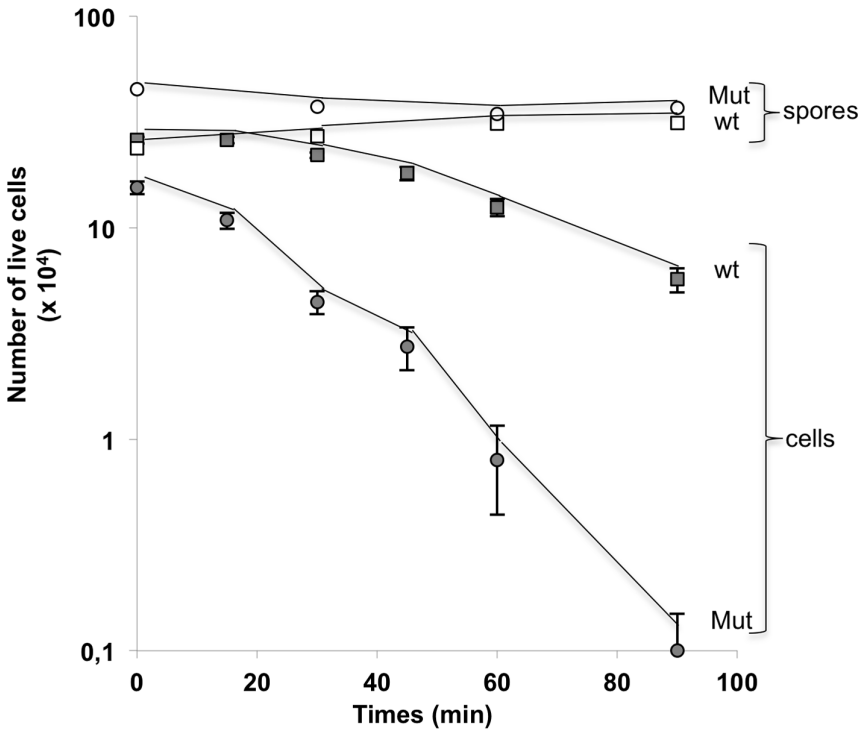

Figure 8. Cell and spore survival after treatment with H_2O_2. Cells and spores were treated with 30 mM H_2O_2 for various times. For each time point the CFU of cells (gray symbols) and spores (white symbols) of the wild type (squares) and the mutant (circles) strains was obtained by plating on LB plates and incubation for 24 hours at 37°C.
doi:10.1371/journal.pone.0062093.g008

Molecular Probe S-2828). The microscope slides were analyzed as described above.

Supporting Information

Figure S1 Western blot analysis of spore coat proteins of SF214 with anti-CotE antobody. Purified spores were extracted by SDS-DTT treatment as previously reported (Nicholson and Setlow, 1990), fractionated on 12% SDS-PAGE and blotted on a PVDF membrane. The membrane was reacted with antibody raised against the CotE protein of *B. subtilis* (Isticato et al., 2010), then reacted against HRP-conjugated secondary antibody and visualized by the ECL method. Coat proteins of a wild type and an isogenic mutant lacking CotE of *B. subtilis* were used as positive and negative control, respectively.
(TIF)

Figure S2 Characterization of TasA of *B. pumilus* SF214. (A) An abundant protein extracted from SF214 spores and corresponding in size to TasA of *B. subtilis* (28 kDa) was transferred to a PVDF membrane and subjected to the Edman degradation reaction. The determined N-terminal 20 residues are reported. A Blast analysis identified the SF214 protein as an homolog of TasA of *B. subtilis* with the homology starting at position 24 of the *B. subtilis* protein. (B) Western blot analysis of spore coat proteins of SF214. Purified spores were extracted with SDS-DTT as previously reported (Nicholson and Setlow, 1990), fractionated on 12% SDS-PAGE and blotted on a PVDF membrane. The membrane was reacted with antibody raised against the TasA protein of *B. subtilis*, then reacted against HRP-conjugated secondary antibody and visualized by the ECL method. Coat proteins of a wild type strain (PY79) of *B. subtilis* were also used.
(TIF)

Figure S3 Isolation of an unpigmented mutant of SF214. (A) SF214 wild type and unpigmented mutant (Mut) on a LB plate grown at 25°C for 48 hours. (B) Survival of SF214 after treatment with 10 mg of NTG for various times. Mid-exponential cells were treated with NTG, washed twice, diluted, plated on LB plates and incubated at 37°C for 36 hours.
(TIF)

Figure S4 Pigment production in SF214 and its unpigmented mutant. Adsorbance spectrum between 300 and 500 nm of 360 mg of cell extracts of SF214 wild type (black symbols) and unpigmented mutant SF214-Mut (white symbols). Cells of both strains were grown at 25°C for 24 hours.
(TIF)

Acknowledgments

We thank Richard Losick for critical reading of the manuscript, Adam Driks for providing the anti-TasA antibody, Saad Fakhry for his contribution to the mutagenesis experiments and Luciano Di Iorio for technical assistance.

Author Contributions

Conceived and designed the experiments: RI ER. Performed the experiments: NM BDL EDA RI. Analyzed the data: NM BDL EDA RI. Wrote the paper: RI ER MDF.

References

1. Hong HA, To E, Fakhry S, Baccigalupi L, Ricca E, Cutting SM (2009) Defining the natural habitat of *Bacillus* sporeformers. Res Microbiol. 160: 375–379.
2. Cutting SM, Hong HA, Baccigalupi L, Ricca E (2009) Oral Vaccine Delivery by Recombinant Spore Probiotics. Int Rev Immunol 28: 487–505.
3. Nicholson WJ, Munakata N, Horneck G, Melosh HJ, Setlow P (2000) Resistance of *Bacillus* endospores to extreme terrestrial and extraterrestrial environments. Microbiol. Mol. Biol. Rev. 64: 548–572.
4. Henriques AO, Moran CP Jr. (2007) Structure, Assembly, and Function of the Spore Surface Layers. Ann. Rev. Microbiol. 61: 555–588.
5. McKenney PT, Driks A, Eichenberger P (2013) The *Bacillus subtilis* endospore: assembly and functions of the multilayered coat. Nat Rev Microbiol 11: 33–44.
6. Setlow P. (2006) Spores of *Bacillus subtilis*: their resistance to and killing by radiation, heat and chemicals. J Appl Microbiol. 101: 514–525.
7. Lopez D, Vlamakis H, Kolter R (2009) Generation of multiple cell types in *Bacillus subtilis*. FEMS Microbiol Rev 33: 152–163.
8. Vlamakis H, Aguilar C, Losick R, Kolter R (2008) Control of cell fate by the formation of an architecturally complex bacterial community. Genes Dev 22: 945–953.
9. Chai Y, Norman T, Kolter R, Losick R (2010) An epigenetic switch governing daughter cell separation in *Bacillus subtilis*. Genes Dev 24: 754–765.
10. Chai Y, Norman T, Kolter R, Losick R (2011) Evidence that metabolism and chromosome copy number control mutually exclusive cell fates in *Bacillus subtilis*. EMBO J. 30: 1402–1413.
11. Lopez D, Vlamakis H, Losick R, Kolter R (2009) Paracrine signaling in a bacterium. Genes Dev 23: 1631–1638.
12. Chai Y, Chu F, Kolter R, Losick R (2008) Bistability and biofilm formation in *Bacillus subtilis*. Mol Microbiol. 67: 254–263.
13. Veening JW, Smits WK, Kuipers OP (2008) Bistability, epigenetics, and bet-hedging in bacteria. Ann Rev Microbiol. 62: 193–210.
14. Fujita M, Losick R (2005) Evidence that entry into sporulation in *Bacillus subtilis* is governed by a gradual increase in the level and activity of the master regulator Spo0A. Genes Dev 19: 2236–2244.
15. Branda SS, Chu F, Kearns DB, Losick R, Kolter R (2006) A major protein component of the *Bacillus subtilis* biofilm matrix. Mol Microbiol 59: 1229–1238.
16. Chu F, Kearns DB, Branda SS, Kolter R, Losick R (2006) Targets of the master regulator of biofilm formation in *Bacillus subtilis*. Mol Microbiol 59: 1216–1228.
17. Romero D, Aguilar C, Losick R, Kolter R (2010) Amyloid fibers provide structural integrity to *Bacillus subtilis* biofilms. Proc Natl Acad Sci USA 107: 2230–2234.
18. Aguilar C, Vlamakis H, Guzman A, Losick R, Kolter R (2010) KinD Is a Checkpoint Protein Linking Spore Formation to Extracellular-Matrix Production in *Bacillus subtilis* Biofilms. mBio 1:1 doi: 10.1128/mBio.00035–10.
19. Hullo M-F, Moszer I, Danchin A, Martin-Verstraete I (2001) CotA of *Bacillus subtilis* is a copper-dependent laccase. J. Bacteriol. 183: 5436–5430.
20. Duc LH, Fraser P, Cutting SM (2006) Carotenoids present in halotolerant *Bacillus* spore formers. FEMS Microbiol Lett 255: 215–224.
21. Khaneja R, Perez-Fons L, Fakhry S, Baccigalupi L, Steiger S, et al (2010) Carotenoids found in *Bacillus*. J. Appl. Microbiol 108: 1889–1902.
22. Manzo N, D'Apuzzo E, Coutinho PM, Cutting SM, Henrissat B, et al (2011) Carbohydrate-active enzymes from pigmented *Bacilli*: a genomic approach to assess carbohydrate utilization and degradation. BMC Microbiol. 11: 198 doi:10.1186/1471–2180–11–198.
23. Steiger S, Perez-Fons L, Fraser PD, Sandmann G. (2012) Biosynthesis of a novel C30 carotenoid in *Bacillus firmus* isolates. J. Appl. Microbiol 110: 888–895.
24. Cremades O, Ponce E, Corpas R, Gutierrez JF, Jover M, et al (2001) Processing of crawfish (*Procambarus clarkii*) for the preparation of carotenoproteins and chitin. J Agric Food Chem 49: 5468–5472.
25. An G-H, Suh O-S, Kwon H-C, Kim K, Johnson EA (2000) Quantification of carotenoids in cells of *Phaffia rhodozyma* by autofluorescence. Biotechnol Letters 22: 1031–1034.
26. Kleinegris D, van Es MA, Janssen M, Brandenburg WA, Wijffels RH. 2010. Carotenoid fluorescence in *Dunaliella salina*. J Appl Phycol 22: 645–649.
27. Pogliano K, Harry E, Losick R (1995) Visualization of the subcellular location of sporulation proteins in *Bacillus subtilis* using immunofluorescence microscopy. Mol Microbiol. 18: 459–470.
28. Zheng L, Donovan WP, Fitz-James PC, Losick R (1988) Gene encoding a morphogenic protein required in the assembly of the outer coat of the *Bacillus subtilis* endospore. Genes Dev. 2: 1047–1054.
29. Isticato R, Pelosi A, De Felice M, Ricca E (2010) CotE binds to CotC and CotU and mediates their interaction during spore coat formation in *Bacillus subtilis*. J. Bacteriol. 192: 949–954.
30. Serrano M, Zilhao R, Ricca E, Ozin AJ, Moran CP, et al (1999) A *Bacillus subtilis* secreted protein with a role in endospore coat assembly and function. J. Bacteriol 181: 3632–3643.
31. Stover AG, Driks A (1999) Secretion, localization, and antibacterial activity of TasA, a *Bacillus subtilis* spore-associated protein. J Bacteriol. 181: 1664–1672.
32. Cutting S, PB Vander Horn (1990) Genetic analysis In: C. Harwood C; Cutting SM, editors. Molecular Biological Methods for *Bacillus*. John Wiley and Sons, Chichester, UK 27–74.

33. Bosak T, Losick RM, Pearson A (2008) A polycyclic terpenoid that alleviates oxidative stress. Proc. Natl Acad Sci USA 105: 6725–6729.
34. Beaumont HJE, Gallie J, Kost C, Ferguson GC, Rainey PB (2009) Experimental evolution of bet hedging. Nature 462: 90–94.
35. Nicholson WL, Setlow P (1990) Sporulation, germination and outgrowth. In: C. Harwood C; Cutting SM, editors. Molecular Biological Methods for *Bacillus*. John Wiley and Sons, Chichester, UK. 391–450.
36. Youngman P, Perkins JB, Losick R (1984) A novel method for the rapid cloning in *Escherichia coli* of *Bacillus subtilis* chromosomal DNA adjacent to Tn917 insertion. Mol. Gen. Genet. 195: 424–433.
37. Azam TA, Hiraga S, Ishihama A (2000) Two types of localization of the DNA-binding proteins within the *Escherichia coli* nucleoid. Genes Cells 5: 613–626.

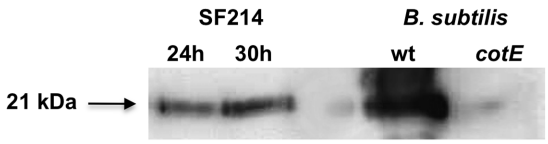

Figure S1: Western blot analysis of spore coat proteins of SF214 with anti-CotE antobody. Purified spores were extracted by SDS-DTT treatment as previously reported (Nicholson and Setlow, 1990), fractionated on 12% SDS-PAGE and blotted on a PVDF membrane. The membrane was reacted with antibody raised against the CotE protein of *B. subtilis* (Isticato et al., 2010), then reacted against HRP-conjugated secondary antibody and visualized by the ECL method. Coat proteins of a wild type and an isogenic mutant lacking CotE of *B. subtilis* were used as positive and negative control, respectively.

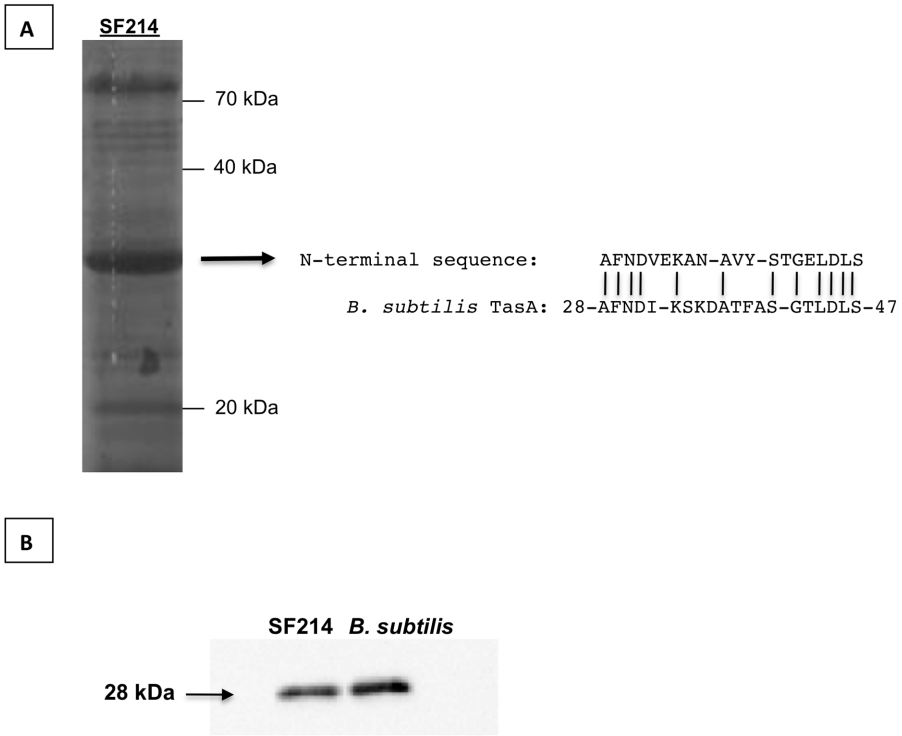

Figure S2: Characterization of TasA of *B. pumilus* SF214. (A) An abundant protein extracted from SF214 spores and corresponding in size to TasA of *B. subtilis* (28 kDa) was transferred to a PVDF membrane and subjected to the Edman degradation reaction. The determined N-terminal 20 residues are reported. A Blast analysis identified the SF214 protein as an homolog of TasA of *B. subtilis* with the homology starting at position 24 of the *B. subtilis* protein. (B) Western blot analysis of spore coat proteins of SF214. Purified spores were extracted with SDS-DTT as previously reported (Nicholson and Setlow, 1990), fractionated on 12% SDS-PAGE and blotted on a PVDF membrane. The membrane was reacted with antibody raised against the TasA protein of *B. subtilis*, then reacted against HRP-conjugated secondary antibody and visualized by the ECL method. Coat proteins of a wild type strain (PY79) of *B. subtilis* were also used.

A

SF214 Wild type

Unpigmented mutant (SF214-Mut)

B

Survival of SF214 cells after NTG treatment

	Time of incubation with 10 μg NTG (min)			
	0	10	20	30
CFU	1.1×10^8	9.8×10^7	2.9×10^7	5.7×10^6
(%)	(100)	(89.1)	(26.4)	(5.2)

Figure S3: Isolation of an unpigmented mutant of SF214. (A) SF214 wild type and unpigmented mutant (Mut) on a LB plate grown at 25°C for 48 hours. (B) Survival of SF214 after treatment with 10 μg of NTG for various times. Mid-exponential cells were treated with NTG, washed twice, diluted, plated on LB plates and incubated at 37°C for 36 hours.

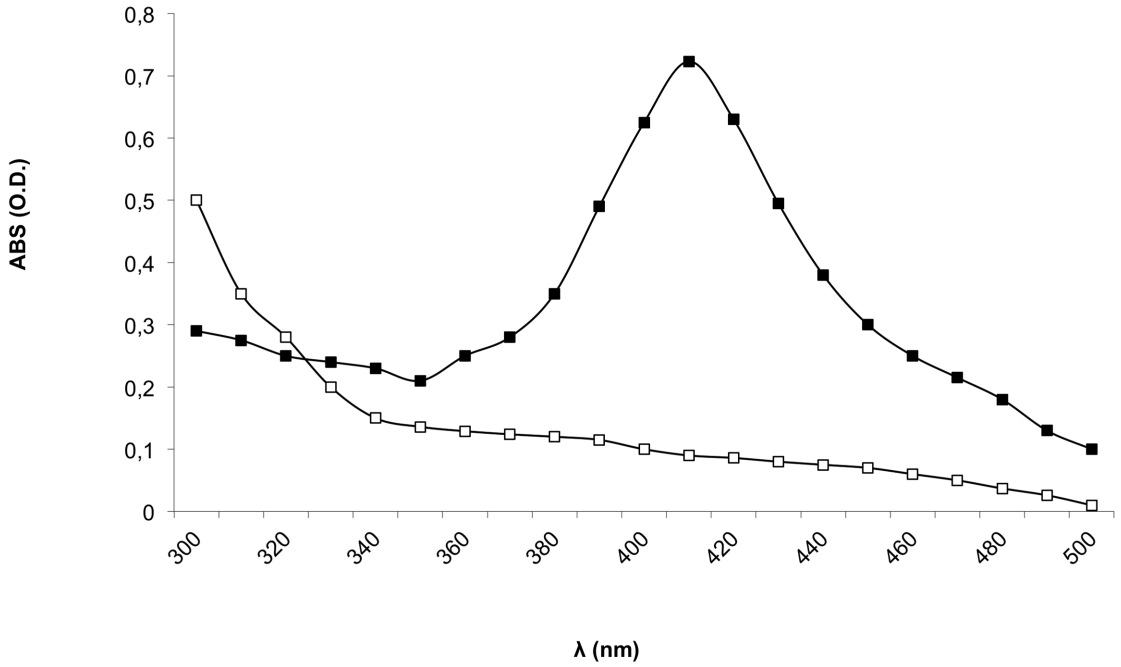

Figure S4: Pigment production in SF214 and its unpigmented mutant. Adsorbance spectrum between 300 and 500 nm of 360 mg of cell extracts of SF214 wild type (black symbols) and unpigmented mutant SF214-Mut (white symbols). Cells of both strains were grown at 25°C for 24 hours.